Universitat de Girona

DOWNWARD FLAME FRONT SPREAD IN THIN SOLID FUELS: THEORY AND EXPERIMENTS

Bruna Comas Hervada

Dipòsit legal: Gi. 1451-2014
http://hdl.handle.net/10803/276957

Universitat de Girona

Doctoral Thesis

Downward flame front spread in thin solid fuels: Theory and experiments

Bruna Comas Hervada

2014

Doctoral Thesis

Downward flame front spread in thin solid fuels: Theory and experiments

Bruna Comas Hervada

2014

Programa de doctorat en ciències experimentals i sostenibilitat

Supervised by:
Toni Pujol Sagaró

Presented in partial fulfilment of the requirements for a doctoral degree from the University of Girona

This Ph.D. Thesis has produced a collection of published articles which are included in the Appendix. The results section of this thesis is formed by the three original papers that have been published in peer-reviewed journals. The impact factors of the journals are from the first and the second quartiles, according to the Journal Citation Reports (JCR) for the year 2012, for the subject categories *Physics, Mathematical* and *Engineering, Multidisciplinary*.

The complete reference of the papers and the impact factor of the journals are:

- B. Comas and T. Pujol. Flame front speed and onset of instability in the burning of inclined thin solid fuel samples. *Physical Review E*, 88: 063019, 2013. (Impact Factor 2.313, journal 6 of 55, Quartile 1, category *Physics, Mathematical*)

- B. Comas and T. Pujol. Energy balance models of downward combustion of parallel thin solid fuels and comparison to experiments. *Combustion Science and Technology*, 185: 1820–1837, 2013. (Impact Factor 1.011, journal 33 of 90, Quartile 2, category *Engineering, Multidisciplinary*)

- B. Comas and T. Pujol. Experimental study of the effects of side-edge burning in the downward flame spread of thin solid fuels. *Combustion Science and Technology*, 184: 489-504, 2012. (Impact Factor 1.011, journal 33 of 90, Quartile 2, category *Engineering, Multidisciplinary*)

Nomenclature

Letters

a	Absorptivity of paper (-)
A_g	Combustion preexponential term ($m^3 kg^{-1} s^{-1}$)
A_s	Pyrolysis preexponential term (s^{-1})
b	constant to express the convective heat flux in Chap. 3.2 (W m^{-2})
B_c	Mass transfer number (-)
c	Specific heat (J kg^{-1} K^{-1})
C	Separation between papers (cm)
d	Function of θ_s (-)
D	Mass diffusivity (m^2 s^{-1})
Da	Damkohler number (-)
E_g	Combustion activation energy term (kJ mol^{-1})
E_s	Pyrolysis activation energy term (kJ mol^{-1})
f	Air to fuel mass ratio (-)
$F_{a \to b}$	View factor from surface a to surface b (-)
F	Factor in Eq. (3.24) (-)
g	Gravity (m s^{-2})
Gr	Grashof number (-)
H_{vap}	Latent heat of vaporization (J kg^{-1})
H_{com}	Heat of combustion (J kg^{-1})
H_{pyr}	Heat of pyrolysis (J kg^{-1})
J	Heat flux in Chap. 3.3 (W m^{-2})
L	Length (mm)
$\dot{m}''$	Mass flux of volatiles (kg m^{-2} s^{-1})
N	Number of papers (-)
Nu	Nusselt number (-)
Pr	Prandtl number (-)
q	Heat flux (W m^{-2})
Q	Heat transfer rate per unit width (W m^{-1})
$\dot{Q}'''_{s-g}$	Volumetric rate of heat transfer from the solid to the gas phase (W m^{-3})
P	Pressure (Pa)

r	Stoichiometric oxidizer to fuel mass ratio (-) in Chap. 3.2 /Correlation coefficient in Chaps. 2 and 3.1 (-)
R	Universal gas constant (8.314 J K^{-1} mol^{-1})
Sc	Schmidt number (-)
T	Temperature (K)
u	x-component of gas phase velocity (m s^{-1})
v	y-component of gas phase velocity (m s^{-1})
v_w	Blowing velocity of volatiles from the solid (m s^{-1})
V_f	Downward flame spread velocity (cm s^{-1})
w	Sample width (mm) / z-component of gas phase velocity in Chap. 1 (m s^{-1})
x	Direction parallel to sample surface (m)
X	Molar fraction (-)
y	Direction normal to sample surface (m)
Y	Mass fraction (-)
z	Direction parallel to sample surface and parallel to flame front (m)

Greek Symbols

α	Thermal diffusivity (m^2 s^{-1})
β	Angle between the flame plane and the paper plane in Chap. 3.3 (deg) / Heating rate in Chap. 2 (K min^{-1})
δ	Constant to express the convective flux in Chap. 3.2 (m) / Thickness of the boundary layer in Chap. 3.3 (m)
δ_i	Length scale (m)
ε	Emissivity (-)
ζ	Integral variable (m)
η	Integral variable (m)
θ	Flame inclination angle (deg)
θ_s	Dimensionless solid temperature, $\theta_s = (T_s - T_\infty)/(T_v - T_\infty)$ (-)
λ	Thermal conductivity (W m^{-1} K^{-1})
μ	Viscosity (Pa s)
ν	Kinematic viscosity (m^2 s^{-1})
ξ	Integral variable (m)
ρ_i	Density (kg m^{-3})
σ	Stefan-Boltzmann constant (W m^{-2} K^{-4})
τ	Thickness (mm)
ϕ	Sample inclination angle (deg)
$\dot{\omega}'''$	Reaction term (kg m^{-3} s^{-1})

Subscripts

$+$	From the upper side
$-$	From the lower side
1	First approximation
2	Second approximation
∞	Ambient
acv	Convective (velocity)
ad	Adiabatic (adiabatic temperature of flame)
com	Combustion
c	Convective
de Ris	Related to de Ris' formula
dx	Differential strip of the sample
d	Downward
e	Ember
f	Flame
g	Gas
h	From paper to flame
i	Dummy index
j	Dummy index
k	Dummy index
l	Dummy index
n	Normal to flame front
N	For N papers (if nothing stated, it refers to 1 paper)
p	Paper
r	Radiative
ref	Reference for calculating gas phase properties
ri	Radiative from $i = f1$ local flame, $i = f2$ nearby flame, $i = s$ surface (losses), $i = p$ nearby paper surface, $i = e$ nearby ember
s	Solid
t	Total
$thin$	Thin solids
$thick$	Thick solids
v	vaporization

List of Figures

List of Tables

Universitat de Girona

El Dr. Toni Pujol i Sagaró, de la Universitat de Girona,

DECLARO
Que el treball titulat *Downward flame front spread in thin solid fuels: Theory and experiments*, que presenta Bruna Comas i Hervada per a l'obtenció del títol de doctora, ha estat realitzat sota la meva direcció i que compleix els requisits per poder optar a Menció Internacional.

I, perquè així consti i tingui els efectes oportuns, signo aquest document.

Signatura

Girona, 26 de maig de 2014.

To my wife and daughter

Acnowledgements

First of all I would like to thank Dr. Toni Pujol for providing the opportunity to conduct this research, he has made a lot of suggestions during these years and has become the principal support of this thesis. This adventure also started under the supervision of Dr. Quim Fort, and would have been impossible to start without him.

I want also to thank my supervisor in Lund University, Dr. Patrick van Hees, for his guidance during my stay there and for having let me conduct some experiments.

This thesis has been possible thanks to FPU (Formación de Profesorado Universitario) fellowship program funded by Ministerio de Educación, Cultura y Deporte.

I wish to extend my gratitude to all my friends and colleagues from Universitat de Girona, the ones from my former department, the Physics Department, and from my new department, the Mechanical Engineering and Industrial Construction department. Specially to my fellow Ph.D. students and my office colleague for the friendship and good times.

I appreciate the friendship and hospitality of the Marie Curie Ph.D. students from Lund University. My stay there wouldn't have been the same without them.

Last but not least, I would like to thank my family for their enormous support and encouragement. This thesis wouldn't have been possible without them. They were the source for my motivation. In particular, my wife Marta and my daughter Lia.

Contents

Resum

La propagació de flames en sòlids és un fenomen complex que inclou processos que passen a la fase sòlida i a la fase gasosa. Diversos autors han estudiat aquest fenomen des de diferents punts de vista ja que és un element clau en l'anàlisi del risc d'incendis i de dinàmica de focs. En aquesta tesi doctoral estudiem la propagació de flames en sòlids prims en processos més complexos que els processos clàssics, on la flama es propaga avall en una mostra vertical o horitzontal.

El Capítol 1 descriu el problema de la propagació de la flama cap avall i dirimeix clarament els objectius del treball. La metodologia aplicada per a obtenir les dades experimentals es descriu al Capítol 2.

El Capítol 3 es compon de tres seccions que són el nucli d'aquesta tesi. La Secció 3.1 fa un estudi complet del mètode experimental i estableix el procediment per a fer proves acurades. També mesura la influència de les vores tot usant diferents tipus de suports de mostra i tot cremant mostres amb un costat sense agafar (amb i sense parets gruixudes properes). Les dades experimentals s'obtenen a fraccions molars d'oxigen diferents i amb mostres de diferents gruixos. A més es deriva un model simple per a la velocitat de propagació del front de flama, que s'ha d'entendre com a una extensió de la fórmula clàssica de de Ris.

La següent secció, la Secció 3.2 estudia l'efecte de la combustió vertical d'un conjunt de mostres paral·leles. Les dades experimentals s'obtenen en funció de la fracció molar d'oxigen i de la separació entre mostres. En aquest capítol generalitzem un model de balanç d'energia detallat que inclou fluxos de calor radiatius per tal que sigui completament predictiu. En aquesta secció també derivem un model analític senzill que és una generalització del model de de Ris, i que inclou explícitament els efectes radiatius. Aquest model reprodueix raonablement bé les velocitats observades.

La Secció 3.3 explora experimentalment i teòricament la propagació cap avall de la flama en mostres inclinades. Es centra en la inestabilitat convectiva que apareix en mostres inclinades que cremen en angles propers a la horitzontal, i proposa una nova metodologia per predir l'angle crític a partir del qual apareix aquesta inestabilitat. La validesa del nostre mètode, basat en el nombre de Nusselt, és confirmada experimentalment amb dades obtingudes a diverses concentracions ambientals d'oxigen.

Resumen

La propagación de llamas en sólidos es un fenómeno complejo que incluye procesos que ocurren en la fase sólida y gaseosa. Diversos autores han estudiado este fenómeno desde distintos puntos de vista, ya que es un elemento clave en el análisis del riesgo de incendios y de dinámica del fuego. En esta tesis doctoral estudiamos la propagación de llamas en sólidos con reducido grosor en procesos más complejos que los procesos clásicos, donde la llama se propaga hacia abajo en una muestra vertical o horizontal.

El Capítulo 1 describe el problema de la propagación de llama hacia abajo y dirime claramente los objetivos del trabajo. La metodología aplicada para obtener los datos experimentales se describe en el Capítulo 2.

El Capítulo 3 se compone de tres secciones que son el núcleo de esta tesis. La Sección 3.1 hace un estudio completo del método experimental y establece el procedimiento para hacer experimentos precisos. También mide la influencia de los lados usando distintos tipos de soportes para la muestra y quemando muestras con un lateral libre (con y sin paredes laterales gruesas). Los datos experimentales se obtienen para fracciones molares de oxígeno distintas y con muestras de distinto grosor. Además se deriva un modelo simple para la velocidad de propagación de la llama, que se debe entender como una extensión de la fórmula clásica de de Ris.

En la siguiente sección, la Sección 3.2, se estudia el efecto de la combustión vertical de un conjunto de muestras paralelas. Los datos experimentales se obtienen en función de la fracción molar de oxígeno y de la separación entre muestras. En esta sección se generaliza un modelo de balance de energías detallado que incluye flujos de calor radiativos para que sea completamente predictivo. También se deriva un modelo analítico simple que es una generalización del modelo de de Ris y que incluye explícitamente los efectos radiativos. Este modelo reproduce razonablemente bien las velocidades observadas.

La Sección 3.3 explora experimentalmente y teóricamente la propagación de la llama hacia abajo en muestras inclinadas. Se centra en la inestabilidad convectiva que aparece en muestras cuyo ángulo de inclinación es próximo a la horizontal, y propone una nueva metodología para predecir el ángulo crítico a partir del cual la inestabilidad aparece. La validez de nuestro método, basado en el número de Nusselt, es confirmada experimentalmente con datos obtenidos en concentraciones ambientales de oxígeno distintas.

Abstract

Flame spread over solid samples has been studied from many points of view, as it is key for fire safety, yet it is a complex phenomenon that involves processes occurring in both the solid and the gas phases. In the present Ph.D. thesis we study flame spread over thin solid samples in processes more complex than the classical cases where a flame spreads downward over a vertical solid sample or horizontally.

Chapter 1 describes the downward flame spread problem and clearly states the objectives of our work. The methodology applied for obtaining the experimental data is detailed in Chapter 2.

Chapter 3 includes the three sections that are the core of this thesis. Section 3.1 makes a thorough study of the experimental method and establishes a procedure for accurately making tests. It also measures the influence of the side effects by using different types of sample holders and by burning the sample with one free edge (with and without nearby sidewalls). The experimental data is obtained at different oxygen molar fractions and with samples of different thickness. A simple model of the flame front speed, that may be understood as an extension of the classical de Ris' formula for thin solid fuels, is derived, acting as a reasonable upper bound of the data we have obtained.

The next section, Section 3.2, shows the effects of a downward combustion of an array of parallel samples. Experimental data are obtained as a function of the oxygen molar fraction and the separation distance between parallel samples. In this chapter we generalize a detailed energy balance model that includes radiative heat transfer in order to be fully predictive. Also in this section, a simple analytical model of the flame front speed is derived, which is a generalization of the de Ris' formula by explicitly including the radiative effects. The models remarkably reproduce the observed data.

Section 3.3 explores the inclined (downward) burning of thin solid samples, both experimentally and theoretically. It focuses on the convective instability that arises when samples are burning almost horizontally, and proposes a new methodology to predict the critical angle at which arises the onset of the instability. The validity of our method, based on the Nusselt number, is experimentally confirmed with data obtained at different oxygen concentrations of the environment.

Chapter 1

Introduction

Flame spread over solid samples is a complex process of great importance from the point of view of fire safety. In addition, it is key for understanding the fundamentals of combustion processes involving pyrolysing materials. Here we restrict our study to downward combustion of thermally thin solids. The latter condition applies to a sample with a thickness smaller than its characteristic thermal length[1]. In the literature, theoretical as well as experimental methods are used for determining the propagation speed of the flame front when burning thin solid fuels. The usual theoretical approach consists of starting from the comprehensive conservation equations and then simplify them after applying some argumented assumptions. The result is either an analytical expression or a set of partial differential equations that form the core of a numerical model whose solution allows us to obtain the flame spread rate. On the other hand, experimental data are usually collected by using a combustion chamber with a given atmospheric concentration and burning a vertical cellulosic-type sample from the top.

This Ph.D. thesis aims to contribute to the knowledge of the downward combustion of thin solid fuels by analysing this phenomenon in more complex situations than those usually applied in common studies (vertical downward combustion with the sample held by both lateral edges). The results obtained in this Ph.D. thesis haven been published in peer-reviewed journals. The results section, Section 3, consists of a transcription of these articles organized in three sections. Section 3.1 experimentally studies the effect of having a free lateral edge on the flame front speed and it develops a simple analytical expression that can be understood as an upper bound of the flame spread rate. Then Section 3.2 generalizes a classical energy balance model in order to include radiative effects and to explain the flame front speed when multiple parallel thin solid sheets are burnt downwards. These sections are focused on vertical burning. In this configuration, convection induces an upward flow parallel to the sample surface and opposed to the flame front velocity. However, in the downward burning of an inclined sample, background flow instabilites arise beyond a critical angle of inclination due to the change of gravity orientation with respect to the sample surface. Section 3.3 investigates this effect and proposes a methodology valid for different atmospheric conditions for predicting such a

[1] $\delta_{gx} = \alpha_g/(V_f + V_g)$; see the nomenclature section for the definition of symbols and variables.

critical angle of inclination.

1.1 The flame spread problem

The flame spread process over solid fuels is described in two steps: first of all there is an endothermic reaction named pyrolysis that takes place in the solid phase. This reaction degrades the solid that produces gases (pyrolysate). After that a strongly exothermic reaction named combustion occurs in the gas phase. There, ambient oxygen and fuel volatiles of the pyrolysate combine to form products and release heat that produces a visible flame. This mechanism starts with an external heat source that pyrolyses the solid until the quantity of fuel volatiles is sufficient to produce a flame. It is sustained by the heat fluxes produced in the combustion process that preheat the virgin solid ahead of the flame front. In Figure 1.1 we can see the schema of the downward flame spread over a thin solid fuel. Only half is depicted, as it is symmetrical with respect to the half thickness of the solid in the vertical burning case.

Besides the articles reproduced in this text, over the course of this Ph.D. we have also developed a transient fully-coupled two-dimensional numerical model of the downward flame spread process. For thin solid fuels and neglecting radiative effects, preliminary results of these simulations allow us to obtain the expected profiles in the gas phase as well as in the solid phase when burning a cellulosic paper with half-thickness $\tau/2 = 0.0933$ mm and density $\rho_s = 461.95$ kg m^{-3} in an environment with no forced flow and oxygen molar fraction $X_{\mathrm{O}_2} = 0.23$.

In Figure 1.2 we can see the solid density and temperature, coupled with the flux of volatiles released by the solid. In the case shown, the flame is propagating to the left (downwards) with the leading edge of the pyrolysis front at 0.003 m approximately. Note the degradation of the solid in the region where pyrolysis exists, with a solid density decreasing to a minimum value (char density) whereas it is almost constant and equal to the virgin value ahead of the front. The volatiles (non-zero values of the mass flux) are released in this pyrolysing region. Also in this region, the solid temperature reaches an almost constant value, whereas there exists a preheating zone with no solid degradation ahead of the front. This behaviour is very similar to that obtained in Refs. [1, 2], being common to all processes of downward flame spread in thin solid fuels.

The next two figures show the characteristic behaviour of the main physical variables in the gas phase. Figure 1.3 displays the fluid density contours in the gas phase at the same time that occurs Figure 1.2 in the solid one. These density variations are due to changes in temperature and induce an opposed buoyancy-driven flow since the propagation is downwards (towards negative x values). Simulations reveal, as in Figure 1.4, that the flame front may be located slightly ahead of the pyrolysis front and that it does not touch the surface. We point out that Figures 1.2-1.4 have been obtained after solving a preliminary version of a numerical model based on the finite volume method. Therefore, the results are solely shown for a qualitative understanding of the flame spread problem. More work is needed for obtaining accurate solutions, especially more effort is required for adequately defining the boundary conditions of the computational domain.

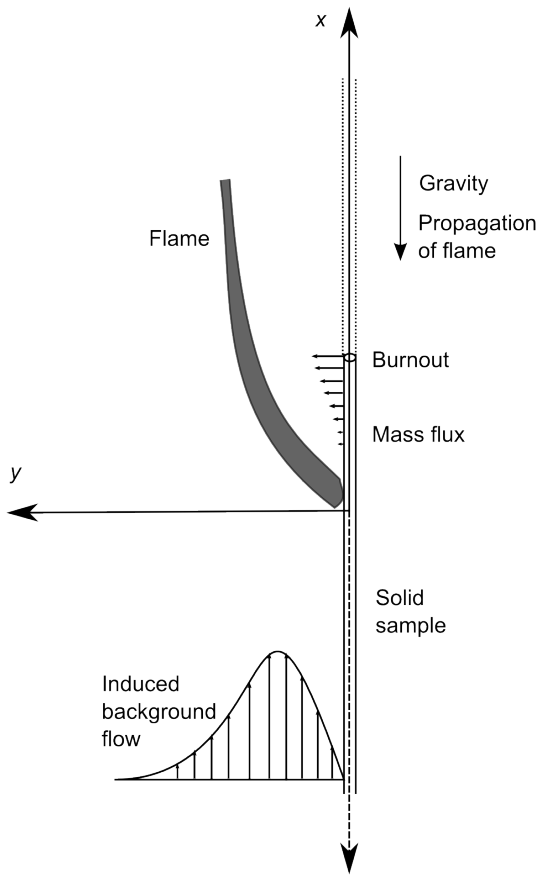

Figure 1.1: Schema of the downward flame spread in a vertical thin solid fuel (symmetry along the x-axis).

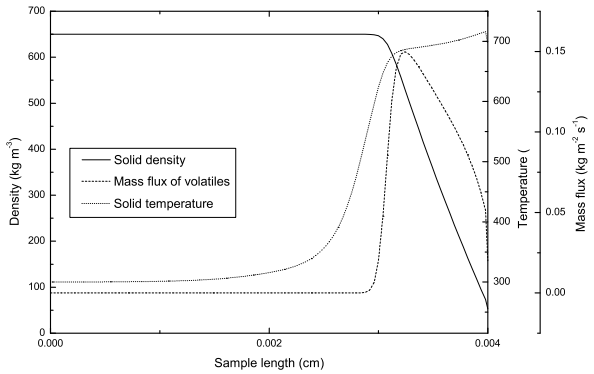

Figure 1.2: Solid density, solid temperature and mass flux of volatiles released by the solid.

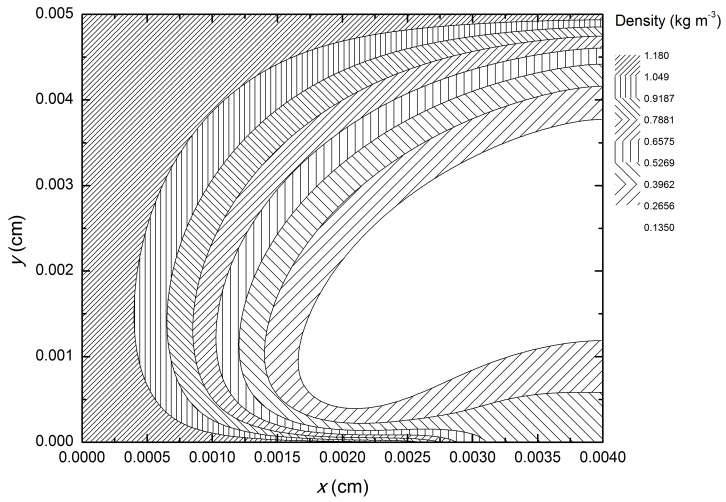

Figure 1.3: Density (kg m^{-3}) contours in the gas phase at the conditions shown in Figure 1.2.

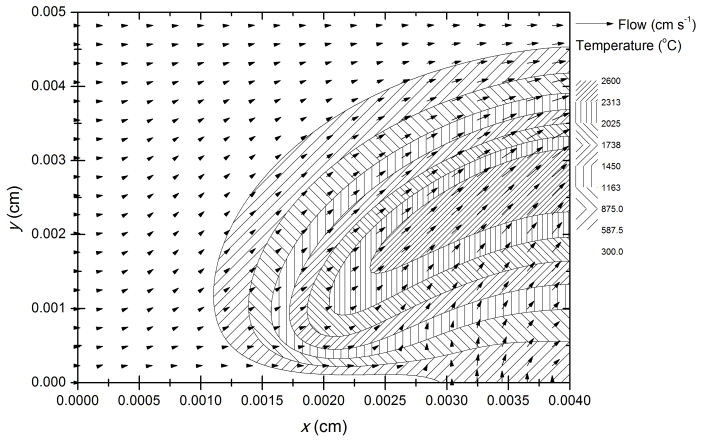

Figure 1.4: Temperature (K) contours and velocity vectors in the gas phase at the conditions shown in Figure 1.2.

1.2 Theory and models

In this section we introduce the comprehensive three-dimensional governing equations for the gas phase reaction (combustion) and the one-dimensional governing equations for the solid phase reaction (pyrolysis) that take place in the flame spread over a thin solid fuel. These equations are used in complex numerical simulations [3]. Under some reasonable assumptions applied to these equations, we may reach analytical expressions for the flame front speed. We then describe the model proposed by de Ris in his Ph.D. thesis [4], which was the first physically-based model that obtained an analytical expression for the flame spread rate based on a simplified version of a two-dimensional model. As stated in the review of the flame spread process over solid fuels written by Wichman [5], the discussion of the physical processes involved in the combustion of solid fuels made in de Ris' Ph.D. thesis is still valid and it becomes a crucial contribution to the field of flame spread.

1.2.1 Governing equations

The pyrolysis process in the solid phase can be described in multiple ways, depending on the material that burns and the degree of complexity wanted. In this thesis we use the word *pyrolysis* meaning a generic reaction that releases gases from a solid, as it is used in the fire research community, nor as it is used in chemical engineering as the anaerobic thermal degradation of solids. We assume that cellulosic materials are charring materials and that melting, bubbling and shrinkage/swelling of the solid can be neglected. The simplest way to model the pyrolysis reaction is using an ablation model that defines a pyrolysis temperature T_v where the reaction takes place. The solid temperature is lower than T_v in the region with no reaction. This model implicitly considers that the pyrolysis

reaction is controlled by heat transfer and that the kinetics of the reaction is infinite [6]. By using this model, pyrolysis is defined with two parameters: the pyrolysis temperature T_v and the heat of pyrolysis H_{pyr}.

The next degree of complexity is to introduce finite-rate kinetics using a one-step Arrhenius reaction term, $\dot{\omega}'''_{fg} = \rho_s A_s exp\left[-E_s/(RT_s)\right]$ (the subscript fg denotes the reaction term from fuel to gas). This was first introduced by Kung [7] for wood pyrolysis. By using finite-rate kinetics, we allow the pyrolysis reaction to happen not only at the surface but throughout the thickness of the solid. This effect is very important in thermally thick solids [3, 6, 8]. Pyrolysis models are reviewed thoroughly in Refs. [6, 9], this not being the objective of this thesis. We suppose that all the fuel burns out and there is no char left. The local mass flux from the solid to the gas phase can be written as

$$\dot{m}''(z) = \int_{\delta}^{z} \dot{\omega}'''_{fg} d\zeta = -\rho v_w(z) \tag{1.1}$$

in the flame front fixed coordinates, with v_w the blowing velocity of the fuel to the ambient, which depends on the gas density and the thickness of the solid [3, 6]. The local energy conservation is

$$\rho_s c_s \frac{\partial T}{\partial t} + \rho_s c_s v_w \frac{\partial T}{\partial z} = -\vec{\nabla} \cdot \vec{J}_s - \dot{\omega}'''_{fg} \nabla H_{pyr} - \dot{Q}'''_{s-g} + \dot{q}'''_r \tag{1.2}$$

where $\dot{Q}'''_{s-g}$ is the volumetric rate of heat transfer from the solid phase to the gas one. By assuming thermal equilibrium between both phases we find $\dot{Q}'''_{s-g} = \dot{m}'' c_g \frac{\partial T_g}{\partial z}$. In Eq. (1.2) $\vec{J}_s$ comprises both radiative and convective heat fluxes. This model is one-dimensional, ignores conductive heat fluxes to other parts of the solid and supposes that all the volatiles generated escape instantaneously [6]. A detailed model of the radiative heat flux can be seen in Bhattacarjee et al.'s work [10] who use a similar model applied to a surface solid element.

On the other hand, the comprehensive gas phase governing equations can be expressed as [3]

- Continuity

$$\frac{\partial \rho}{\partial t} + \nabla \cdot \left(\rho \vec{V}_g\right) = 0 \tag{1.3}$$

- x-momentum

$$\begin{aligned} \frac{\partial (\rho u)}{\partial t} + \nabla \cdot \left(\rho u \vec{V}_g - \mu \nabla u\right) = -\frac{\partial (p - p_\infty)}{\partial x} + \left\{ \frac{\partial}{\partial x} \left[\frac{1}{3} \mu \frac{\partial u}{\partial x} - \right.\right. \\ \left.\left. -\frac{2}{3} \mu \left(\frac{\partial v}{\partial y} + \frac{\partial w}{\partial z} \right) \right] + \frac{\partial}{\partial y} \left[\mu \frac{\partial v}{\partial x} \right] + \frac{\partial}{\partial z} \left[\mu \frac{\partial w}{\partial x} \right] \right\} + g\left(\rho_\infty - \rho\right) \end{aligned} \tag{1.4}$$

with z the coordinate along the width of the sample and x positive in the direction opposite to the propagation.

- y-momentum

$$\frac{\partial(\rho y)}{\partial t} + \nabla \cdot \left[\rho v \vec{V_g} - \mu \nabla v\right] = -\frac{\partial(p - p_\infty)}{\partial y} + \left\{\frac{\partial}{\partial x}\left[\mu \frac{\partial u}{\partial y}\right] + \frac{\partial}{\partial y}\left[\frac{1}{3}\mu \frac{\partial v}{\partial y} - \frac{2}{3}\mu\left(\frac{\partial u}{\partial x} + \frac{\partial w}{\partial z}\right)\right] + \frac{\partial}{\partial z}\left[\mu \frac{\partial w}{\partial y}\right]\right\} \tag{1.5}$$

- z-momentum

$$\frac{\partial(\rho w)}{\partial t} + \nabla \cdot \left[\rho w \vec{V_g} - \nabla w\right] = -\frac{\partial(p - p_\infty)}{\partial z} + \left\{\frac{\partial}{\partial x}\left[\mu \frac{\partial u}{\partial z}\right] + \frac{\partial}{\partial y}\left[\mu \frac{\partial v}{\partial z}\right] + \frac{\partial}{\partial z}\left[\frac{1}{3}\mu \frac{\partial w}{\partial z} - \frac{2}{3}\mu\left(\frac{\partial u}{\partial x} + \frac{\partial v}{\partial y}\right)\right]\right\} \tag{1.6}$$

- Species equation

$$\frac{\partial(\rho Y_i)}{\partial t} + \nabla \cdot \left(\rho Y_i \vec{V_g} - \rho D_i \nabla Y_i\right) = \dot{\omega}_i''' \tag{1.7}$$

  for $i =$ F, O_2, CO_2, H_2O, N_2. The source (or sink) term for species i is

$$\dot{\omega}_i''' = f_i \dot{\omega}_F''' = f_i A_g \rho^2 Y_F Y_O \exp\left(\frac{-E_g}{RT}\right) \tag{1.8}$$

  Considering that the fuel is cellulose, the stoichiometric combustion can be written as $C_6H_{10}O_5 + 6(O_2 + 3.76N_2) \rightarrow 6CO_2 + 5H_2O + 22.56N_2$, so that the stoichiometric ratios are $f_F = -1$, $f_{O_2} = -1.1852$, $f_{CO_2} = 1.6296$, $f_{H_2O} = 0.5556$ and $f_{N_2} = 3.901$.

- Energy equation

$$\frac{\partial(\rho c_g T)}{\partial t} + c_g \nabla \cdot \left[\rho T \vec{V_g} - \left(\frac{\lambda}{c_g} \nabla T\right)\right] = \sum_{i=1}^{N} \rho D_i c_{p,i} (\nabla Y_i \cdot \nabla T) - \sum_{i=1}^{N} \dot{\omega}_i''' h_i + \nabla c_g \cdot \nabla T \left(\frac{\lambda}{c_g}\right) \tag{1.9}$$

  with c_g the weighted specific heat.

The most common boundary equations for combustion within an enclosure at downstream ($x = x_{min}$), upstream ($x = x_{max}$), fuel surface ($y = 0$), chamber walls ($y = y_{max}$

or $z = z_{max}$) and center line of the sample ($z = z_{min}$) are

$$\text{at} \quad x = x_{max} \quad \begin{cases} u = \bar{V}_{g,\infty} - V_f, & v = 0, & w = 0 \\ T = T_\infty, & Y_{\mathrm{O_2}} = Y_{\mathrm{O_2},\infty} & Y_{\mathrm{F}} = Y_{\mathrm{CO_2}} = Y_{\mathrm{H_2O}} = 0 \end{cases} \tag{1.10}$$

$$\text{at} \quad x = x_{min} \quad \begin{cases} \frac{\partial u}{\partial x} = 0, & \frac{\partial v}{\partial x} = 0, \frac{\partial w}{\partial x} = 0 \\ \frac{\partial T}{\partial x} = 0, & \frac{\partial Y_i}{\partial x} = 0 (i = \mathrm{F}, \mathrm{O_2}, \mathrm{CO_2}, \mathrm{H_2O}) \end{cases} \tag{1.11}$$

$$\text{at} \quad y = 0 \quad \begin{cases} u = -V_f, \quad v = v_w, \quad w = 0 \\ T = T_s, \ \dot{m} Y_{F,w} = \dot{m} \frac{\rho D_F}{Le_F} \left(\frac{\partial Y_F}{\partial y} \right)_w, \\ \dot{m} Y_{i,w} = \dot{m} \frac{\rho D_i}{Le_i} \left(\frac{\partial Y_i}{\partial y} \right)_w (i = \mathrm{O_2}, \mathrm{CO_2}, \mathrm{H_2O}) \end{cases} \tag{1.12}$$

$$\text{at} \quad y = y_{max} \quad \begin{cases} u = -V_f, & v = 0, \quad w = 0 \\ T = T_\infty, & \frac{\partial Y_i}{\partial y} = 0 (i = \mathrm{F}, \mathrm{O_2}, \mathrm{CO_2}, \mathrm{H_2O}) \end{cases} \tag{1.13}$$

$$\text{at} \quad z = z_{min} \quad \begin{cases} u = 0, & \frac{\partial v}{\partial z} = 0, \quad w = 0 \\ \frac{\partial T}{\partial z} = 0, & \frac{\partial Y_i}{\partial z} = 0 (i = \mathrm{F}, \mathrm{O_2}, \mathrm{CO_2}, \mathrm{H_2O}) \end{cases} \tag{1.14}$$

$$\text{at} \quad z = z_{max} \quad \begin{cases} u = -V_f, & v = 0, \quad w = 0 \\ T = T_\infty, & \frac{\partial Y_i}{\partial z} = 0 (i = \mathrm{F}, \mathrm{O_2}, \mathrm{CO_2}, \mathrm{H_2O}) \end{cases} \tag{1.15}$$

The previous equations are used in numerical simulations [3], although for typical configurations the solid can be considered infinitely wide and only two-dimensional equations (x, y) need to be considered [2, 10, 11]. In some cases, we use this assumption, among others, in order to find analytical expressions for the flame spread rate. The validity of this assumption is questioned in Section 3.1 where side effects are investigated. Another major assumption done in most combustion studies [2, 11] is to simplify the combustion reaction in terms of a global reaction with stoichiometry $f\mathrm{Fuel} + \mathrm{O_2} \rightarrow P\mathrm{Products} + Heat$. This assumption reduces the number of species equations needed. It also allows us to introduce another typical assumption done in combustion models, Le = 1, where the Lewis number Le is the ratio between thermal and mass diffusivities,

$$\mathrm{Le} = \frac{\alpha}{D} = \frac{\lambda}{\rho c_g D} \tag{1.16}$$

1.2.2 The de Ris' model

John Norval de Ris in his Ph.D. thesis [4] derived an analytical model of the flame spread over solid fuels. Starting from the two-dimensional conservation equations (infinitely wide sample) for both gas and solid phases, he proposed a set of physically realistic assumptions. These simplified the system of equations that finally allowed an analytical solution, even for the gas phase region. We can see the flame spread schema proposed by de Ris in Figure 1.5.

The main assumptions made by de Ris were:

1. To neglect gravitational effects. There was not an induced flow due to gravity, so he could center his attention in the heat transfer mechanisms.

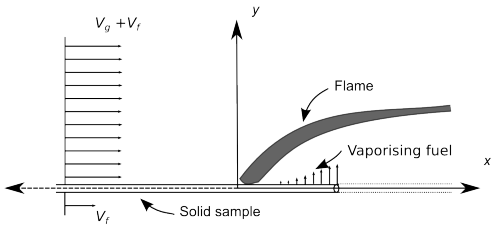

Figure 1.5: Schema of the downward flame spread in a thin solid fuel used in de Ris' model.

2. Simplification of vaporization processes (sublimation, pyrolysis, melting and evaporation) to sublimation. Thereby solids had a constant heat of vaporisation and a defined vaporization temperature (infinite pyrolysis reaction rate).

3. Simplification of the flame structure as a simple diffusion flame (infinite combustion reaction rate). The processes in the solid phase were simplified in a way that when the solid was heated and reached the vaporization temperature, it released gases with a given heat of vaporization. This allowed a great simplification of the governing equations, although it led to a higher reaction rate than the actual one. For this reason, he applied an 'ad hoc' factor to decrease the mass flux of volatiles ($\ln(1 + B_c)$ where B_c is the Spalding, or mass transfer, B_c number [12]). He also discussed the flame structure near the tip, and pointing out that it should be a triple-flame near the cold wall, the main flame front where reactants reacted in stoichiometric proportions and two secondary flame fronts, one ahead of the flame front, lean (with a higher proportion of oxygen), and one after, rich (with more fuel). After defining that, he avoided the problem by setting the ignition temperature below the vaporization temperature of the solid. Thus the flame touched the cold sample surface, with no oxygen after the flame and no fuel in front. He used the model for diffusion flames from Schvab and Zeldovich [13] that considered infinite the chemical reaction rate, so the flame was confined in a thin sheet and fuel and oxygen were consumed at stoichiometric proportions.

4. Oseen flow approximation. The environment would move, either by an opposing flow fed by the lab design or by an induced flow due to buoyancy effects. He considered this opposed flow as a laminar flow with a constant velocity V_g parallel to the fuel, thus using the Oseen flow approximation. Note that this approximation breaks the no-slip condition at the solid surface, although it is a valid solution for the Navier-Stokes equations.

5. Lewis number equal to unity. De Ris set the Lewis number to 1, as the air Lewis

number is Le ≈ 0.9. By setting it to 1, one term dropped from the equations after combining them. This approximation is commonly used in other studies [2, 11] and it is also used in this Ph.D. thesis. The effect of taking into account a mass diffusion by setting Le $\neq 1$ is to change the flame spread rate in the way pointed out in Refs. [3, 14, 15, 16].

6. To neglect radiative heat transfer. De Ris did not consider radiative heat fluxes in his main flame spread rate expressions. He discussed them supposing an exponential net radiative heat flux from the gas to the solid surface, and arrived to the conclusion that radiative effects could be accounted by reducing the heat of combustion or, equivalently, the effective adiabatic stoichiometric flame temperature $T_{f,ad}$. Posterior studies showed that the radiative heat transfer term could be neglected in the thermal regime or, equivalently, far away from combustion limits due to reduced oxygen environmental contents and/or to low gravity values [17]. Radiative effects are also important for various simultaneously burning samples, where the main interaction mechanism between them is the radiative heat transfer. These effects are investigated in Section 3.2 of the results chapter.

With all these assumptions, de Ris derived two formulas for the flame spread rate for both thermally thin and thermally thick solids:

$$V_{f,thin} = \frac{\pi}{4} \frac{\lambda_g}{(\tau/2)\, c_s \rho_s} \frac{(T_{f,ad} - T_v)}{(T_v - T_\infty)} \tag{1.17}$$

$$V_{f,thick} = \sqrt{2} \frac{\alpha_s}{\tau} \frac{\lambda_s}{\lambda_g} \sqrt{\frac{\rho_g c_g \lambda_g}{\rho_s c_s \lambda_s}} \frac{(T_{f,ad} - T_v)}{(T_v - T_\infty)} \tag{1.18}$$

where it is assumed that conduction effects through a thin solid sheet are negligible as the sample has the same T_s value for the whole thickness.

The transition from thermally thin to thick fuel occurs when the solid half-thickness τ_s satisfies $\tau_s \geq \sqrt{\alpha_s \alpha_g / \left[(V_f + V_g)\, V_f\right]}$ [18], which is equivalent to say when the square of the solid half-thickness is greater than the product of the characteristic thermal lengths of gas $\delta_{gx} = \alpha_g/(V_f + V_g)$ and solid $\delta_{sx} = \alpha_s/V_f$ phases.

1.2.3 Energy balance models

The objective of global energy balance models is to apply the conservation of energy to the desired control volume or surface. All the heat fluxes that enter or exit this control volume have to be identified and added to the energy conservation equation. Global energy models are mainly useful for thermally thin solids, as conductive heat fluxes through the solid would make difficult to find an analytical expression for the flame spread rate in thermally thick ones.

Energy balance models are used in Sections 3.1, 3.2 and 3.3 of Chapter 3 in order to derive an expression for the flame spread rate. In Section 3.2 the control volume is an infinitesimal length of the preheated zone of the sample (which is burning downwards).

The flame spread of a wide enough sample can be described as a one-dimensional phenomena, and for thermally thin solids the temperature of the whole thickness can be considered constant. As we will derive in Section 3.2, the energy balance for one element of the preheated zone is then

$$\lambda_s \frac{d^2 T_s}{dx^2} + \rho_s c_s V_f \frac{dT_s}{dx} + \frac{1}{\tau}\left(q_c + q_r\right) = 0 \tag{1.19}$$

where the convective heat flux is due to the environmental gas flow and the radiative heat fluxes have to be identified for every source, being usually modeled as gray-body emitters.

1.2.4 Experimental studies

The experimental work related with the flame spread can be done in a combustion chamber [19, 20], in a wind tunnel (as in the narrow channel apparatus employed in Ref. [21, 22]) or in open air [23]. The combustion chamber is a closed device that can be totally vacuumed and filled with the desired gases at the desired concentration. Data are collected with the background flow at rest. In the wind tunnel configuration a background flow of known composition and velocity flows over the sample. Wind tunnels with very narrow channels are employed in order to suppress convection effects and to simulate microgravity conditions (e.g., [21, 22]).

The main measurement done in these types of studies is the flame spread rate via recordings of the pyrolysis front position at determined times, although other measurements can be done [24]. Temperature measurements can also be obtained by using thermocouples placed at the desired locations or through laser interferometry [5, 25]. A qualitative evaluation of the gas phase around the flame can be done using Schlieren photography [26].

The materials used for these types of experiments are mainly PMMA and cellulosic samples [5, 6]. The experiments can be done either with thermally thin or thermally thick samples. While this classification does not change substantially the experiment done, being an *ad-hoc* differentation, it is used in theoretical work [27] to simplify the set of equations employed to simulate the process. In this Ph.D. thesis we use thermally thin samples.

The air flow can be forced by an external source in a wind tunnel or it can be induced (by gravity), and its direction can be opposed or concurrent to the flame propagation. Concurrent flow flame spread can be divided into three regimes regarding the sample thickness: 1) the kinetic regime, where spread rates increase with the thickness, and where both pyrolysis and flame lengths are short ($\tau < 0.4 \cdot 10^{-4}$ m); 2) the thermally thin regime, where flame spread rates decrease as the solid thickness increases and where both pyrolysis and thermal lengths increase, and 3) the thermally thick regime, where flame spread rate is constant ($\tau > 0.25 \cdot 10^{-2}$ m) [24]. Opposed flow flame spread has also a similar classification regarding the flame thickness.

This thesis deals with opposed flow flame spread induced by buoyancy flows. Downward flame spread (vertical or inclined) arises after igniting the sample at the top. Short

after ignition the front propagation reaches a steady spread rate downward the sample. We experiment with changing thickness, width and lateral holders in Section 3.1, with the effects of having a parallel array of samples in Section 3.2 and with the effects of varying the sample angle of inclination in Section 3.3.

1.3 Objectives

The aims of this thesis are to: (1) Study the flame front propagation in processes more complex than the classical vertically downward one and understand its behaviour; (2) Develop new analytical models that generalize the classical ones and apply them to new conditions (e.g. by including radiative effects in analytical models); (3) Go beyond the balance energy models and explain the convective instabilities that arise in the downward combustion of inclined samples.

Chapter 2

Methodology

This Ph.D. thesis is made as a collection of articles that are included in the following chapters. Each article briefly describes the methodology employed, which usually consists of developing a model for deriving an expression of a key parameter involved in the combustion process (e.g. the flame spread rate) and testing it experimentally. Models will be defined in detail in the following chapters. The experimental design, which is common for all the articles, is here explained for the sake of completeness.

2.1 Experimental Setup

Figure 2.1 shows the combustion chamber used in our experiments. It is a cylindrical galvanized steel chamber with a volume of 0.0458 m^3. It has a 29.5×10 cm width PMMA transparent window in order to record the tests. The chamber can also be inclined at any desired angle.

Vacuum can be made inside the chamber by means of a Telstar Torricelli 2G-6 vacuum pump. We can reach an absolute pressure less than 0.25% of the external (ambient) one. Pressure values inside the chamber are measured with a Wika CPG1000 digital manometer. The system that supplies gases allows us to fill the chamber with oxygen O_2, and a diluent at the desired partial pressures. The diluent used in this Ph.D. thesis has been nitrogen N_2. Tests are done at an absolute pressure of 10^5 Pa, with various concentrations of oxygen (ranging from $X_{O_2} = 20\%$ to 100%).

2.2 Samples

The samples used in our studies are cellulosic sheets of half-thickness $\tau/2 = 0.0933$ mm and a density of $\rho_s = 461.95$ kg m^{-3}. The length of the sheets used differs in each chapter of the thesis, ranging from 16 cm to 27 cm, with a typical width of 4 cm. From the study of the side-effects carried out in Chapter 3.1, this width is a good compromise between being insensitive to side effects and not depleting an excessive amount of oxygen as the sample is burnt. We note that in any case the sample length is chosen so that the oxygen depletion inside the chamber due to the burning process is always less than 2%.

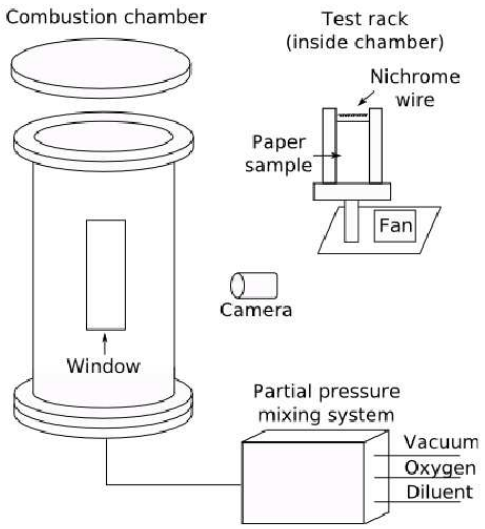

Figure 2.1: Schema of the experimental setup.

The physical properties of our cellulosic sheets have been investigated. The thermal conductivity λ_s is determined using a hot plate at 50^oC with cellulose on and a PMMA plate covering it. This experiment is described in Chapter 3.1. It uses three thermocouples placed at the central point of the interface hot plate-cellulose, cellulose-PMMA and on top of the PMMA plate, and works under the assumption that the heat flux through both solids is the same. Then, using Fourier's law and knowing the thermal conductivity of PMMA, we determine that $\lambda_s = 0.101$ Wm^{-1}K^{-1} with a 5% of error near ambient temperature.

The specific heat capacity c_s curve for our cellulose sample is obtained by using a Differential Scanning Calorimetry (DSC) technique, and it is shown in Figure 2.2. It increases from 1180 J kg^{-1} K^{-1} at 300 K to 2370 J kg^{-1} K^{-1} at 530 K. A linear fit in this range gives $c_s(T) = (6.104 \pm 0.003)T + (954.7 \pm 0.4)$ J kg^{-1} K^{-1}.

We have performed a Thermogravimetric Analysis (TGA) to study the pyrolysis of our sheets. Tests were performed at constant heating rates of $\beta = 2$, 5, 10, and 20 K min^{-1}. Figure 2.3 shows the result of one test done at $\beta = 20$ K min^{-1}. We can see that there are two degradation processes, one near 620 K and the other near 750 K, which is coherent with the models and the experiments reviewed by Milosavljevic [28] for cellulose. By using an Arrhenius first-order one step model for the main solid decomposition[29], we have analysed the main degradation process using the Kissinger method, from which we have obtained the preexponential term $A_s = 3.457 \times 10^{10}$ s^{-1} and the activation energy $E_s = 145.716$ kJ mol^{-1}.

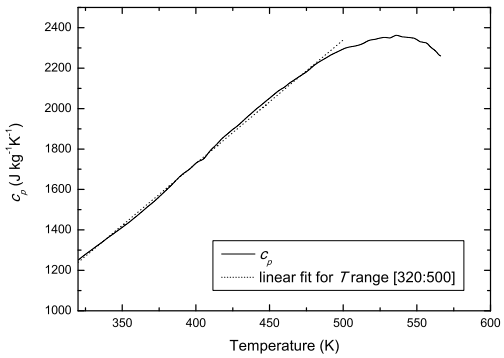

Figure 2.2: Specific heat curve of the cellulose sheets.

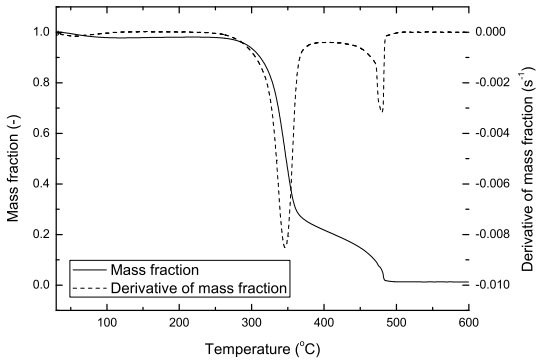

Figure 2.3: Mass fraction and derivative of the mass fraction obtained by means of thermogravimetric analysis of the cellulosic sheets in air and a heating rate $\beta = 20$ K min^{-1}.

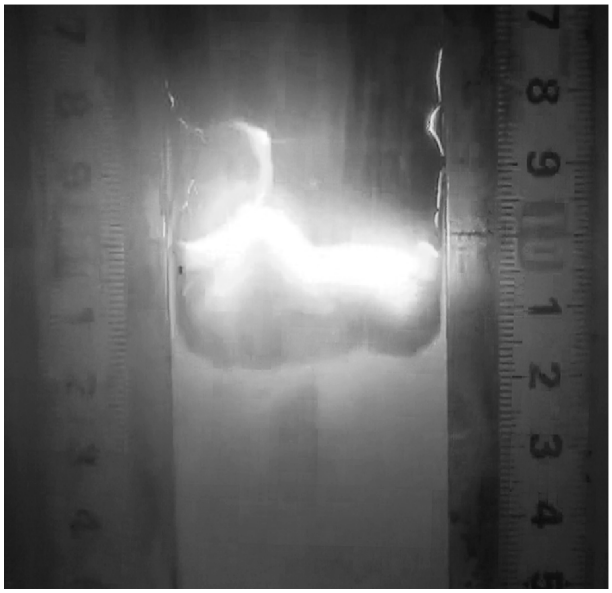

Figure 2.4: Image from one experiment done in a 50% O_2 50% N_2 atmosphere with an inclination of 70^o with respect to the horizontal.

2.3 Experimental procedure

Before starting each experiment, samples are dried for 2 h in an oven at 105 ^{o}C and stored for a minimum of 24 h in a dessicator, to ensure that all samples have the same moisture content. The procedure for making a test consisted of holding the samples with lateral plates and fixing them inside the combustion chamber. The typical holders used are made of aluminium 4 cm wide and 2 mm thick, although in Chapter 3.1, where side effects are investigated, we use other types of paper holders (wider and/or ceramic).

We close the combustion chamber and make the vacuum inside until the inside pressure is less than 0.25% the ambient one. Then the chamber is filled with the desired gases up to an absolute pressure of 10^5 Pa. We mix the gases using a fan for 2 minutes, and then they are left at rest for 3 minutes to ensure that no remaining currents exist inside the chamber when the test is done. The validity of these time periods have been confirmed experimentally. The samples are ignited using a coiled nichrome wire. The experiments carried out using $N > 1$ parallel samples used a nichrome wire for each paper as well, which ignited each sample simultaneously. In the latter case, small nitrocellulose strips between the sample and the wire were used in order to ensure simultaneity of the ignition.

Every test is recorded with a Sony Handycam HDR-CX105E digital camcorder that records 50 interlaced frames per second (25 usable images per second). A typical image from one experiment can be seen in Fig. 2.4. These images are later analysed in the computer. The position of the flame front is obtained with a precision of 1/25 s by identifying it as the visible pyrolysis front (change from white to black in the colour of

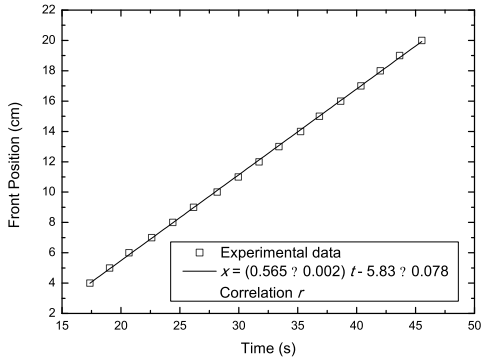

Figure 2.5: Flame position vs. time and linear regression of a test done vertically downward for one paper of width 4 cm in an atmosphere of 30% O_2 - 70% N_2.

the sample). This approach to the flame front is valid and used in other studies [5, 26] as both the pyrolysis and the flame fronts move at the same rate.

The flame spread rate is obtained making a lineal regression of flame positions vs. time. The correlation coefficient for the linear regression r is higher than 0.98 for every test. As an example, Figure 2.5 shows the output of one experiment and the lineal regression obtained in one test. At least three repetitions with the same experimental conditions are carried out to ensure repeteability of the experiments.

Chapter 3

Results

This chapter consists of three sections, being each one a transcription of a published article. A copy of these articles can be found in the Appendices.

3.1 Experimental study of the effects of side-edge burning in the downward flame spread of thin solid fuels

This section is a transcription of the contents of the following paper (a copy of the published version can be found in Appendix A):

B. Comas and T. Pujol. Experimental study of the effects of side-edge burning in the downward flame spread of thin solid fuels. *Combustion Science and Technology*, 184: 489-504, 2012.

Abstract

A comparison between the downward flame spread rate for thermally thin samples with one or two inhibited edges is done in multiple situations. The effects of atmospheric composition as well as the width and thickness of a cellulosic-type fuel are tested experimentally. We have found that the normal velocity to the inclined flame front in a side-edge burning is very similar to the downward flame front speed when the sample is inhibited by both edges. Also, the effect of locating a sidewall close to the free edge of the sample is investigated. All these results may be important in order to validate or refute possible models of downward flame spread that take into account side effects.

Keywords: Downward combustion; Flame spread; Side burning.

3.1.1 Introduction

The flame spread over solid fuels is one of the classical topics in combustion. There have been many theoretical and experimental studies that have investigated downward flame spread, where the flame spreads vertically down against gravity (e.g., [14, 27, 30, 31, 32]). In most of these experimental studies, samples were rectangular, held by the two long

Ref.	Method	Case	Fuel	w (cm)	$\rho_s(\tau/2)$ (kg m^{-2})	X_{O_2} (%)	Results[1]
[3]	Sim.	1 in. edge, 2 in.edges	Cellulose	2	0.046	20 to 25	$V_{f,d}$, θ, fluid fields, etc.
[23]	Exp.	1 in. edge	Fabric, PMM	14	0.2057 (and others)	A	$V_{f,d}$
[36]	Exp.	1 in. edge	PMMA	8	0.58 to 3.48[2]	A	$V_{f,d}$, θ
[37]	Exp.	1 in. edge	Cellulose	2	0.080	21, 30, 50	θ
[38]	Exp. Sim.	1 in. edge	Cellulose	4	0.0385	A	$V_{f,d}$
Present	Exp.	1 in. edge, 2 in. edges, lateral blockage	Cellulose	2, 4, 6	0.043, 0.086, 0.129, 0.172	22, 25, 27, 30, 40, 50	$V_{f,d}$, θ

Table 3.1: Summary of previous works that obtain data related to the downward combustion of solid fuels with free edges at absolute pressure $P = 10^5$ Pa (or similar), normal gravity and initially quiescent environment.

vertical sides and burned from the top horizontal side to the bottom one (e.g., [15, 19, 33, 34]). Using this configuration, the pyrolysis front is nearly flat and perpendicular to the side edges. When only one of the edges is inhibited, either by metallic support strips or chemically, the flame spread is faster along the free edge, this effect being only analyzed, as far as we know, in the studies listed in Table 3.1, where we also include the contribution of the present paper. We note, however, that Emmons and Shen [35] were the first authors who studied the flame front velocities in paper arrays with a free side edge for several densities and separation distances in a quiescent environment (although for horizontal flame propagation instead of downward).

Later, Markstein and de Ris [23] studied flame spreading from a point source of ignition on the edge of textile and plastic samples. They found that under all conditions examined, all with environmental air atmosphere, the downward velocity along the edge $V_{f,d}$ was faster than the velocity normal to the flame front $V_{f,n}$ and assumed that both velocities could be related as $V_{f,n} = V_{f,d}\sin\theta$, where θ is the angle between the vertical side edge and the inclined flame front. Creeden and Sibulkin [36] studied the downward flame propagation on PMMA sheets with an uninhibited side edge, and they found that after a transient phase, θ remained constant ($\theta \approx 30^o$ in air). They compared the downward flame spread rate $V_{f,d}$ with flame front velocities V_f of PMMA sheets with

[1] Exp.= Experimental, Sim.= Simulation, in.= Inhibited, A= Ambient

[2] Assuming $\rho_s = 1160 \text{kgm}^{-3}$

two edges inhibited found in the literature and obtained that, in all conditions studied, $V_{f,n} = V_{f,d}\sin\theta$ coincided with V_f within a 20% interval. After that, Vedha-Nayagam et al. [37] found a relationship between the angle θ and the downward spread rate $V_{f,d}$ based on the exothermic surface reaction model of Sirignano [39]. However, their measurements for various atmospheric concentrations and total pressure were only carried out for free side paper samples, and only the angle θ was reported.

Mell and Kashiwagi [40] and Mell et al. [38] worked experimentally and with three dimensional (3-D) numerical simulations to find out what happened when a horizontal sample with two free edges was ignited in the middle with forced flow, mainly in microgravity conditions but also in normal gravity. The flame reached the free edges, and depending on the flow conditions imposed, it spread only upstream or both upstream and downstream. The flame spread was faster at the edge than in the center. They obtained that in spite of the flame spread rates being steady, the process as a whole was unsteady because the edge and center flames had different spread rates. This was explained as being caused by a greater oxygen supply in the edge and a greater heat transfer from the gas to the solid, which is consistent with previous observations in the transient phase. However, Mell et al. [38] used a small size of the sample (4 cm $\times$ 10 cm), which may not be large enough to reach the steady state. More recently, Kumar and Kumar [3] studied the effect of side-edge burning in normal gravity and in microgravity using computational methods with a steady 3-D model. They found that free edge burning samples had higher spread rates than side inhibited ones, this effect being magnified in a microgravity environment. This was explained because of the effect of buoyant convection that generates an opposed induced flow in normal-gravity situations. There were other effects that, despite the increment of velocity, had different behaviors in normal or microgravity configurations. One of the results of their simulations was that the flame temperature was higher in the uninhibited case than in the inhibited one, and this could explain their differences between velocities normal to the flame front, as we will explain later.

Thus, very few experiments have been carried out with side-edge burning, so our aim is to shed light onto the effects of having an inhibited side edge on the downwards flame spread rate of thin solid fuels. For doing so, we have carried out experiments with different widths and thicknesses of a cellulosic-type fuel and with different atmospheric compositions, as summarized in Table 3.1. In comparison with other experimental studies, we do here report measurements of the downward spread rate for both two sides inhibited and one side uninhibited samples, as well as the inclination angle of the flame front in the latter cases. We have also performed experiments with samples with one inhibited edge and with the free edge having a very close lateral blockage (large sidewall) in order to clarify the role of both oxygen shortage and heat loss effects on the side-edge burning case. In addition, we have developed a simple control volume analysis in order to predict an upper boundary for the downward flame front speed in the uninhibited side edge case that reasonably agrees with our measurements.

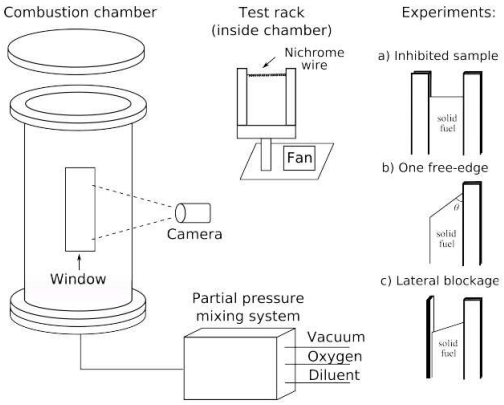

Figure 3.1: Schema of the experimental setup.

3.1.2 Experimental Setup

In the present study, the fuel samples were cellulose sheets having a length of 27 cm, a width varying from 2 cm to 6 cm, and a half-thickness of $(\tau/2) = 0.0933$ mm. Experiments with other thicknesses were obtained by putting together several sheets of cellulose (from two to four). The surface density of one cellulosic sheet defined as $\rho_s(\tau/2)$ was found to be 0.0431 kg m^{-2} where ρ_s is the solid density. Properties of cellulose were investigated with thermogravymetric analysis, using air as the environmental gas and ambient pressure. Kinetic data were obtained with a linear heating at rates of 2, 5, 10, and 20 K min^{-1}. Data were then analysed with the Kissinger method, and both the pre-exponential term A_s and the activation energy E_s for the one-step first order Arrhenius type pyrolysis reaction were found, with values $A_s = 3.457 \times 10^{10}$ s^{-1} and $E_s = 145.716$ kJ mol^{-1}. These values are not used in the present study, but are part of the characterization of the solid and may be used in posterior studies. Comparing them with other values found in the literature, we find that A_s is 38% higher than di Blasi [41] and 30% lower than West et al. [42], which are representative of the range of values used for A_s in other studies. Differences in E_s values are smaller, being 2% and 4% lower in comparison with di Blasi [41] and West et al. [42]. Differential scanning calorimetry (DSC) was used in order to obtain the heat capacity c_s curve of cellulose as a function of temperature that increases almost linearly from 1180 J kg^{-1}K^{-1} at 300 K to 2370 J kg^{-1}K^{-1} at 530 K.

Thermal conductivity was determined using a hot plate at 50 ^{o}C with cellulose on and PMMA covering it. The key concept for this experiment was the assumption that the heat flux that passed through the two materials was unidimensional and equal for both solids. We measured the temperature of the hot surface, the temperature at the cellulose-PMMA interface and the temperature at the external surface of PMMA with

three thermocouples placed in the central point of the samples. Three tests with different sample thicknesses were performed, measuring thermocouple values three times per test. Thickness of the samples was measured with a vernier, being 1.81 mm, 2.58 mm, and 4.67 mm and 3.75 mm for the PMMA plate. The width of both materials was 20 cm, being long enough to discard lateral effects. From these results, using Fourier's law and knowing the thermal conductivity of PMMA (0.197 W $m^{-1}K^{-1}$), we could conclude that the thermal conductivity of our samples was $\lambda_s = 0.101$ W $m^{-1}K^{-1}$ at ambient temperature within a 5% error. In comparison with other values found in the literature, our λ_s coincides within the error band with the value used by di Blasi [41], although other authors employ thermal conductivities for cellulose samples that are 20% higher (see e.g., [1, 2, 43, 44]).

Tests were performed in a combustion chamber of a volume slightly greater than 0.045 m^3, with an absolute pressure of 10^5 Pa and various oxygen concentrations (see Table 3.1). Figure 3.1 shows a schematic view of the experimental design. The volume of the chamber is large enough to ensure that the oxygen depletion of the chamber is smaller than 2%, as explained in Pujol and Comas [8].

Before each experiment, samples were dried for a minimum of 2 h at 100 ^{o}C, then stored for a minimum of 24 h in a dry chamber to ensure homogeneity. During the experiment, the sample was positioned in the middle of the chamber, and was held at one side and at the bottom with two L-shaped supports (one side inhibited case and lateral blockage case), or held by the two sides with straight supports (two inhibited edges case). Unless otherwise stated, these supports were 5 cm wide, 2 mm thick, and were made of aluminium. The lateral blockage is a piece of aluminium, either 1 cm or 2 cm thick, placed near the paper end on the free edge side but not in contact with it.

Vacuum was created in the chamber, and then it was filled with O_2 and N_2 at the desired concentrations. The gases were mixed for 2 min with a fan and then left for 3 min to ensure steadiness of the mixture. The sample was uniformly ignited at the top with a coiled nichrome wire.

Every experiment was recorded through a window of the chamber with a high definition camera at 50 Hz. Frames clearly showed the pyrolysis front, whose location is obtained from a ruler marked in the middle and also on the free side of the paper. The video was then analysed frame by frame in order to determine the spread rate, which corresponds to the slope of the distance versus time location of the flame front. The flame tilt angle was obtained a posteriori by analysing the position of the pyrolysis front in the middle and in the free edge of the paper. As an example, Figure 3.2 shows an image obtained by the camera for the $X_{O_2} = 30\%$ case with a sample 4 cm width, 0.0933 mm half-thickness, and one inhibited edge. A more detailed explanation of the experimental setup for the two inhibited edges case can be found in Pujol and Comas [8].

3.1.3 Results

Every configuration of the experiment was tested three times, and in all cases, the flame spread rate was greater in the one-side inhibited configuration. After ignition and in the transient phase of the process, the flame propagated down more rapidly through the

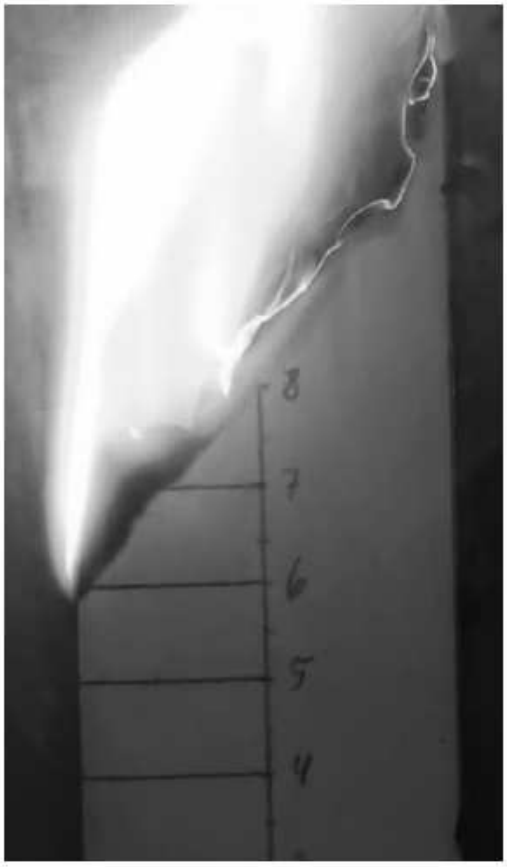

Figure 3.2: Image obtained by the camera for the $X_{O_2} = 30\%$ case with a sample 4 cm width, 0.0933 mm half-thickness and one inhibited edge.

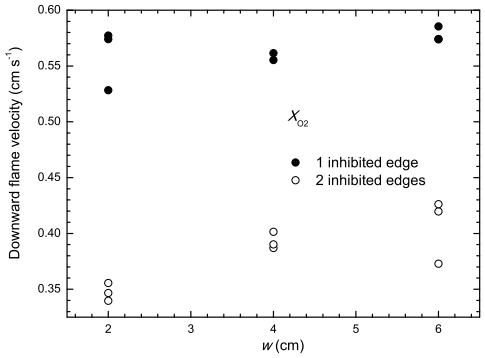

Figure 3.3: Downward flame spread rates for samples with different widths and half-thickness of 0.0933 mm in an atmosphere with $X_{O_2} = 25\%$.

uninhibited edge than in the middle of the sample, thus developing an inclined pyrolysis region, as also reported by Markstein and de Ris [23] and Creeden and Sibulkin [36]. This inclined region spread slowly across the sample width, until it reached the inhibited edge and the inclination angle and the downward flame spread rate became constant (see Figure 3.2). The effects on the flame spread rate of changing the width of the sample, the atmospheric mixture, the thickness of the sample, and of fixing a large sidewall close to the free edge are reported below. In what follows, $V_{f,d}$ and $V_{f,n}$ stand for the downward flame speed and the velocity normal to the inclined flame front for the one-side inhibited case, respectively, and V_f corresponds to the downward flame front velocity for the two-side inhibited case.

Effect of Sample Width

The effects of modifying the separation distance between the two metallic holders in inhibited samples were already investigated by Frey and T'Ien [34], who obtained a clear trend to extinction as the paper width decreased. For samples with a half-thickness $(\tau/2) = 0.095$ mm, 0.3 oxygen mass fraction, and 0.66 bar absolute pressure, the decrease of the flame velocity due to the shortening of the sample width became important for separation distances smaller than 2 cm [34]. Flame front speeds for greater separation distances were similar and, therefore, were insensitive to side-edge effects.

Here, our aim is to study the side-edge burning in samples where the flame front velocity is not affected by side-edge effects when they are inhibited (i.e., two-dimensional flame). Therefore, we tested samples with three different widths w (2 cm, 4 cm, and 6 cm) and half-thickness $(\tau/2) = 0.0933$ mm at different atmospheric mixtures and absolute pressure 10^5 Pa. We found that the downward flame velocity for the inhibited case substantially decreased for the smaller width (2 cm) at values of the molar atmospheric mixture X_{O_2} lower than 30%, as in the work of Zhang and Yu [45]. For the case with

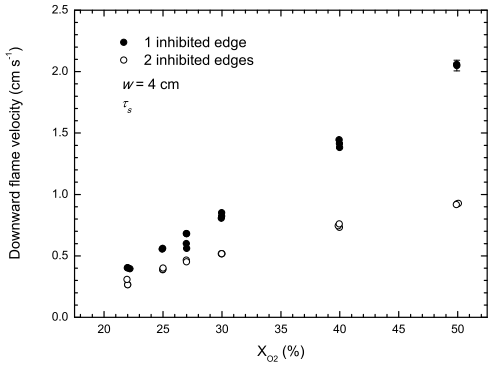

Figure 3.4: Downward flame spread rates for samples of 4 cm width, with one edge uninhibited and with both edges inhibited as a function of oxygen molar concentration X_{O_2}.

one uninhibited edge, however, the downward flame speed did not vary for the three widths except for very low values of the atmospheric mixture (X_{O_2} lower than 25%). This is because the influence of the holder was just to one side of the sample, so the lateral energy losses through the holder and the lateral barrier of the oxygen supply were smaller than for the two-inhibited edge case. Figure 3.3 shows the effect of the width on the downward flame spread for the $X_{O_2} = 25\%$ case. Note that downward flame speeds $V_{f,d}$ for the one inhibited edge (closed circles in Figure 3.3) are substantially greater than those corresponding to the two inhibited edges case V_f (open circles in Figure 3.3), which clearly decrease as the width reduces. Thus, the extinction limit in the one inhibited edge cases seems to arise at smaller separation distances than in the two inhibited edges cases.

For larger widths (4 and 6 cm), the flame velocity stabilized and remained almost constant ($< 7\%$ variation) for the same atmospheric composition. The width of 4 cm has been chosen as a standard in most of the experiments because it is large enough to be in the region where V_f is insensitive to side-edge effects but small enough to not to note the effects of oxygen depletion of the chamber.

Effect of Oxygen Concentration

Downward flame speeds $V_{f,d}$ for the one uninhibited edge cases (closed circles) and downward flame front speeds V_f for the inhibited edge cases (open circles) as a function of the oxygen concentration for samples with width $w = 4$ cm are shown in Figure 3.4. In Figure 3.4, it can be seen that for all atmospheric mixtures, the downward flame spread rate was greater for the samples with an uninhibited edge, with a difference increasing as oxygen concentration increases, varying from a 30% increase when $X_{O_2} = 22\%$ to a 55% increase when $X_{O_2} = 50\%$. The effect of the oxygen atmospheric concentration on $V_{f,d}$ was also greater in the one edge uninhibited case, where the trend for the $X_{O_2} = 22\% - 50\%$

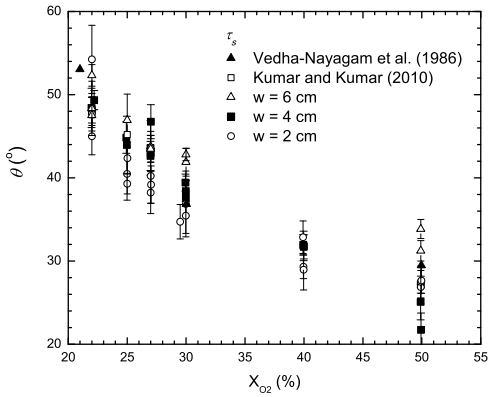

Figure 3.5: Angles of the pyrolysis front with respect to the vertical side for samples with half-thickness of 0.0933 mm and different widths.

range is almost linear, since a linear fit of the data gives $V_{f,d} = 5.58X_{O_2} - 0.83$ with a linear regression coefficient $r = 0.989$ (speed in cm s^{-1} and dimensionless oxygen molar fraction). A better linear fit ($r = 0.994$) is obtained for data extracted from the $w = 6$ cm case (not shown), with a slope equal to 4.89 cm s^{-1}. The $w = 2$ cm data obtained the worst linear fit, since $V_{f,d}$ substantially reduces at very low X_{O_2} values due to side edge effects as explained above. Note that from the linear fit, a 1% increase in oxygen concentration leads to an increase in the downward flame velocity $V_{f,d}$ of the order of 0.05 cm s^{-1}.

For the two-dimensional flame (two inhibited edges), a linear fit for the entire range of oxygen levels analyzed here does not appear reasonable, since V_f rapidly increases as a function of X_{O_2} near the extinction and increases slowly as a function of X_{O_2} at large values of oxygen concentration. We point out that the flame front velocities for the inhibited case are within the range of the values found in the literature (see, e.g., the discussion in [8]).

Although the above data may suggest that the extinction limit for the one inhibited edge case occurs at lower X_{O_2}, Kumar and Kumar [3] found that by doing simulations with and without side-burning, the extinction point is at $X_{O_2} = 20\%$ for the inhibited case and $X_{O_2} = 20.5\%$ for both uninhibited sides cases, although the velocity at the extinction point is higher in the uninhibited case. Unfortunately, we have not been able to experimentally confirm such behaviour due to experimental difficulties found near the extinction point.

In addition, the angle θ measured from the vertical side edge to the inclined pyrolysis front was obtained after analysing the recorded data in the uninhibited cases. These are reported in Figure 3.5 as a function of the oxygen concentration level X_{O_2} where we also include results obtained from the $w = 2$ cm and $w = 6$ cm cases. In Figure 3.5, we also show how our results are consistent with the experimental angles obtained by

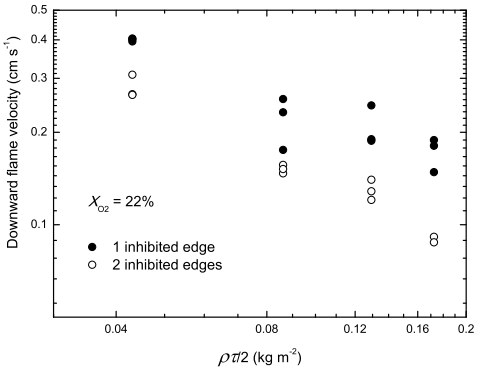

Figure 3.6: Downward flame spread rates for samples with different thicknesses and a width of 4 cm in an atmosphere with $X_{O_2} = 22\%$.

Vedha-Nayagam et al. [37] (see Table 3.1) and the one extracted from the 3-D simulations carried out by Kumar and Kumar [3] both using cellulosic type fuels with width $w = 2$ cm (see other sample details in Table 3.1). We note that the angle reduces (the inclination of the front increases) as X_{O_2} increases, this being related with both the downward flame spread $V_{f,d}$ and the normal velocity to the flame front $V_{f,n}$, as we shall discuss in the Discussion subsection.

Effect of Sample Thickness

Four distinct thicknesses τ of cellulose were tested. Following Bhattacharjee et al. [18], the characteristic thermal length of the solid fuel can be written as $L_s = \sqrt{\alpha_s \alpha_g}/V$, where α_s and α_g are the solid phase and gas phase thermal diffusivities, respectively. From the physical properties of our sample detailed in the Experimental Setup subsection, the solid phase thermal diffusivity is $\alpha_s = \lambda_s/(c_s \rho_s) = 1.85 \times 10^{-7}$ m^{2}s^{-1}. The gas phase thermal diffusivity $\alpha_g = \lambda_g/(c_g \rho_g) = 2.16 \times 10^{-5}$ m^2 s^{-1}, where values of thermal conductivity $\lambda_g = 0.0256$ W K^{-1}m^{-1}, specific heat $c_g = 1000$ J K^{-1} kg^{-1}, and gas density $\rho_g = 1.19$ kg m^{-3} at room conditions follow from Frey and T'Ien [1]. We define the solid fuel as thermally thin if $L_s > (\tau/2)$ or thick if $L_s < (\tau/2)$. Note that this definition depends on the flame spread rate V_f, so it could change in every experiment depending on the composition of gases or the type of experiment. However, for all cases analyzed here, the condition $L_s > (\tau/2)$ is satisfied, so our analyses correspond to thermally thin fuels.

A standard half-thickness of 0.0933 mm (sheets having a surface density $(\tau/2)\rho_s = 0.0431$ kg m^{-2}) was chosen for the majority of experiments. Other thicknesses were obtained by putting together sheets of cellulose. The main difficulty of this method was in preventing sheets from separating during the experiment. This was done by folding the sheets on the uninhibited edge. Figure 3.6 shows the downward flame spreading rates in an atmosphere of $X_{O_2} = 22\%$ as a function of the surface density. The trend of the

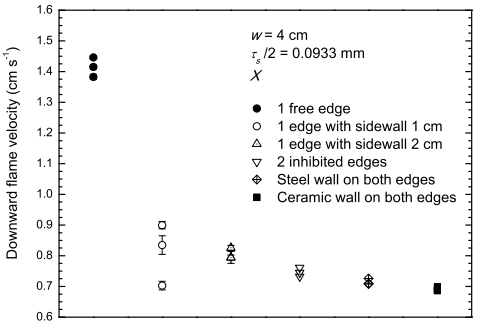

Figure 3.7: Downward flame spread rates for samples with different edge conditions, all with a width of 4 cm in an atmosphere with $X_{O_2} = 40\%$.

downward flame spread rate to decrease as thickness increases can be seen; this is due to the increasing importance of solid conduction between the whole thickness that reduces the amount of energy available to pyrolize the solid. It was also found that the difference in the flame front speed between the inhibited and the uninhibited case was greater for small thicknesses, varying from a 30% difference at $\rho_s(\tau/2) = 0.172$ kg m^{-2} to a 50% at $\rho_s(\tau/2) = 0.043$ kg m^{-2}. This may be caused by the increase in the pyrolysis mass flux from the lateral side when we reduce the thickness, an effect that is related with the thermal conduction through the solid, as we have explained above. Note that Figure 3.6 is a log-log plot where data do not exactly follow a -1 slope, as suggested from the analytical expression of de Ris [27]. We suspect that it is due to the fact that sheets attached together for the high thickness cases separate slightly during the combustion process, increasing the flame spread rate.

Lateral Blockage

Detailed numerical simulations from a 3-D model have recently revealed the importance of lateral oxygen supply for the free edge burning condition [3]. Here we investigated this effect by placing a thick sidewall close to the uninhibited edge. We tested two different thicknesses of the sidewall, one of 10 mm and the other with 20 mm wide in the direction normal to the sample surface, being centred at the sample location. This means that the two sidewalls avoid the lateral entrainment for perpendicular distances from the solid surface lower than 5 mm or 10 mm. Note that the metallic holders on the inhibited side were 2 mm wide in the direction perpendicular to the sample surface. In addition, two tests with holders 8 mm thick and 40 mm wide, made of aluminium and also of ceramic, were done in order to clarify the effect of heat transfer to holders.

The effect of having the lateral blockage on the side was tested with a thermally thin sample ($(\tau/2) = 0.0933$ mm) in an atmosphere of $X_{O_2} = 40\%$. A comparison between

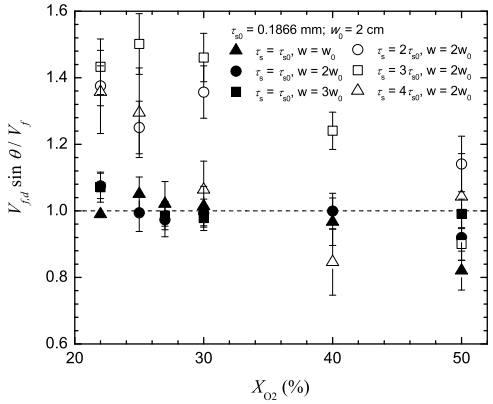

Figure 3.8: Ratio of the velocity normal to the flame front in free edge experiments $V_{f,n} = V_{f,d}\sin\theta$ and the downward flame front speed V_f when both edges are inhibited as a function of the oxygen concentration for different sample conditions.

the six cases (only one side inhibited, one inhibited with the uninhibited having a lateral blockage 5 mm or 10 mm wide and both inhibited with 2 mm thick aluminium clamps, 8 mm thick aluminium clamps, and 8 mm thick ceramic clamps) can be seen in Figure 3.7. Although the side-edge was burning, the shape of the flame front was almost horizontal in the cases with lateral blockage. Indeed, it was very similar to the flame front shape of the cellulose with both edges inhibited. The downward velocity of the flame front was found to be similar to that case, far different from the case with one free edge. In addition, the two experiments with both sides inhibited that used thick walls had similar spread rates, although the heat conductivity of both holders was very different. Note that the results of cases with both sides inhibited for aluminium clamps are not exactly the same. Since losses to the holder are small (from comparison with results obtained using ceramic clamps), this may be due to the increase on the opposed flow by a channelling effect when the holder thickness is large enough to act as a lateral wall. Indeed, some tests done with ceramic clamps had a slower spread rate than those obtained with aluminium ones, most likely due to its roughness, which would tend to reduce the lateral entrainment and enhance the channelling effect. Therefore, these experiments with lateral blockage clearly showed that the main effect of inhibiting an edge corresponded to the shortage of oxygen supply rather than to the increase in the heat losses due to the contact with the holder.

3.1.4 Discussion

We have studied free edge effects experimentally in multiple circumstances. It has been shown that for all cases, the downward flame spread rate $V_{f,d}$ for free edge situations has increased in comparison with the same situation but with both edges inhibited. In terms

of the speed normal to the flame front $V_{f,n}$, we may assume that $V_{f,n} = V_{f,d}\sin\theta$, where $V_{f,d}$ and θ are measured data. The ratio $V_{f,n}/V_f$, where V_f is the flame front velocity for the two-side inhibited case, as a function of the atmospheric mixture is shown in Figure 3.8, where error bars arise from assuming the errors for $V_{f,d}$ and θ as one standard deviation of the statistics applied for obtaining them.

From Figure 3.8, we note that $V_{f,n}/V_f = 1$ within a 5% range for the thickness corresponding to a single sheet, with a slight trend to decrease as X_{O_2} increases when using small widths. In these particular cases, large X_{O_2} values imply large inclination angles, so $V_{f,n}$ substantially departs from the vertical direction and propagates toward the inhibited side. The existence of the aluminium clamp two millimetres wide in the inhibited side may substantially reduce the entrainment of fresh air in a similar way as in the lateral blockage case explained previously. This may lead to $V_{f,n}$ values smaller than the downward flame front velocity V_f obtained with the burning of a sample inhibited in both sides. We also note that the condition $V_{f,n}/V_f \approx 1$ is not satisfied for larger thicknesses, since the multiple sheets attached together are likely to separate (especially in the free edge case), which compromises the assumption of being a single solid fuel.

In comparison with other studies, and from the cellulose-type fuel simulations of Kumar and Kumar [3], we may deduce a ratio $V_{f,n}/V_f = 1.14$. It can be shown, however, that a fraction of this 14% difference of flame front spread rates seems to be due to flame temperature differences between the uninhibited and the fully inhibited cases. Thus, we can calculate the influence of the flame temperature on the front spread rate by using de Ris' [27] formula[3], $V_f \sim \lambda_g / \left(\rho_s c_s (\tau/2)\right) \left(T_f - T_v\right) / \left(T_v - T_\infty\right)$, where T_f is the flame temperature, T_v is the temperature of vaporization, and T_∞ is the ambient temperature. When using the flame temperature corresponding to the free side edge burning case of Kumar and Kumar [3] in the two side inhibited case, the flame front velocity modifies accordingly to the dependence of V_f on T_f shown in the expression above. By using this new flame front velocity for the inhibited case, the ratio $V_{f,n}/V_f$ derived from Kumar and Kumar's [3] data is very similar to 1, with less than a 7% discrepancy.

Once we accepted the relationship $V_{f,n}/V_f \approx 1$, one of our main purposes became to estimate the downward flame spread from the known experimental conditions. For doing this, we derived an upper bound for the downward flame speed $V_{f,d}$ by applying a simple control volume analysis near the free edge of the sample. This analysis is similar to that developed in Bhattacharjee et al. [18] for two dimensional flames except for the introduction of a new term corresponding to the lateral heat flux into the sample from the free edge side. Three simple control volumes have been used, two in the gas phase and one in the solid phase, as shown in Figure 3.9. The solid phase control volume is at T_v and corresponds to the vaporizing part. There is one gas phase control volume on top of the solid one and another gas phase control volume on the lateral side, both at T_f. We assume that the solid in front of the control volume shown in Figure 3.9 is at ambient temperature T_∞. Considering that conduction through the gas phase is the main heat

[3]The de Ris' model assumes an infinite fast reaction kinetics, so the model here developed may lose applicability in fires where the chemical kinetics may be slow, as vitiated fires or fires with high flow velocity.

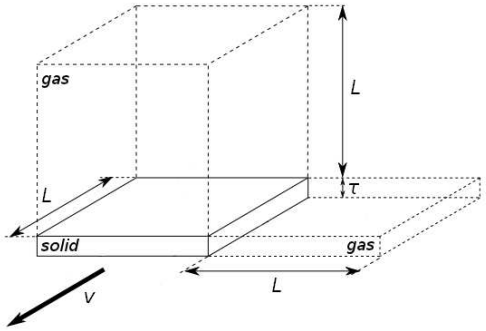

Figure 3.9: Solid and gas phase control volumes at the flame leading edge.

transfer mechanism from the flame to the solid surface, the energy balance equation for the solid phase control volume becomes

$$\rho_s c_s V_{f,d} \frac{(T_v - T_\infty)}{L} L^2(\tau/2) \sim \lambda_g \frac{(T_f - T_v)}{L^2} L^3 + \lambda_g \frac{(T_f - T_v)}{L^2} L^2(\tau/2) \tag{3.1}$$

where, for simplicity, we use $L = \alpha_g / V_g$ as the characteristic size of the control volume in all directions except for that perpendicular into the solid fuel where we use the solid half-thickness $(\tau/2)$ (the solid is thermally thin). In the definition of L, α_g is the gas phase diffusivity at room conditions, and V_g is the induced flow velocity. The flame temperature T_f is calculated using the equation

$$T_f = T_\infty + \frac{H_{com} Y_{o,a}}{f c_s} \left[1 - \frac{B_c H_{vap}}{H_{com} \ln(1 + B_c)} \right], \tag{3.2}$$

where the heat of reaction is $H_{com} = 1.67 \cdot 10^7$ J kg^{-1}, the latent heat of vaporization is $H_{vap} = 7.5 \cdot 10^5$ J kg^{-1}, $f = 1.185$ is the air to fuel mass ratio and the mass transfer number B_c is calculated as $B_c = \frac{Y_{o,a} H_{com}}{f H_{vap}} - c_g \frac{(T_v - T_\infty)}{H_{vap}}$ (values extracted from Greenberg and Ronney [14]), where $Y_{o,a}$ is the oxygen mass fraction at ambient conditions. The value used for temperature of vaporization, $T_v = 620$ K, is extracted from our thermogravimetric analysis, and it is consistent with other values found in literature [18]. In comparison with the analysis carried out by Bhattacharjee et al. [18], we add here the last term in Equation (3.1) that corresponds to the heat flux from the lateral flame into the solid at the free edge side. By rearranging terms in Equation (3.1), we found

$$V_{f,d} / V_f \sim 1 + \frac{(\tau/2)}{L}, \tag{3.3}$$

where $V_f \sim \lambda_g / (\rho_s c_s (\tau/2)) (T_f - T_v) / (T_v - T_\infty)$ follows de Ris' [27] expression for a two-dimensional downward flame front velocity of a thin fuel. The estimated values

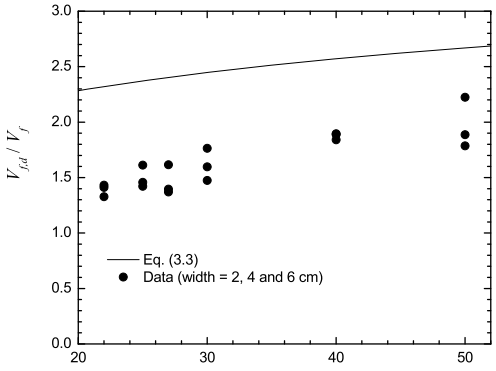

Figure 3.10: Ratio of the downward flame spread rate $V_{f,d}$ in the free edge and the flame front speed V_f when both edges are inhibited as a function of the oxygen concentration for samples with 0.0933 mm half-thickness. The solid line corresponds to the estimation provided by Eq. (3.3).

provided by Equation (3.3) may be seen as upper bounds for the actual $V_{f,d}/V_f$ figures, since we neglect energy losses in the process.

Figure 3.10 shows the prediction $V_{f,d}/V_f$ from Equation (3.2) as a function of the oxygen mixture concentration in comparison with the values obtained from our experiments for the $(\tau/2) = 0.0933$ mm cases. Here $V_{f,d}$ and V_f correspond to our measured data for both the free edge and the fully inhibited cases, respectively. Note that L in Equation (3.3) is a function of the oxygen level X_{O_2} through the induced flow velocity V_g. An increase in the oxygen concentration will lead to an increase in the flame temperature T_f, and, therefore, in the buoyant induced flux V_g, which, from Frey and T'Ien [1], satisfies $V_g \sim [\alpha_g (T_f - T_\infty)/T_\infty]^{1/3}$. Results from Equation (3.3) assume a value of $V_g = 0.3$ m s^{-1} for an oxygen mass fraction $Y_{O_2} = 0.23$ [41], with other V_g values in agreement with $V_g \sim [\alpha_g (T_f - T_\infty)/T_\infty]^{1/3}$, where T_f is the adiabatic flame temperature that depends on X_{O_2} [see Eq. (3.2)].

3.1.5 Conclusions

We have carried out experiments of the downward burning of thin solid fuels with and without a free edge and also varying the width and thickness of the sample and the oxygen molar fraction X_{O_2} in an O_2-N_2 atmosphere at 10^5 Pa. The results we obtained show that the extinction limit that arises when we reduce the width of the sample is attained at lower values of X_{O_2} for the free edge case in comparison with the fully inhibited one. The flame spread rate of samples with a free edge is greater than in samples without free edges due to the increase of oxygen supply along the free edge.

The variation of atmospheric composition for the free edge cases not only caused an

increase in the velocity of the flame front but also an increase of the inclination of the front with respect to the horizontal. This implies that the same increase of X_{O_2} has a greater effect in the downward spread rate for free edge samples than in inhibited ones.

Indeed, although the variation of the X_{O_2} affects the angle of the flame front in the free edge case, our results showed that the velocity normal to the flame front appeared very similar for samples with one or none free edges for all of our experiments with half-thickness $(\tau/2) = 0.0933$ mm. This was not totally satisfied with thicker samples, although we suspect that such a discrepancy may arise from the fact that thicker fuels were obtained by adding sheets of $(\tau/2) = 0.0933$ mm, which may separate during the burning process, especially in the free edge case.

We did perform studies with samples with both inhibited edges employing holders of different thermal conductivity. The results showed that lateral heat losses through the holders are of minor importance. This was also confirmed when having a lateral blockage close to the free edge, which clarified that the main effect of inhibiting an edge is the oxygen shortage that it produces, being more important than the increase in the heat losses to the lateral holders. In addition, a simple control volume analysis gave us a reasonable estimate for the downward flame speed along the free edge in terms of the oxygen level concentration.

Acknowledgements

B.C. acknowledges the support of a FPU program grant. J. Vicens and S. Saus provided very helpful technical assistance. P. Bertran and E. Vives obtained some of the experimental data. This work has been partially funded by the Generalitat de Catalunya under grant 2009-SGR-374, the MICINN-FEDER under grant FIS-2009-13050, and the European Commission under grant NEST-28192-FEPRE.

3.2 Energy Balance Models of Downward Combustion of Parallel Thin Solid Fuels and Comparison to Experiments

This section is a transcription of the contents of the following paper (a copy of the published version can be found in Appendix A):

B. Comas and T. Pujol. Energy balance models of downward combustion of parallel thin solid fuels and comparison to experiments. *Combustion Science and Technology*, 185: 1820–1837, 2013.

Abstract

We analyse the flame front speed in the downward combustion of multiple parallel samples of thermally thin fuels at normal gravity and far from extinction conditions. In contrast with the single sample case, where conduction through the gas phase is the dominant heat transfer mechanism, in the multiple parallel samples case, radiative heat fluxes may become very relevant, which compromises the application of the well-known formula of de Ris for determining the burning rate. Here we study the downward combustion of multiple parallel sheets by (1) obtaining new experimental data at different oxygen atmospheric levels; (2) generalizing a previous comprehensive energy balance model now expected to be valid for a wide range of scenarios; and (3) deriving an analytical approximation for the burning rate that generalizes the classical de Ris formula for those cases where radiative effects cannot be neglected. The comparison with own as well as with external data reveals the strengths and weaknesses of these types of models.

3.2.1 Introduction

In a recent work that studied the downward combustion over thin solid fuels, Bhattacharjee et al. [46] have derived new expressions for describing the main flame geometrical parameters in terms of both gas and solid properties. Here we use these expressions for generalizing a comprehensive energy balance model of the downward combustion in multiple parallel samples. For a single sample, the downward flame front speed in the thermal regime of a thin solid fuel follows the well-known de Ris's expression [27]:

$$V_{f,deRis} = \frac{\pi}{4} \frac{\lambda_g \left(T_{f,ad} - T_v\right)}{(\tau/2)\, c_s \rho_s \left(T_v - T_\infty\right)} \tag{3.4}$$

where the $\pi/4$ term has been included after the exact solution derived by Delichatsions [31] (see the Nomenclature for the description of the variables and parameters).

Equation (3.4) assumes that conduction through the gas phase is the main contribution for preheating the virgin solid ahead of the pyrolysis zone. The excellent agreement of the values predicted by Eq. (3.4) with a wide variety of experimental data (see, e.g., [33]) corroborates that conduction through the solid phase as well as radiative heat fluxes are of secondary importance when burning thin solid fuels far from the extinction limits.

This contrasts with the radiative regime found in the microgravity environment where natural convection as well as conduction through the gas phase are obviously suppressed. In this case, the flame spread rate strongly depends on radiative effects [18]. At normal gravity and far from the extinction, radiation may also play a major role when multiple samples are burned simultaneously and radiative heat fluxes emitted from neighbour high temperature flames may not be neglected. A strong re-radiation effect also arises in many real fires caused by the combustion of nearby solids. This has led to studies of fire propagation at several scales, ranging from bench- to full-scale fire tests. One of the intermediate-scale fire tests consists of two parallel samples with a gas burner at the surface [47, 48]. This parallel panel configuration has been recently employed as a tool for predicting costly full-scale fire tests (e.g., [49]). In the parallel panel test, samples are burned upward in order to reproduce the most hazardous configuration, and many efforts have been devoted to properly simulate such an upward flame spread (see, e.g., [50]). In solid fuels ignited at the top, however, flames propagate downward, and the flame front speed is substantially lower than that predicted for an upward burning configuration. Therefore, it is important to predict the downward flame spread as accurately as possible.

For an array of cellulosic-type samples, Kurosaki et al. [51] and Itoh and Kurosaki [52] developed a model for the propagation speed of the flame front V_f with a simplified expression for both convective and radiative heat fluxes. Although it correctly predicted the behaviour of experimental data, Kurosaki and Itoh's models rely on many values extracted from their own data such as flame temperature, height, and length. This compromised the validity of the model when it is used for predicting other scenarios.

The main motivation for conducting the present study was to generalize the comprehensive model of the downward burning of several parallel samples of Itoh and Kurosaki [52] in order to be fully predictive. This is expected to be accomplished by employing the recent parametrizations of the flame geometry derived by Bhattacharjee et al. [46]. We also propose an approximation to our simple model in terms of a simple analytical expression for the flame front speed that generalizes Eq. (3.4) by including radiative fluxes and interaction with multiple samples. The predictions of our models are compared with experimental data.

3.2.2 Experimental Set-up

Very few experimental works have been devoted to study the downward burning rate of multiple parallel cellulosic-type samples. Emmons and Shen [35] analysed the horizontal burning of an array of vertical paper strips. Kim et al. [53] obtained the flame spread rate between two parallel fuel surfaces using methanol-soaked slabs as a test fuel. Kurosaki et al. [51] measured the downward flame front speed when two parallel papers were burned at different separation distances at ambient conditions. This work was generalized by Itoh and Kurosaki [52] by burning several papers simultaneously (up to 10) at ambient conditions, whereas micro- and normal gravity studies at low atmospheric pressure of downward combustion of two parallel thermally thin solid fuels were carried out by Urban et al. [54]. Here we obtain new data in the downward burning of parallel thin solid fuels at different oxygen concentration levels.

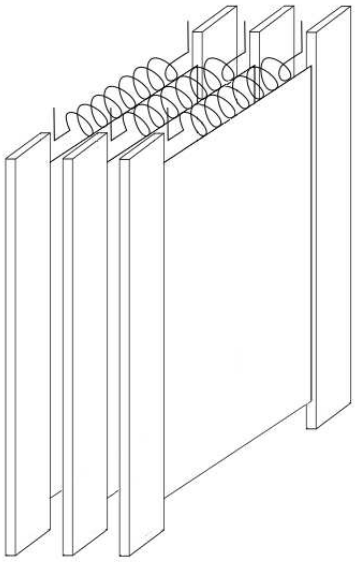

Figure 3.11: Schematic view of the experimental setup for an array of three papers equally spaced, with a view of the coiled nichrome wires used to ignite them at the same time.

Our experiments were carried out in a combustion chamber used in our previous research [55, 56]. Fuel samples consisted of cellulosic papers of thickness 0.187 mm, width 4 cm, and length 16 cm, which were long enough to ensure a stationary spread rate but short enough to ensure that oxygen depletion within the chamber was less than 2%. Lateral effects due to holders were almost negligible since the flame spread rate was very similar for samples 4 cm wide and 6 cm wide [56]. Properties of our paper samples are conductivity $\lambda_s = 0.101$ W m^{-1}K^{-1}, density $\rho_s = 461.95$ kg m^{-3}, specific heat $c_s = 1180$ J kg^{-1}K^{-1} (all at 20 ^{o}C), and vaporization temperature $T_v = 620$ K.

Before a test, papers were heated for 2 hours in an oven at 105 ^{o}C and 24 h in a desiccator. Sheets of paper were held vertically by aluminium plates 2 mm wide located at fixed distances by spacers. Vacuum was made inside the chamber, and then it was filled with a mixture of N_2 and O_2 at the desired proportion with a final pressure of 10^5 Pa. Gases were mixed with a fan for 2 min. Then, the system rested for 3 min to ensure a correct mixture with no remaining currents inside the chamber as it was confirmed in previous studies. A coiled nichrome wire placed at the top of each paper ignited them all at the same time. Simultaneity was ensured by using a small amount of nitrocellulose between the sample and the wire. In Figure 3.11, we can see an schema of an array of parallel papers.

Experiments were recorded with a high definition camera as in [52]. The analysis clearly showed the flame front, whose location was obtained from a ruler marked in the

Figure 3.12: Image of one experiment. Case $N = 2$, $X_{O_2} = 30\%$, and $C = 28$ mm.

edge of the aluminium plate. The spread rate corresponds to the slope of the distance vs. time location of the flame front during a steady propagation. The behaviour of the flame spread rate was the same as that observed or modelled in other studies [51, 52, 54]. A typical image from the experiments can be seen in Figure 3.12. Note that for experiments with multiple sheets of paper (i.e., $N > 1$), the camera was placed in the plane of one of the papers in order to assure the alignment of the marks in the holder with the position of the flame front behind it. We did not take into consideration experiments of parallel samples that showed delayed flame fronts due to a non-simultaneity of the burning at the ignition time.

3.2.3 Models

Kurosaki et al. (K) Model

Kurosaki et al. [51] developed a one-dimensional steady flame model (coordinate system attached to the flame front) for obtaining the downward flame spread rate when burning two parallel sheets of paper. Sheets are considered thermally thin, and the physical properties of the unburned paper are considered constant. With all these assumptions, the energy balance of an element of the preheated zone of one paper is

$$\lambda_s \frac{d^2 T_s}{dx^2} + \rho_s c_s V_f \frac{dT_s}{dx} + \frac{1}{\tau}\left(q_c + q_r\right) = 0 \tag{3.5}$$

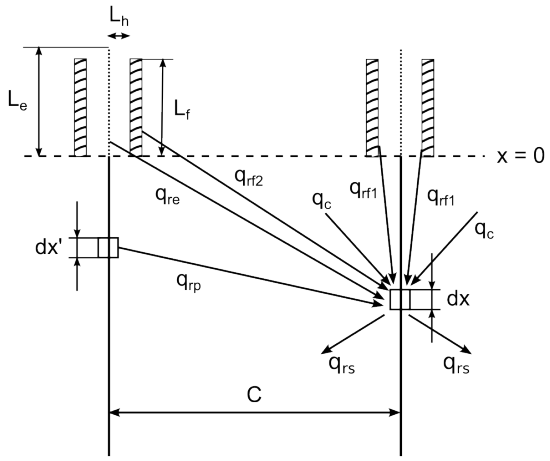

Figure 3.13: Heat fluxes received on an element of the preheated zone of the paper (as in [51], and [52]). See text for details.

where x is the coordinate parallel to the surface, being positive pointing downward (direction of propagation) and with the pyrolysis zone starting at $x = 0$. Note that the equation of propagation exclusively depends on the coordinate of the direction of propagation x since the heat fluxes are expressed as a function of x only. The dependence on the other two coordinates is parametrized in the calculation of the radiative heat transfer rates by using separation distances from paper to flame, from paper to other paper C and the width of the samples w (see Figure 3.13). The solution of Eq. (3.5) with the boundary conditions $T_s = T_v$ at $x = 0$ and $T_s = T_\infty$ at $x = \infty$, the assumption of constant temperature in the pyrolysis zone, and the condition that the temperature profile must be continuous and derivable at $x = 0$ leads to the temperature profile of the preheated zone,

$$T_s(x) = T_v - \frac{1}{\rho_s c_s \tau V_f} \int_0^x \left[1 - e^{V_f(x-\xi)/\alpha_s}\right] q(\xi)\, d\xi \tag{3.6}$$

where $\alpha_s = \lambda_s (\rho_s c_s)$ is the sample thermal diffusivity. Eq. (3.6) for $x = \infty$ allows us to derive an expression for the flame spread rate,

$$V_f = \frac{Q_f}{\rho_s c_s \tau (T_v - T_\infty)} \tag{3.7}$$

where Q_t is the total heat transfer rate per unit width.

Convective q_c and radiative q_r heat fluxes are calculated for two sheets assuming that

emitting surfaces in Figure 3.13 behave as gray bodies, being

$$q_c = \lambda_g \frac{\partial T_g}{\partial y} \mid_{y=0} \tag{3.8}$$

$$q_{rf1} = a\epsilon_f \sigma T_f^4 F_{f1\to dx}, \qquad q_{rf2} = a\epsilon_f \sigma T_f^4 F_{f2\to dx} \tag{3.9}$$

$$q_{rs} = \epsilon_s \sigma \left(T_s^4 - T_\infty^4\right), \qquad q_{rp} \int_0^\infty a\epsilon_s \sigma T_s^4 F_{dx'\to dx} \tag{3.10}$$

$$q_{re} = a\epsilon_e \sigma T_e^4 F_{e\to dx} \tag{3.11}$$

with q_{rf1} and q_{rf2} the radiative heat fluxes received from the flame itself and nearby flames, respectively; q_{rs} and q_{rp} the radiative heat fluxes emitted [negative contribution in Eq. (3.7)] and received from the local and the nearby paper, respectively; and q_{re} the radiative heat flux received from the nearby ember. Thus, for the two parallel sample problems, $Q_t \equiv \int_0^\infty (2q_c + 2q_{rf1} + 2q_{rs} + q_{rf2} + q_{re} + q_{rp})\, dx$ (see Figure 3.13).

Kurosaki et al. [51] assume that $q_c = be^{-x/\delta}$, with constants b ($= 5 \times 10^4$ W m^{-2}) and δ ($= 1250$ m^{-1} fitted to reproduce measured data. Radiative heat fluxes use constant flame height L_h ($= 0.15$ cm), flame length L_f ($= 1.5$ cm), and ember length L_e ($= 1.2$ cm) for calculating the view factors F in Eqs. (3.9), (3.10), and (3.11). The flame temperature T_f ($= 1300$ K) is set as the mean temperature of the flame region, whereas the flame emssivity $\epsilon_f = 0.05$, the ember emissivity $\epsilon_e = 0.85$, and the emissivity ϵ_s of the virgin paper and its absorptivity a with $\epsilon_s = a = 0.92$ were taken from previous works. The model also assumes a separation of 0.2 cm along the x direction between the edge of the flame front and the edge of the ember zone.

Itoh and Kurosaki (I) Model

Itoh and Kurosaki [52] extended the previous model to multiple ($N > 2$) parallel sheets of paper by assuming that the total heat transfer rate per unit width for all papers is

$$Q_{tN} = (Q_r)_{i=1} + (Q_r)_{i=N} + 2\sum_{i=2}^{N-1} (Q_r)_i + 2\sum_{i=1}^{N} \left[(Q_c)_i + (Q_{rf1})_i + (Q_{rs})_i\right] \tag{3.12}$$

where $Q_r = Q_{rf2} + Q_{rp} + Q_{re}$ with $Q_i = \int_0^\infty q_i dx$ for $i = c$, $rf1$, $rf2$, re, rp, and rs.

Since the experiments showed that, after a transient phase, the downward spread rate became stationary and equal for all sheets, Itoh and Kurosaki [52] assumed the same heat transfer rate for each sample, this being calculated as

$$Q_t = \frac{Q_{tN}}{N} = 2\left(Q_c + Q_{rf1} - Q_{rs}\right) + 2\frac{N-1}{N}\left(Q_{rf2} + Q_{re} + Q_{rp}\right) \tag{3.13}$$

which, substituted into Eq. (3.7), allows us to calculate the flame front speed V_f.

In addition, Itoh and Kurosaki [52] expressed both flame L_f and ember L_e lengths as a function of the flame front speed, $L_e = V_f/K$ and $L_f = AL_e$, with A ($= 0.9$) and K ($= 0.04$ s^{-1}) experimental constants.

Generalized Itoh and Kurosaki (I-G) Model

Here we generalize the previous model in order to be totally predictive, thus being only dependent on the physical properties of the samples and on the ambient conditions.

We assume that the relevant length scale where the convective heat flux q_c is important corresponds to $\delta_g \equiv \alpha_g / (V_g + V_f)$, as it was determined in [18]. Therefore, we state that $\delta = \delta_g$ in the exponential shape for the convective flux $q_c = be^{-x/\delta}$. On the other hand, we assume that Eq. (3.7) for the one sheet case neglecting radiation must reduce to the de Ris velocity Eq. (3.4) since it is accepted to be valid for the thermal regime. With this condition, the coefficient b of the exponential expression for the convective flux reads

$$b = \frac{\pi}{4} \frac{\lambda_g}{\delta_g} (T_{f,ad} - T_v) \tag{3.14}$$

The adiabatic flame temperature used in Eq. (3.14) follows [14],

$$T_{f,ad} = T_\infty + \left(1 - \frac{1}{1 + Y_{O2}/r}\right) \left[T_v - T_\infty + \frac{1}{c_g} (H_{com} - H_{vap})\right] \tag{3.15}$$

Note also that $T_{f,ad}$ differs from the flame temperature T_f employed in the calculation of the radiative fluxes, the latter being the mean temperature calculated using the one-dimensional vertical model of a diffusion flame described in [14]. In Eq. (3.15), we use the mass fraction of oxygen at ambient conditions,Y_{O2}; the stoichiometric oxidizer to fuel mass ratio, r; the gas specific heat, c_g; the latent heat of vaporization, H_{vap}; and the heat of combustion, H_{com}. The gas specific heat c_g in Eq. (3.15) is evaluated at the mean temperature $(T_{f,ad} + T_\infty)/2$ [14].

The opposed flow gas velocity V_g is assumed to vary accordingly to the expression [1] $V_g / V_{g,ref} = [\alpha_g (T_{f,ad} - T_\infty)]^{1/3} / [\alpha_{g,ref} (T_{f,ad,ref} - T_\infty)]^{1/3}$, where the reference values correspond to those at $X_{O_2} = 21\%$ with $V_{g,ref} = 0.3$ m s^{-1}.

On the other hand, flame L_f, ember L_e, and separation from flame to paper L_h lengths are calculated using Bhattacharjee et al. [46] work:

$$L_h = \frac{1}{10} r \frac{\rho_s}{\rho_g} \frac{\tau}{Y_{O2}} \frac{V_f}{V_f + V_g} \tag{3.16}$$

$$L_f = 0.0345 \cdot 5 L_h^2 \frac{V_f + V_g}{\alpha_g} \tag{3.17}$$

and assuming that the relationship between ember and flame lengths is $L_e \approx L_f / 0.9$ [52]. Unless otherwise stated, gas transport coefficient values are evaluated at the vaporization temperature [46].

We point out that Bhattacharjee et al. [46] obtain Eqs. (3.16) and (3.17) after correlating data for single sheet cases. We assume here that these expressions are still valid for multiple sheets of paper when the separation distance C is reasonably large. Indeed, experimental values for the burning of two parallel sheets of paper revealed that the flame structure is essentially the same as for a single sample case when C is above a given value C_l (e.g., $C_l \approx 10$ mm for $X_{O_2} = 21\%$ and two parallel samples [51]).

Since δ, b, L_h, L_f, and L_e depend on the flame spread rate V_f and these terms are needed in order to compute the total heat transfer rate Q_t, an iterative method of solution has to be used. On the first iteration, an initial value for lengths is assumed ($L_f = 15$ mm, $L_e = 12$ mm, and $L_h = 2$ mm), and q_{rp} and q_{rs} are set to 0. The flame spread rate V_f and the temperature profile $T_s(x)$ are calculated, and then all the parameters and expressions are varied accordingly to these new values. This is done iteratively until V_f converges within a prescribed value ($< 0.1\%$ difference).

Analytical (A) Model

The generalization of Itoh and Kurosaki's model in the previous subsubsection still requires an iterative process for obtaining the flame front speed. Here, we derive an analytical approximation to the flame spread rate with the aim of generalizing Eq. (3.4) by including radiative effects in the burning of multiple parallel samples. The model is essentially the same as that shown in Figure 3.13 except with the unburned paper region assumed to have a constant temperature T_∞. This substantially simplifies the expressions for the radiative fluxes, and a simple energy balance similar to that developed in [18] leads to

$$V_f = V_{f,deRis}\left[1 + \frac{q_{rf1}}{q_c v} + \frac{2\,(N-1)}{N}\frac{(q_{rf2}+q_{re})}{q_{cv}}\right] \tag{3.18}$$

where $q_{cv} = \pi\lambda_g\,(T_{f,ad} - T_v)\,/\,(4\delta_g)$, $q_{rf1} = a\epsilon_f\sigma T_f^4 F_{f1\to 1}$, $q_{rf2} = a\epsilon_f\sigma T_f^4 F_{f2\to 1}$, and $q_{re} = a\epsilon_e\sigma T_e^4 F_{e\to 1}$. Here, $F_{S\to 1}$ corresponds to the view factor of finite area S (local flame $f1$, nearby flame $f2$ and nearby ember e) to finite area 1 (paper at uniform temperature T_∞; see Appendix). In contrast with the previous subsubsection, values of the parameters δ_g, L_h, L_f, and L_e needed in q_{cv}, q_{rf1}, q_{rf2}, and q_{re} have been evaluated at $V_{f,deRis}$ instead of at V_f. This makes Eq. (3.18) fully explicit. Note that in Eq. (3.18) we have neglected the contribution of the q_{rp} term due to its small relevance in the total heat transfer rate as noted in [51]. We point out that Eq. (3.18) reduces to Eq. (3.4) for the non radiative case or for scenarios where conduction through the gas phase q_{cv} is the dominant effect.

3.2.4 Results

One Sample

Figure 3.14 shows the results for a downward burning of one sample at different ambient oxygen molar fractions X_{O_2}. In comparison with data, de Ris expression Eq. (3.4) overestimates the flame speed at low–moderate values of X_{O_2}, whereas it underestimates it at high X_{O_2} values where radiation, due to high energy flames, may play an important role. The analytical model (A model in Figure 3.14), which generalizes the de Ris expression by including radiation, predicts higher values of the spread rate due to the positive contribution of the radiative terms in Eq. (3.18), as already expected. This analytical model matches the data at $X_{O_2} = 50\%$ but fails to reproduce the observed behavior at greater atmospheric concentrations, underestimating by 19% the flame front speed at $X_{O_2} = 100\%$. The generalized model gives slightly greater values of V_f than the

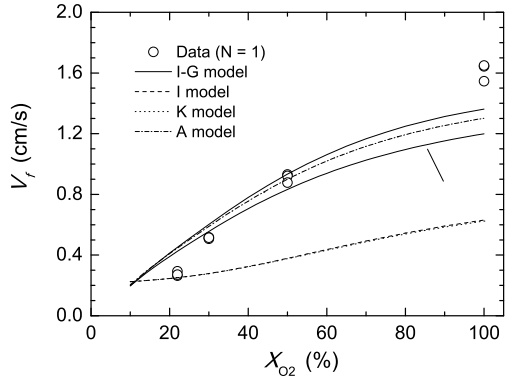

Figure 3.14: Downward burning rate V_f as a function of the oxygen molar fraction X_{O_2} for a single sheet. Our experimental data is compared with the Kurosaki et al. model (K model) [51], Itoh and Kurosaki model (I model) [52], our generalization of Itoh and Kurosaki model (I-G model), and an analytical model (A model). Values of Eq. (3.4) are also shown (de Ris).

analytical model, but not higher enough to correctly report the measured data at high X_{O_2}. In comparison with de Ris Eq.(3.4), and for a single sheet, the differences with the generalized (I-G) model arise from the radiative flux from the flame (q_{rf1}) and the radiative losses from the paper (q_{rs}). This radiative correction may lead to a negative value for losses higher than the gain from the flame. However, this is not observed in our model due to the assumed flame shape. In our model, the flame is a rectangle parallel to the paper, separated from it by a length L_h (see Figure 3.13). This provides a view factor of the flame to a differential element of the preheated zone of the paper greater than it would be if a more realistic shape was assumed, which overestimates q_{rf1}. Note also that the q_{rf1} value predicted by the I-G model is greater than the value obtained from the A model since it applies the V_f value instead of the $V_{f,deRis}$ for determining the geometrical flame parameters.

In contrast, Kurosaki et al. [51] and Itoh and Kurosaki [52] models clearly underestimate the experimental observations at moderate–high values of X_{O_2}, only correctly predicting the flame spread rate at environmental values $X_{O_2} = 21\%$, which correspond to the conditions that they were developed. Both K and I models shown in Figure 3.14 adopt a variable value of the flame temperature T_f as a function of X_{O_2}, being the same as that employed in A and I-G models.

Two Parallel Samples

For two parallel sheets of paper with a separation distance $C = 25$ mm and burning at different X_{O_2}, Figure 3.15 reveals that I and K models behave better than the generalized version at low X_{O_2}. At the maximum X_{O_2} value, the I-G model underestimates V_f by

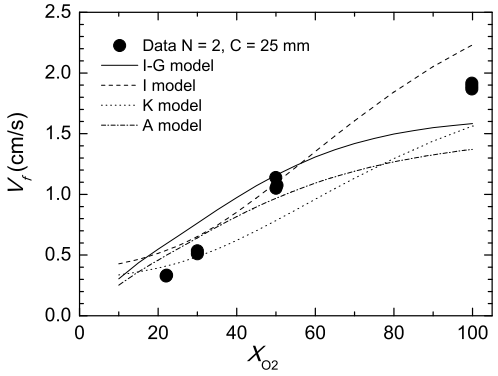

Figure 3.15: As in Figure 3.14 but for a two parallel sheets case with a separation distance $C = 25$ mm.

16%, being similar to the result from the K model, whereas the I model overestimates it by a 18%. In comparison with the flame front speed obtained for the one sample case, the generalized model correctly predicts the observed change ΔV_f, thus indicating a successful simulation of the effect of the nearby radiative fluxes. This is not accomplished when fixing L_f, L_e, and L_h values (K model) or L_f and L_e values directly proportional to V_f (I model), since very high discrepancies in comparison with data are obtained.

Radiative heat fluxes from the local flame q_{rf1} and the nearby flame q_{rf2} highly depend on the flame temperature T_f. As explained above, T_f is obtained by averaging the vertical temperature profile in a one-dimensional vertical diffusion flame model that reaches a maximum temperature $T_{f,ad}$ at the flame height. By applying this procedure, $T_f/T_{f,ad}$ ranges from $T_f/T_{f,ad} = 0.54$ at $X_{O_2} = 20\%$ to $T_f/T_{f,ad} = 0.43$ at $X_{O_2} = 100\%$. Figure 3.16 shows the results of the flame front speed for two parallel samples separated $C = 25$ mm with the generalized I-G model as a function of (a) oxygen molar fraction X_{O_2} and (b) T_f while keeping the $T_{f,ad}$ value calculated with Eq. (3.15). At moderate–low levels of X_{O_2}, the burning spread rate V_f is almost independent of the flame temperature, thus indicating that radiation plays a minor role. However, at larger values of X_{O_2}, we observe a strong dependence of V_f on T_f since radiative fluxes are becoming important. In comparison with data, a better behavior of the I-G model would be obtained by deriving T_f values from $T_{f,ad}$ with a different $T_f/T_{f,ad}$ ratio than that provided by the one-dimensional vertical diffusion model of [14].

In Figure 3.17 we can see the downward spread rate of flames for the two parallel papers case at $X_{O_2} = 30\%$ depending on the separation distance C predicted by the K model, the I model, and our generalization (I-G model). We also include the analytical A model, and the results obtained with the I-G model when using a characteristic length $\delta = 4\delta_g$ and a height of the flame L_h 1.5 times that obtained in Eq. (3.16). These figures are chosen in order to produce values of b, δ, L_f, and L_h at $X_{O_2} = 21\%$ very similar to those adopted in [51]. The latter case correctly reproduces our measured data,

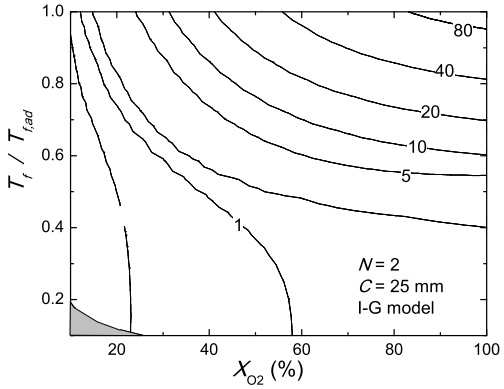

Figure 3.16: Downward burning rate V_f contours (cm/s) as a function of the ratio between the flame temperature T_f and the adiabatic flame temperature $T_{f,ad}$, and of the oxygen molar fraction X_{O_2}. Nonpropagation is predicted in the gray region. See text for details.

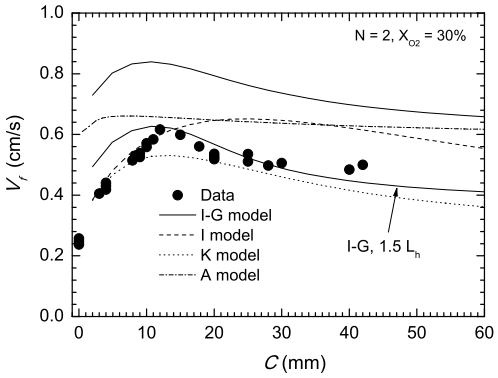

Figure 3.17: Downward burning rate V_f as a function of the separation distance C between two parallel sheets at $X_{\mathrm{O}_2} = 30\%$ for the models described in Figure 3.14 and including a modified I-G model (see text).

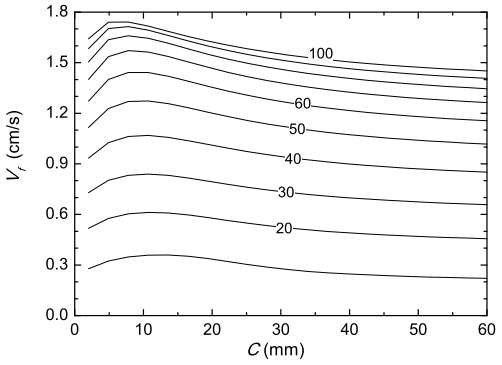

Figure 3.18: As in Figure 3.17 but for the I-G model only and at different oxygen molar fractions (in %).

with a peak at $C \approx 14$ mm. Data show a maximum in the spread rate at $C = 12$ mm ($V_f = 0.62$ cm s^{-1}), which is 24% higher than the velocity at $C = \infty$ ($V_f = 0.50$ cm s^{-1}). The behaviour of the flame as a function of the separation distance C is as follows: when the separation is narrow, there is no flame between the two sheets and the main heat transfer mechanism is convection. Then there is a transition region, where a unstable flame appears between both papers, and later appears a stable flame between them. First it is a united flame and then becomes a separated flame for each paper as the separation becomes wider. This produces the behaviour observed and predicted for the spread rate: a slow downward flame spread rate when the two papers are separated a small distance, an increase as a function of the separation C with a maximum when the flame between them is higher, and finally the downward spread rate approaches asymptotically that for a single flame. In our observations at $X_{O_2} = 30\%$, and in agreement with the behaviour noted in [51] at $X_{O_2} = 21\%$, the region of a stable flame arises at $C > 5$ mm, which is well below the region of separation distances that gives a maximum in the flame front speed ($10 < C < 15$ mm; see Figure 3.17). Note that models tested here are only applicable for C values large enough to ensure that a stable flame exists between papers (i.e., $C > 5$ mm). In those very few cases where the simulation predicts a flame height L_h higher than half the separation distance C between papers, we force L_h to be $C/2$.

In Figure 3.17, the analytical A model does not show an abrupt peak at intermediate values of the separation distance. This may be caused by the simplified expression of the radiation effects that employs a view factor between two finite areas. The generalized I-G model reproduces the behaviour of data, with a maximum velocity at $C = 11$ mm but at a higher value (0.84 cm s^{-1}).

The effect of increasing the oxygen concentration level is shown in Figure 3.18 for the I-G model. The maximum in the flame front speed shifts to lower values of the separation distance C as the oxygen molar fraction X_{O_2} increases. However, at large X_{O_2} values, the region with a stable flame between papers will begin at larger C values than at low

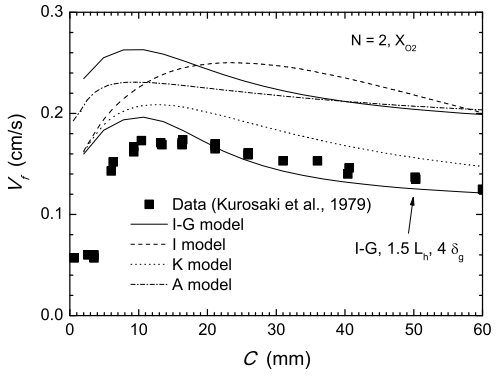

Figure 3.19: As in Figure 3.17 but for cellulosic-type samples as in Kurosaki et al. [51]. See text for details.

X_{O_2}. Thus, at high X_{O_2} conditions, this implies that the maximum in the flame speed will arise just at the point C of formation of a stable flame between papers.

Finally for the two parallel sheet problem, we have also analysed the data obtained in [51]. Samples have the following properties $k_s = 0.577$ W m^{-1}K^{-1}, $\rho_{=}$901 kg m^{-3}, $c_s = 1670$ J kg^{-1}K^{-1}, and $\tau = 0.2$ mm with $T_v = 533$ K and $T_e = 800$ K. The experiment was carried out at $X_{O_2} = 21\%$ and $T_\infty = 298$ K. Results are shown in Figure 3.19 where the generalized I-G model with the modified L_h and δ parameters also performs better than the other models, including the Kurosaki et al. [51] one (K model), that was fitted to reproduce the data.

Multiple ($N > 2$) Samples

We have also simulated the effect of using a high number of samples, and the results of the flame speed as a function of the separation distance C are shown in Figure 3.20 for the $X_{O_2} = 30\%$ case. Experimental data shown in Figure 3.20 have been obtained in our combustion chamber with $C = 15$ mm. For comparison purposes, the I model has been also shown. Note that the solution reaches an asymptotic value as N increases, with the maximum in the burning rate shifted to higher C. As expected, the contribution of more papers increases the total heat available, and therefore the flame front speed V_f also increases. Note that the I model assumes a very strong dependence of V_f as a function of N due to the overestimation of the radiation fluxes previously explained when discussing Figure 3.15.

3.2.5 Conclusions

We have compared several comprehensive energy balance models developed for deriving the downward flame front speed V_f in the burning of parallel thin cellulosic-type samples. In these cases, a model beyond the classical de Ris [27] one is needed since radiation may

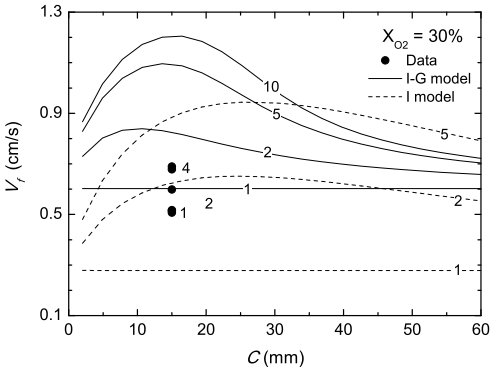

Figure 3.20: Downward burning rate V_f as a function of the separation distance C between two parallel sheets at $X_{O_2} = 30\%$ for different number of parallel samples. Itoh and Kurosaki model (I model) and our generalized model (I-G model) are shown.

play an important role. The Kurosaki et al. [51] model (K model) uses constant values of the main flame geometrical dimensions and flame temperatures. The Itoh and Kurosaki [52] model (I model) assumes flame and ember lengths proportional to V_f. Our generalization of the I model employs the parameterizations of the flame geometrical dimensions of Bhattacharjee et al.[46] and a variable convective flux (I-G model). In addition we derive an analytical expression (A model) that employs a simplified expression for radiative heat fluxes with a constant temperature for the unburned solid.

K and I models show a good performance at ambient conditions ($X_{O_2} = 21\%$) only, since they have several parameters estimated using experimental data. At other X_{O_2} atmospheric levels, these models clearly fail to predict the burning rate of a single and/or of two parallel sample cases. In comparison, our generalized I-G model better predicts the observed behavior for a wider range of X_{O_2} concentration (up to 50%). For very high values of X_{O_2}, however, the I-G model underestimates V_f since the approximation of the flame as a sheet parallel to the surface of the paper may not be appropriate enough, and may produce radiative heat fluxes values lower than the actual ones.

For a fixed (moderate to low) X_{O_2} concentration, the behaviour of the burning rate as a function of the separation distance between parallel papers is very well predicted by our (slightly modified) I-G model when comparing with our experimental data as well as with data obtained by [51] with a different type of solid fuel.

These comprehensive models contrast with the recently developed model of Shih [57] that explicitly includes fluid dynamics and is able to simulate both counter and coflow conditions. However, such a type of model requires costly methods, which limits the number of cases that can be studied.

As we have shown here, energy balance models may capture the essential physics of the problem and correctly reproduce flame front speed data in a wide variety of cases. Therefore, we think that there is still room for this type of modelling as long as they

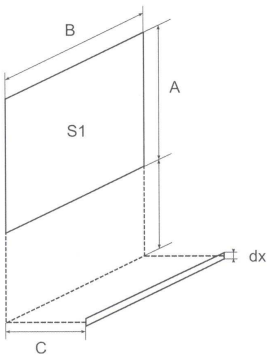

Figure 3.21: View factor of surface $S1$ to a differential strip dx (K, I, and I-G models).

keep their simplicity. Indeed, a simpler model than the one shown here has been used by Bhattacharjee et al. [18] with the purpose of deriving a flammability map in the microgravity regime. For multiple parallel sheets, our results suggest the need of a good calculation of radiative fluxes for better determining the downward flame spread in a wider range of atmospheric oxygen concentration.

Acknowledgements

B.C. acknowledges the support of a FPU grant. Jordi Vicens and Sergi Saus provided very helpful technical assistance. J. Jaggopota obtained some of the experimental data. This work has been partially funded by the Generalitat de Catalunya under grant 2009-SGR-374 and the MICINN-FEDER under grant FIS-2012-31307.

Appendix: view factors

Surface $S1$ to a differential strip dx (Figure 3.21):

$$F_{s1\to dx} = \frac{1}{\pi}\left[\frac{\sqrt{B^2+C^2}}{B}\left(\tan^{-1}\frac{A+x}{\sqrt{B^2+C^2}} - \tan^{-1}\frac{x}{\sqrt{B^2+C^2}}\right)\right.$$
$$-\frac{C}{B}\left(\tan^{-1}\frac{A+x}{C} - \tan^{-1}\frac{x}{C}\right) \qquad (3.19)$$
$$\left.+\frac{A+x}{\sqrt{(A+x)^2+C^2}}\tan^{-1}\frac{B}{\sqrt{(A+x)^2+C^2}} - \frac{x}{\sqrt{x^2+C^2}}\tan^{-1}\frac{B}{\sqrt{x^2+C^2}}\right]$$

Surface $S1$ to surface $S2$ (Figure 3.22):

$$F_{s1\to s2} = \frac{1}{S_1}\sum_{l=1}^{2}\sum_{k=1}^{2}\sum_{j=1}^{2}\sum_{i=1}^{2}(-1)^{i+j+k+l}\,G\left(x_i, y_j, \eta_k, \xi_l\right) \qquad (3.20)$$

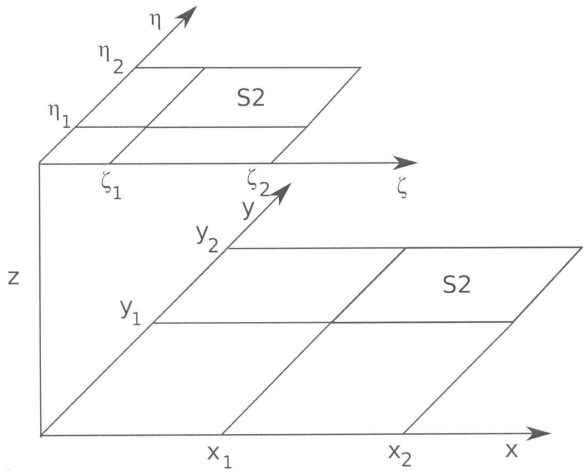

Figure 3.22: View factor of surface $S1$ to a surface $S2$ (A model).

$$
\begin{aligned}
G = & \frac{1}{2\pi}(y-\eta)\left[(x-\xi)^2+z^2\right]^{1/2}\tan^{-1}\left\{\frac{y-\eta}{\left[(x-\xi)^2+z^2\right]^{1/2}}\right\} \\
& + \frac{1}{2\pi}(x-\xi)\left[(y-\eta)^2+z^2\right]^{1/2}\tan^{-1}\left\{\frac{x-\xi}{\left[(y-\eta)^2+z^2\right]^{1/2}}\right\} \\
& - \frac{z^2}{4\pi}\ln\left[(x-\xi)^2+(y-\eta)^2+z^2\right]
\end{aligned}
\tag{3.21}
$$

3.3 Flame front speed and onset of instability in the burning of inclined thin solid fuel samples

This section is a transcription of the contents of the following paper (a copy of the published version can be found in Appendix A).

B. Comas and T. Pujol. Flame front speed and onset of instability in the burning of inclined thin solid fuel samples. *Physical Review E*, 88: 063019, 2013.

Abstract

We focus on the front propagation of diffusive flames obtained from the downward burning of inclined thermally thin solid fuels. This process consists of a pyrolysis reaction in the solid phase and a combustion reaction in the gas phase. The solid phase model is based on two coupled one-dimensional equations of temperature and solid density. We reduce the system into a single one-dimensional equation from which we obtain an analytical expression for the flame front speed. This expression may be understood as an upper bound of the burning spread rate in inclined samples. The gas phase model is based on four coupled two-dimensional equations. These are employed to derive a criterion for determining the critical inclination angle beyond which the flame behaviour becomes unstable. The comparison with the experiments confirms the validity of our predictions.

PACS numbers: 47.70.Pq, 47.70.Fw, 47.20.−k, 82.33.Vx

3.3.1 Introduction

Combustion is an exothermic process of chemically reacting flows that may produce either a premixed or a nonpremixed flame [58]. Premixed flames occur when both fuel and oxidizer are mixed before burning. In laminar flows of flat premixed gaseous flames, several methods applied to the one-dimensional reaction-convection-diffusion equations that correspond to the conservation equations of mass and energy lead to analytical approximations of the flame front speed [59, 60, 61].

On the other hand, diffusion (or, equivalently, nonpremixed) laminar flames arise when the mixing and burning occur simultaneously, like in the downward burning of a cellulosic type sample. In contrast with flat premixed gaseous flames, the combustion of thin solid fuels is, at least, a two-dimensional process, since it involves the mass flux of volatiles at the solid surface and the combustion reaction at the flame height. For such a process, analytical expressions for the speed of the flame front V_f have been obtained after reducing complex two-dimensional reaction-convection-diffusion equations into a single one-dimensional one [5, 56]. Although some of these approximations successfully predict the downward flame speed, they fail to explain the burning spread rate over inclined samples where flame instabilities may arise [62].

In this work, we use the solid phase equations in Subsec. 3.3.3 to derive an analytical expression of the upper bound of the flame spread rate. This expression generalizes previous equations and it is valid for inclined surfaces. In Subsec. 3.3.4 we use the gas phase equations to obtain stationary solutions that allow us to calculate the Nusselt

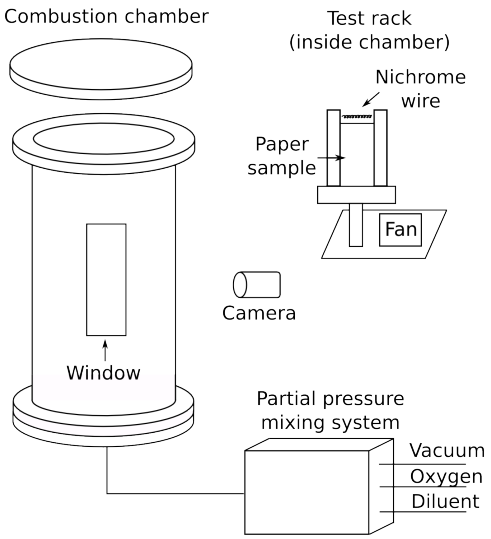

Figure 3.23: Schema of the combustion chamber.

number at first-order approximation (equivalent to assume only the gravity component parallel to the surface) and at second-order approximation (equivalent to assume the gravity component normal to the surface). A given value of the ratio of these Nusselt numbers will provide an instability threshold when comparing with experimental data as shown in Subsec. 3.3.5. Here, our approach differs from Refs. [21, 63] since it is based on the fundamental governing equations.

3.3.2 Experimental setup

The experiments were carried out in a combustion chamber, using a controlled atmosphere of 10^5 Pa with a mixture of O_2 and N_2. Figure 3.23 shows a schematic view of the experimental design. The combustion chamber could be inclined at the angle required for the test.

Cellulosic samples of half-thickness 0.0933 mm and surface density 0.0431 kg m^{-1} were used. The length and width of the samples were 24 $\times$ 4 cm, long enough to ensure steady spread and wide enough to minimize effects of lateral heat losses. More details about the samples and justification of the sizes can be found in Ref. [8].

Samples were dried for 2 h at 100 ^{o}C and stored for a minimum of 24 h before each experiment. Then they were held by aluminium holders, 2 mm thick and 40 mm wide, in the middle of the chamber; the chamber was closed and inclined to the desired angle. A vacuum was created inside the chamber and then it was filled with O_2 and N_2 at the desired concentration. Gases were mixed during three minutes with a fan and then they were left at rest for 2 min. Samples were ignited uniformly at the top with a coiled nichrome wire. Three repetitions with the same sample configuration and atmospheric

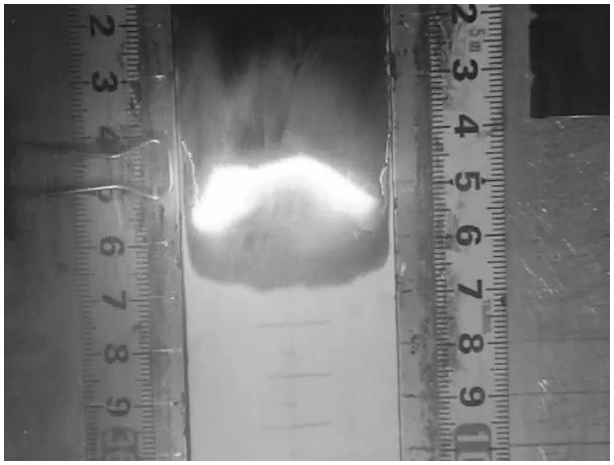

Figure 3.24: Image from one experiment made at 30% of O_2, with an inclination of 70^o respect to the horizontal.

concentration were done.

Every experiment was recorded with a high-definition camera at 50 Hz. Videos were later analysed frame by frame to determine the position of the flame front and the existence (if observed) of an erratic flame behaviour that may cause instabilities and produce a substantial variability of the flame front speed once the experiment is repeated under the same conditions. A typical image of the experiment can be seen in Fig. 3.24. Flame spread velocities were obtained through lineal regression of the front position with respect to time, with a correlation factor of 0.996 or better for all cases.

3.3.3 Flame spread rate

The combustion of a vertical cellulosic-type sample ignited at the top produces a flame front that propagates downwards at a given speed V_f . For thermally thin solids, many authors have proposed analytical expressions for calculating V_f based either on an energy balance of the solid phase [46] or on an energy balance of the gas phase [56]. Here, we generalize the broadly accepted model of de Ris [27] based on the solid phase equations in order to study the flame spread rate of inclined samples. This model assumes unit Lewis number (equal thermal and mass diffusivities) and constant transport coefficients.

The burning process of cellulose consists of two main chemical reactions. The first is the endothermic pyrolysis reaction in the solid phase that releases fuel volatiles. The second is the exothermic combustion reaction in the gas phase (oxygen and fuel volatiles) that produces a diffusive flame. The transfer of heat from the flame to the virgin solid ahead preheats the sample, produces the pyrolysis, and sustains the propagation of the flame front.

The governing equations for the solid phase temperature T_s and solid phase density

ρ_s are

$$c_s\rho_s\frac{dT_s}{dt} = -\nabla\cdot\overrightarrow{J_s} - \frac{d\rho_s}{dt}\left[H_{vap} + (c_s - c_g)\,(T_s - T_\infty)\right] \tag{3.22}$$

$$\frac{d\rho_s}{dt} = -A_s\rho_s e^{-E_s/(RT_s)} \tag{3.23}$$

where c_s and λ_s, used in the conductive heat flux term, are the specific heat and conductivity of the solid, H_{vap} is the heat of vaporization, c_g is the gas specific heat, and T_∞ is the room temperature. The term $\overrightarrow{J_s}$ in Eq. (3.22) includes radiative as well as conductive heat fluxes. In Eq. (3.23), E_s and A_s are the activation energy and the preexponential term of the pyrolysis reaction, respectively, with R the universal gas constant.

By applying the classical analysis of Benguria and collaborators [59] to the set of Eqs. (3.22) and (3.23), Ref. [8] obtained an upper bound of the flame front speed,

$$V_f < V_{f,deRis} - 2\int_0^1 2\sqrt{F\theta_s}d\theta_s \tag{3.24}$$

where

$$F = \frac{\alpha_s T_v A_s\rho_s e^{-E_s/(RT_s)}\left[H_{vap} + (c_s - c_g)\,(T_v - T_\infty)\,\theta_s\right]d}{c_s^2\rho_{s\infty}^2\,(T_v - T_\infty)^2} \tag{3.25}$$

with α_s the solid thermal diffusivity, T_∞ and T_v the room and the vaporization temperatures, respectively, θ_s a dimensionless variable defined as

$$\theta_s = \frac{(T_s - T_\infty)}{(T_v - T_\infty)} \tag{3.26}$$

and d a function of θ_s such as $d = 0$ at $\theta_s = 1$ and $d = 1$ at $\theta_s = 0$.

In Eq. (3.24), the term

$$V_{f,deRis} = \frac{2\lambda_g\,(T_{f,ad} - T_v)}{\tau c_s\rho_{s\infty}\,(T_v - T_\infty)} \tag{3.27}$$

corresponds to the de Ris equation with τ the solid thickness, λ_g the gas phase conductivity and $T_{f,ad}$ the adiabatic flame temperature (excluding a $\pi/4$ multiplying factor that arises after solving the gas phase equations).

Equation (3.24) applies only to the downward combustion of vertical samples. In this configuration, the background convective flow induced by density variations through the flame region opposes the direction of propagation of the flame front. However, as the angle of inclination of the sample increases, the convective flow parallel to the sample decreases in intensity and, therefore, the velocity of the flame front increases. Here, we develop an analytical expression that aims to include this effect.

According to Ref. [64], our model assumes no pyrolysis (constant solid density) ahead of the flame front. Then, in a coordinate system attached to the flame front, Eq. (3.22) applied to the preheated region (negative x') reduces to

$$c_s\rho_s V_f\frac{dT_s}{dx'} = \lambda_s\frac{d^2T_s}{dx'^2} - \frac{\partial J_s}{\partial y}. \tag{3.28}$$

The integration of Eq. (3.28) through the sample thickness (from $y = -\tau$ to $y = 0$) and with the dimensionless variables θ_s (3.26) and $x = x'/L_{gx+}$ with L_{gx+} as the characteristic gas phase thermal length along x (parallel to the solid surface) of the upper side + of the inclined sample leads to

$$\begin{aligned} V_f \frac{d\theta_s}{dx} &= \frac{\alpha_s}{L_{gx+}} \frac{d^2\theta_s}{dx^2} - \\ &- \frac{L_{gx+}}{\tau c_s \rho_s \left(T_v - T_{s\infty}\right)} \left(J_{cv,y=0} - J_{cv,y=-\tau} + J_{rd,y=0} - J_{rd,y=-\tau}\right), \end{aligned} \tag{3.29}$$

where J_{cv} and J_{rd} are the conductive and radiative heat fluxes on the upper $y = 0$ and lower $y = -\tau$ sides of the inclined sample. In Eq. (3.29), we have assumed a uniform temperature across the y direction within the paper sample, which agrees with the thin solid fuel case studied.

The conductive flux in the preheated region is commonly expressed in terms of exponentially decaying functions with a maximum value at the flame leading edge ($x = 0$) [52, 64]. At this point, we assume the adiabatic flame temperature $T_{f,ad}$ as the characteristic gas phase temperature and T_v as the characteristic solid temperature. Therefore, the conductive heat flux at the solid surface at $x = 0$ is equal to $\lambda_g \left(T_{f,ad} - T_v\right)/L_{gy}$ with L_{gy} the characteristic thermal length along y. Thus, the upper $J_{cv,y=0}$ and lower $J_{cv,y=-\tau}$ conductive fluxes in the preheated region are

$$J_{cv,y=0} = -\frac{\lambda_g \left(T_{f,ad} - T_v\right)}{L_{gy+}} e^x, \; J_{cv,y=-\tau} = \frac{\lambda_g \left(T_{f,ad} - T_v\right)}{L_{gy-}} e^{xL_{gx+}/L_{gx-}}, \tag{3.30}$$

where L_{gy+}, L_{gy-} and L_{gx-} are the characteristic gas phase thermal lengths along y or x in the upper + or lower − sides of the inclined sample.

The radiative flux emitted by the flame and absorbed at the virgin solid ahead of the flame front is obtained by using a simplified model in which both flame and paper are constant temperature planes that intersect at the flame leading edge. From the above, the integration of the radiative fluxes from $x = -L/L_{gx+}$ to $x = 0$, where L is the length of the paper, gives

$$\int_{-L/L_{gx+}}^{0} \left(J_{rd,y=0} - J_{rd,y=-\tau}\right) dx = \varepsilon_f a \sigma T_f^4 \left(F_{s-f}^{+} + F_{s-f}^{-}\right) \frac{L}{L_{gx+}} \tag{3.31}$$

where ε_f is the flame emissivity, a is the absorptivity of the paper and T_f is the mean flame temperature. As pointed out in Ref. [52], T_f must be lower than the adiabatic value $T_{f,ad}$ and here is taken as the mean value of the gas phase temperature obtained in the one-dimensional flame model of Ref. [14]. The view factors from the paper plane to the flame plane are

$$F_{s-f}^{+,-} = \frac{1}{2} \left(1 + \frac{L_f}{L} - \sqrt{1 + \frac{L_f^2}{L^2} - 2\frac{L_f}{L^2} \cos \beta^{+,-}} \right) \tag{3.32}$$

with β^+ and β^- the angle between the flame plane and the paper plane in the upper and lower sides of the sample, respectively.

The integration of Eq. (3.29) from $x = -L/L_{gx+}$ to $x = 0$ gives

$$V_{f,g} = \frac{\alpha_s}{L_{gx+}} \left.\frac{d\theta_s}{dx}\right|_{x=0} + \frac{2\alpha_s}{\tau}\frac{\lambda_g\left(T_{f,ad} - T_v\right)}{\lambda_s\left(T_v - T_{s\infty}\right)}\left[\frac{L_{gx+}}{L_{gy+}}\left(1 - e^{-L/L_{gx+}}\right)\right. \\ \left. + \frac{L_{gx-}}{L_{gy-}}\left(1 - e^{-L/L_{gx-}}\right)\right]\frac{\alpha_s}{\tau}\frac{\varepsilon_f a\sigma T_f^4 L}{\lambda_s\left(T_v - T_{s\infty}\right)}\left(F_{s-f}^{+} + F_{s-f}^{-}\right). \tag{3.33}$$

Note that Eq. (3.33) for the case with no radiation and no conduction through the solid phase reduces to the classical de Ris Eq. (3.27) for $L_{gx+} = L_{gx-} = L_{gy+} = L_{gy-}$ and $L = \infty$ as it should. Also note that for our radiative calculation, the temperature of the virgin solid is assumed constant and equal to that for the room. This implies no net radiative losses that would tend to lower the velocity in Eq. (3.33). Therefore, Eq. (3.33) will overestimate the flame front speed and may be understood as an upper bound to the actual value. This is confirmed by comparison with the experiments as we show in Subsec. 3.3.5.

3.3.4 Instability

The momentum and continuity gas phase equations for a steady diffusion laminar flame upon an inclined angle ϕ from the vertical are the starting point of the instability analysis. The classical analysis of these equations ignores the gravity component normal to the surface [53, 65, 66], either by considering only vertical combustion or low-enough inclination angles ϕ. Our analysis aims to find the critical point where instability arises, and since it is located at angles near $\pi/2$, we must maintain the gravity component normal to the surface. This implies a nontrivial equation for the normal momentum that cannot be solved analytically.

In this subsection the flame plane is modelled parallel to the surface of the paper ($\beta^+ = \beta^- = 180^o$ in Eq. (3.32)) in order to use Boussinesq approximation for the density. We note that the flame speed Eq. (3.33) decreases by less than 4% only when varying the β angles from 140^o to 180^o for the 30% oxygen concentration case. We have experimentally seen with the aid of lateral mirrors inside the combustion chamber that the flame plane does not substantially deviate from the surface until the angle is close to the horizontal, where the flame becomes unstable.

Continuity, momentum, and energy equations will be

$$\frac{\partial\left(\rho u\right)}{\partial x} + \frac{\partial\left(\rho v\right)}{\partial y} = 0 \tag{3.34}$$

$$u\frac{\partial u}{\partial x} + v\frac{\partial u}{\partial y} = \nu\frac{\partial^2 u}{\partial y^2} + g cos\phi\frac{\left(\rho_\infty - \rho\right)}{\rho} \tag{3.35}$$

$$u\frac{\partial v}{\partial x} + v\frac{\partial v}{\partial y} = \nu\frac{\partial^2 v}{\partial y^2} + g sin\phi\frac{\left(\rho_\infty - \rho\right)}{\rho} \tag{3.36}$$

$$u\frac{\partial\left(T - T_\infty\right)}{\partial x} + v\frac{\partial\left(T - T_\infty\right)}{\partial y} = \alpha\nabla^2\left(T - T_\infty\right) \tag{3.37}$$

where boundary-layer assumptions have been made [53, 65, 67]. In the above equations we have supposed constant transport properties, unit Lewis number, and velocities much less than the speed of sound. Equations (3.34), (3.35), (3.36), and (3.37) provide the starting point of a natural convection flux. From these equations we can reach the equations in integral form,

$$\nu \left.\frac{\partial^2 u}{\partial y^2}\right]_0^\delta + g cos\phi \left.\frac{\rho_\infty - \rho}{\rho}\right]_0^\delta - g sin\phi \int_0^\delta \frac{\partial}{\partial x}\left(\frac{\rho_\infty - \rho}{\rho}\right) dy = 0 \tag{3.38}$$

$$\frac{\partial}{\partial x}\int_0^\delta u(T - T_\infty)dy - \alpha \left.\frac{\partial (T - T_\infty)}{\partial y}\right]_0^\delta = 0 \tag{3.39}$$

The detailed analysis from Eqs. (3.34), (3.35), and (3.36) to the equations in integral form is not given here for the sake of brevity and may be found in the literature [53, 68]. For a downward (or inclined) spreading flame, the reference frame is defined as traveling at the steady flame spread rate V_f. The boundary conditions of the fluid will be

$$\left.\begin{array}{l} u = V_f \\ \rho = \rho_f \\ T = T_f \end{array}\right\} \quad \text{for} \quad y = 0 \tag{3.40}$$

$$\left.\begin{array}{l} u = V_f \\ T = T_\infty \\ \rho = \rho_\infty \\ \frac{\partial u}{\partial y}, \frac{\partial (T - T_\infty)}{\partial y}, \frac{\partial [(\rho_\infty - \rho)/\rho]}{\partial y} = 0 \end{array}\right\} \quad \text{for} \quad y = \delta \tag{3.41}$$

The assumed velocity profile is similar to the velocity profile obtained in the numerical model of Ref. [11],

$$u = u_1 \frac{y}{\delta}\left(1 - \frac{y}{\delta}\right)^2 + V_f \tag{3.42}$$

where δ is the thickness of the boundary layer. The density profile is normalized from 1 to 0,

$$\frac{(\rho_\infty - \rho)\rho_f}{(\rho_\infty - \rho_f)\rho} = \left(1 - \frac{y}{\delta}\right)^2. \tag{3.43}$$

Setting these profiles in the integral equations (3.38) and (3.39) gives a set of differential equations that in dimensionless form are

$$\frac{6u_1'}{\delta'^2} = \mathrm{PrGr} cos\phi + \frac{1}{3} sin\phi \mathrm{PrGr}\frac{d\delta'}{dx'} \tag{3.44}$$

$$\frac{1}{30}\frac{d}{dx'}\left(u_1'\delta' \mathrm{Gr}\right) = 2\frac{\mathrm{Gr}}{\delta'} \tag{3.45}$$

where the dimensionless quantities are $u_1' = u_1 L/\alpha$, $\delta' = \delta/L$, $x' = x/L$, being L a characteristic length scale. The Grashof and Prandtl numbers are defined as follows:

$$\mathrm{Gr} = g\frac{\rho_\infty - \rho_f}{\rho_{ref}}\frac{L_f^3}{\nu_{ref}^2} \tag{3.46}$$

$$\mathrm{Pr} = \frac{\nu_{ref}}{\alpha_{ref}} \tag{3.47}$$

where the subscript ref means that properties are evaluated at the reference temperature. The set of dimensionless equations (3.44) and (3.45) might be solved for an inclined plate first neglecting the term with $d\delta'/dx$ from both equations. This is equivalent to consider only the gravity component parallel to the surface. This first approximation gives

$$\delta_1' = \left(\frac{480}{\mathrm{PrGr}cos\phi}\right)^{1/4} x'^{1/4} \tag{3.48}$$

$$u_{1,1}' = \left(\frac{40}{3}\right)^{1/2} (\mathrm{PrGr}cos\phi)^{1/2}\, x'^{1/2} \tag{3.49}$$

The Nusselt number is the ratio of the heat transfer convected by the heat transfer conducted. For natural convection, it is a function of Prandtl and Grashof numbers [67]. It may be expressed as $Nu = 2/\delta'$ [53]. Then

$$\mathrm{Nu}_1 = \frac{2}{480^{1/4}} (\mathrm{PrGrcos}\phi)^{1/4} \tag{3.50}$$

Taking into account the gravity component normal to the surface allows us to make a second approximation,

$$\delta_2' = \delta_1' \frac{\left[1 - \frac{1}{6} tan\phi \left(\frac{480}{\mathrm{PrGr}x'}\right)^{1/4}\right]^{1/2}}{1 - \frac{1}{3} tan\phi \left(\frac{480}{\mathrm{PrGr}x'}\right)^{1/4}} \tag{3.51}$$

$$u_{1,2}' = u_{1,1}' + \frac{10^{3/4}}{3^{5/4}} tan\phi \left(\frac{\mathrm{PrGr}cos\phi}{x'}\right)^{1/4} \frac{1 - \frac{1}{6} tan\phi \left(\frac{480}{\mathrm{PrGr}x'}\right)^{1/4}}{\left[1 - \frac{1}{3} tan\phi \left(\frac{480}{\mathrm{PrGr}x'}\right)^{1/4}\right]^2} \tag{3.52}$$

where the second approximation to the Nusselt number gives

$$\mathrm{Nu}_2 = \mathrm{Nu}_1 \frac{1 - \frac{1}{3} tan\phi \left(\frac{480}{\mathrm{PrGr}}\right)^{1/4}}{\left[1 - \frac{1}{6} tan\phi \left(\frac{480}{\mathrm{PrGr}}\right)^{1/4}\right]^{1/2}} \tag{3.53}$$

3.3.5 Results

Figure 3.25 shows the experimental results of the flame spread rate as a function of the angle of inclination of the sample for (a) different values of room oxygen concentration (new data, three repetitions on every environmental conditions) and (b) ambient conditions obtained by Refs. [26] and [69]. In Ref. [62] there was also an experimental analysis of the flame front speed for different angles of inclinations but with an external heating supply. In contrast with the results of Kurosaki and coworkers [26, 69], Kashiwagi and Newman [62] found that there exists a threshold angle of inclination beyond which the instabilities of the flow lead to large variations on the value of the flame front speed. This critical angle reduces as the value of the external heat supplied to the system increases. This effect is not clearly observed at near-ambient conditions without an external heat supply. However, at higher room oxygen concentration X_{O_2} , we do capture an onset of instability (see Fig. 3.25) that arises at lower angles of inclination as X_{O_2} increases.

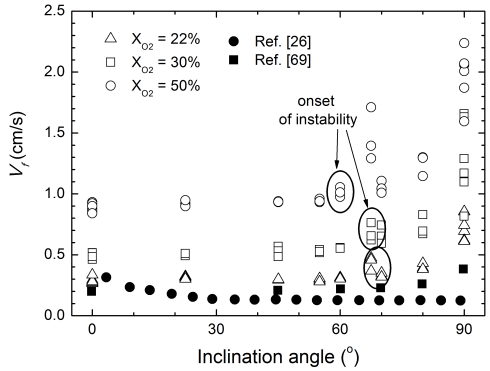

Figure 3.25: Flame spread rate versus angle to vertical of the samples.

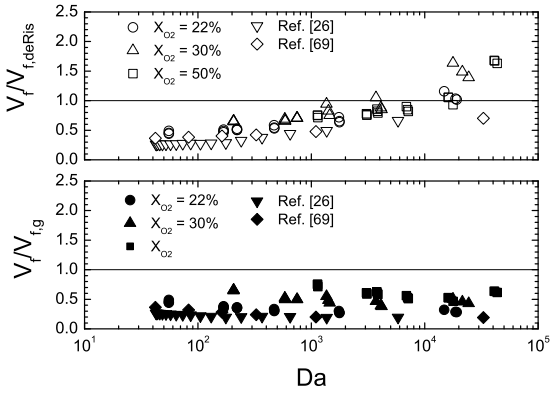

Figure 3.26: Normalized values of flame front speed as a function of Damkohler number.[5]

Note in Fig. 3.25 that the flame spread rate is almost constant for a wide range of angles of inclination until a point where the three repetitions of the experiments produce a variation of 20% or higher between flame spread values.

Although such an instability makes it difficult to reproduce the observed flame spread rate by means of an analytical model, a generalization of the de Ris expression (3.27) in order to predict the trend of data is of great importance, especially at low oxygen concentrations. Figure 3.26 shows the normalized values of the flame front speeds shown in Fig. 3.25 as a function of the Damkohler number Da. In Fig. 3.26, $V_{f,deRis}$ follows Eq. (3.27) and $V_{f,g}$ is obtained from Eq. (3.33) by using the characteristic gas phase thermal lengths as

$$L_{gx+} = \frac{\alpha_g}{V_{acv}\cos\phi + V_f}, \tag{3.54}$$

[5]The x-values of this figure are different from those of the article as we found an error in the Damkohler number calculations. It has no implications in the conclusions of our work.

and $L_{gx-} = L_{gy+} = L_{gy-} = L_{gx+}(\phi = 0^o)$. In Eq. (3.54) α_g is the gas phase thermal diffusivity and V_{acv} is the convective velocity itself, which is calculated as $V_{acv} = [g\alpha(\rho_\infty - \rho_f)/\rho_{ref}]^{1/3}$ (the formula is obtained equating buoyancy and inertia forces [11]). Note that $V_{acv}\cos\phi$ is the component parallel to the sample surface on the upper side. Below, the paper acts as a barrier for the upward convective flow and, for simplicity, we have employed $L_{gx-} = L_{gy+} = L_{gy-} = L_{gx+}(\phi = 0^o)$. The effect of the radiative flux from the flame is taken into account by using a constant value of $\beta^+ = \beta^- = 140^o$, although different values of these angles did not produce significant changes on the burning rate, which confirms the small relevance of radiative fluxes in the flame front propagation within the thermal regime [18]. Conduction through the solid in Eq. (3.33) has been also neglected, since it is not considered of importance in the burning of thin samples [5].

The Damkohler number is the ratio of the residence time for the gas mixture in the flow and the chemical time for the second-order Arrhenius-type reaction [33], being

$$\mathrm{Da} = \frac{\alpha_g}{\rho_g}\frac{Y_F Y_O A_g e^{-E_g/RT_{f,ad}}}{\left(V_{acv}\cos\phi + V_f\right)^2} \tag{3.55}$$

where $A_g (= 3.57\times10^7\ \mathrm{m^3\ kg^{-1}\ s^{-1}})$ is the preexponential factor, E_g $(= 125\times10^5\ \mathrm{J\ mol^{-1}})$ is the activation energy and Y_O and Y_F are the room oxygen and fuel mass fractions, respectively. Following [33], the fuel mass fraction follows $Y_F = \mathrm{Sc}\ln(1+B_c)/B_c^{0.15}$ where B_c is the mass transfer number and Sc is the viscous to mass diffusivity ratio. We note that higher values of the Damkohler number are obtained for higher values of inclination angle and/or higher values of room oxygen concentration level (fast reaction).

In Fig. 3.26, the normalized flame front speed data with respect to the de Ris expression shows a trend to increase as a function of the Damkohler number Da. A similar behavior was already observed in Ref. [33] for the downward ($\phi = 0^o$) combustion of thin solid fuels. Our simple analytical model (3.33) improves the classical one since the normalization of V_f with Eq. (3.33) tend to be almost independent on Da. However, Eq. (3.33) overpredicts the flame front speed for a factor of 1.3 to 5, depending on the data and angle employed. In contrast with the classical de Ris expression, however, Eq. (3.33) behaves as an upper bound whose range of values are even below than those obtained applying Eq. (3.24) (see Fig. 3 in Ref. [8]).

The onset of the instability can be tracked using the quotient of Nusselt numbers exposed in Subsec. 3.3.4. Figure 3.27 shows the ratio of Nusselt numbers calculated as in Eq. (3.54) for all the situations tested and the theoretical behavior expected. There is a good agreement between the expected curves and experimental values of the quotient of Nusselt numbers; they differ less than 1.5%. The values of $\mathrm{Nu_2/Nu_1} = 0.9$ are chosen as the theoretical critical angle in Fig. 3.27, being 64.2 and 55.4 for $X_{\mathrm{O_2}} = 30\%$ and 50%, respectively. This coincides with the experimental angles showing unstable values seen in Fig. 3.25. For the $X_{\mathrm{O_2}} = 22\%$ case, there is no instability due to the low energy of the flame as also observed in thermally thicker samples [26, 69].

The Grashof number is computed using as a reference length the flame length L_f, calculated using the formula obtained in [46], $L_f \approx 0.0345\left\{(T_f - T_v)/\left[(T_v - T_\infty)Y_{O2\infty}\right]\right\}^2 \alpha/(V_{acv} + V_f)$, with the flame spread rate V_f being either the experimental value or the calculated

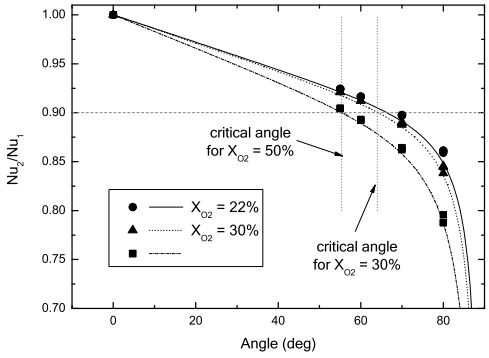

Figure 3.27: $\mathrm{Nu}_2/\mathrm{Nu}_1$ for all X_{O_2} tested, experimental results and expected curves.

using de Ris' formula ($V_f = (\pi/4)\lambda/(\tau\rho_s c_s)(T_f - T_v)/(T_v - T_\infty)$ [27], i.e., Eq. (3.33) for $\phi = 0^o$ with no radiation neither conduction through the solid phase). The experimental values of the flame length were not used because of experimental difficulties. The temperature of flame used is the mean of temperatures of the flame zone computed as in [14]. The reference temperature used for calculating the transport properties from the gas was the vaporization temperature ($T_v = 620$ K).

For nearly horizontal samples, the experiments show an unstable spread rate that may be triggered by curling of ashes and may be due to the flame in the lower side of the sample, as stated in Ref. [62]. The instability observed can be explained through the importance of the gravity component normal to the surface.

The importance of the normal component of gravity can be traced through the correction done to the Nusselt number $\mathrm{Nu}_2/\mathrm{Nu}_1$. After doing the tests, it has been seen that when this correction is greater than 10% of Nu_1, flame spread rates become unstable and expand for a large range of values.

3.3.6 Conclusions

The flame spread down thermally thin inclined samples is controlled by heat transfer to the unburned part of the sample. For vertical or slightly inclined surfaces, the behavior can be explained using only the component of gravity parallel to the surface. The component of gravity normal to the surface of the sample gains importance as the surface becomes more horizontal and may trigger an instability. In this paper we have generalized the classical analytical expression of the flame front speed [27] in order to be valid for the downward burning of an inclined sample. We have also developed a method to show the importance of the normal component of gravity via the quotient of Nusselt numbers having and not having into account this component. We have found that the instability arises when the correction is greater than a 10%, this being valid for different X_{O_2} concentration values.

Acknowledgements

B.C. acknowledges the support of a FPU grant from the MICINN. Some data were obtained by Adrià Carmona. We also thank Jordi Vicens and Sergi Saus for their technical assistance. This work has been partially funded by the Generalitat de Catalunya under Grant No. 2009-SGR-374 and the MICINN-FEDER under Grant No. FIS-2012-31307.

Chapter 4

Discussion

Since the results of this Ph.D. thesis has been published in three articles, the previous sections of the results chapter contain separated discussions. The present chapter aims to unite them in order to have a deeper insight of the flame spread problem.

4.1 Comparison with previous studies

Previous authors have dealt with the flame spread problems here analysed. In this section, we list the studies that, at our knowledge, have experimentally worked on the topics discussed in Section 3.1, 3.2 and 3.3. Thus, the following tables contribute to put our results in the context of the current knowledge of the flame front propagation over thin solid fuels.

Table 4.1 summarizes the main features of the works carried out by other authors in the study of the side effects on the burning of thin sheets. In addition, we also include data corresponding to the work done in Section 3.1. We point out that Table 4.1 reproduces Table 3.1 found in Section 3.1. Note that our study extends the previous works by analysing the effects of using lateral walls. These tend to reduce the lateral entrainment of air. This blockage phenomenon has been here investigated for the first time by using lateral holders of different materials. This has shed light into the relevance of the heat conduction through the holding plates as discussed in the following subsection.

The case of burning multiple parallel thin sheets has been investigated by a more reduced number of authors. The list of the previous works on this topic, including their characteristics, is found in Table 4.2. The first studies carried out by Ref. [70] were focused on explaining the channel effect of two burning surfaces. They found the spread rate and the temperature profile without radiation and assuming an infinite combustion reaction rate of plates soaked in methanol, heptane and cellulose. They concluded that the flame front speed was controlled by the Grashof number and the length and width of the channel. A great step on the understanding of this problem was due to the excellent paper of Kurosaki et al. [51] who not only derived a comprehensive, physically-based

[1]Exp.= Experimental, Sim.= Simulation, in.= Inhibited, A= Air

[2]Assuming $\rho_s = 1160 \text{kgm}^{-3}$

Ref.	Method	Case	Fuel	w (cm)	$\rho_s(\tau/2)$ (kg m^{-2})	X_{O_2} (%)	Results[1]
[3]	Sim.	1 in. edge, 2 in.edges	Cellulose	2	0.046	20 to 25	$V_{f,d}$, θ, fluid fields, etc.
[23]	Exp.	1 in. edge	Fabric, PMM	14	0.2057 (and others)	A	$V_{f,d}$
[36]	Exp.	1 in. edge	PMMA	8	0.58 to 3.48[2]	A	$V_{f,d}$, θ
[37]	Exp.	1 in. edge	Cellulose	2	0.080	21, 30, 50	θ
[38]	Exp. Sim.	1 in. edge	Cellulose	4	0.0385	A	$V_{f,d}$
Sec. 3.1	Exp.	1 in. edge, 2 in. edges, lateral blockage	Cellulose	2, 4, 6	0.043, 0.086, 0.129, 0.172	22, 25, 27, 30, 40, 50	$V_{f,d}$, θ

Table 4.1: Summary of previous works that obtain data related to the downward combustion of solid fuels with free edges at an absolute pressure of $P = 10^5$ Pa (or atmospheric pressure), normal gravity and initially quiescent environment. We include the work done in Section 3.1. Same as Tab. 3.1.

Ref.	Method	Case	Fuel	w (cm)	ρ_s (kg m^{-3})	τ (mm)	X_{O_2} (%)	Results
[51]	Exp. Sim.	$N = 2$, $C = 0$ to 6 cm	Paper	4	901	0.2	A	V_f, q_r, q_c, T
[52]	Exp. Sim.	$N = 1$ to 10, C= 0 to 6 cm	Paper	4	901	0.2	A	V_f
[70]	Exp. Sim.	$N = 2$,	Heptane, Methanol, Cellulose	$0.3 - 10$	791.80	100	A	T_g, V_g
Sec. 3.2	Exp. Sim.	$N = 1$ to 4, $C = 0$ to 6 cm	Paper	4	461.95	0.187	0-100	V_f

Table 4.2: Summary of previous works that obtain data related to the downward combustion of solid fuels with more than one sample at an absolute pressure of $P = 10^5$ Pa (or atmospheric pressure), normal gravity and initially quiescent environment. We include the work carried out in Section 3.2.

model able to explain the main mechanisms involved in this problem but also obtained experimental data with a high level of accuracy. The posterior work of Itoh and Kurosaki [52] was a continuation of their preliminary work in order to extend the model (as well as the comparison with the experiments) to more than two parallel thin solid fuels. The contribution of this thesis to this problem, as noted in Table 4.2, has consisted of analysing cases at different controlled oxygen concentrations and, more importantly, to generalize the previous simple model in order to be fully predictive.

The effect of varying the angle of inclination of the sample on the flame front speed has been extensively studied in solid fuels, since the prediction of its behaviour in upward burning may have great applications in fire safety issues (e.g., in fires in stairs as the King's Cross fire in 1987 [71]). In thin solid fuels, however, the number of studies is relatively low, as it is shown in Table 4.3. Kashiwagi and Newman [62] already noted that at angles of inclination close to the horizontal in downward burning, flow instabilities appear and make difficult to predict the flame front spread. The estimation of the conditions that lead to this onset of instability has been the purpose of our study shown in Section 3.3.

4.2 Experimental results

Although Sections 3.1, 3.2 and 3.3 of this thesis analyse laboratory data, Section 3.1 sets the experimental basis of the subsequent studies. It is in Section 3.1 where we obtain the physical properties of our cellulose fuel samples that are used throughout our whole work. These data do not only include information about the sample density, thickness, thermal conductivity and heat capacity but also of the kinetic data related with the pyrolysis

Ref.	Method	Case	Fuel	w (cm)	ρ_s (kg m^{-3})	τ (mm)	X_{O_2} (%)	Results
[26]	Exp.	-90^o to 90^o	Cellulose	6.4	901	0.16	A	V_f, T_g
[53]	Sim.	0^o to 90^o , Cylindrical	Various	-	Various	-	A	V_f, ϕ, T
[62]	0^o to 90^o	Cellulose	14	470	1.0	A	V_f, θ_c	
[65, 66]	Theo.	Vertical, Horizontal	PMMA	-	-	-	A	θ
[69]	Exp.	0^o to 90^o	Cellulose	0.6 - 7.6	433.3	0.21	A	V_f
[72]	Exp.	-90^o to 0^o	Cellulose, PMMA	1 - 10	450, 1180	0.18, 6	A	V_f, T_s
[73]	Exp.	-90^o to 0^o	Paper and other	5.4	220 (and other)	0.168	A	V_f
Sec. 3.3	Exp. Sim.	0^o to 90^o	Cellulose	4	461.95	0.187	22 to 50	V_f, ϕ_c

Table 4.3: Summary of previous works that obtain data related to inclined downward combustion of solid fuels at an absolute pressure of $P = 10^5$ Pa (or atmospheric pressure), normal gravity and initially quiescent environment. We include the work carried out in Section 3.3.

process obtained by means of a thermogravymetric analysis. Therefore, it is in Section 3.1 where we get the values of both the preexponential term and the activation energy of a one-step first order Arrhenius reaction related with the pyrolysis phenomenon and determine a temperature value for the vaporization temperature that is used in simpler definitions of the pyrolysis reaction.

In addition, it is also in Section 3.1 where we clearly state the experimental methodology in order to gather flame front velocities with the required accuracy. With the aim of investigating the appearance of three-dimensional effects when varying the width of the sample in the vertically downward burning configuration, the results obtained in Section 3.1 reveal that samples 4 cm wide behave very similar than wider samples in the typical configuration of holding the sample with two lateral plates. Therefore, this width of 4 cm is chosen as the minimum width where the flame is essentially two-dimensional and it is also employed in subsequent studies. The flame front speed in samples with less than 4 cm wide is affected (and reduced) by the presence of lateral holders. This result is similar to that found in Ref. [34] when studying a thin solid fuel with different physical properties than those of our samples.

From all the above, the work carried out in Section 3.1 may be essentially understood as a methodological study in order to establish a successful experimental protocol. Although the previous sentence is essentially true, we point out that Section 3.1 also includes new data related to the burning of fuel samples with 1) one free lateral edge (i.e., end lateral sheet not compressed with holding plates), 2) lateral walls located very close to the free lateral edge and 3) holding plates of materials with different thermal conductivities. The experimental data collected for all these cases indicate that the blockage effect due to the lateral walls substantially reduces the flame front speed. This oxygen shortage phenomenon is much more important than the use of holding materials with

different heat conductivities (that enhance the heat transfer to the surrounding elements).

The experiments carried out in Section 3.2 and 3.3 allow us to validate the theoretical models described in the following subsection. In Section 3.2 we study the burning of multiple parallel samples. Although the methodology employed follows that set in Section 3.1, we slighlty modify the process by placing a small strip of nitrocellulose between the coiled nichrome wires and the paper samples. This assures the simultaneity of the ignition of the multiples samples, which is a requirement for these types of experiments. From the experimental results of multiple parallel samples, it is clearly observed that for a fixed value of oxygen molar fraction, the downward flame front speed reaches a maximum at intermediate separation values between samples. As expected, at the limit of very close samples the burning rate tends to the value of a thicker fuel sample (which is lower than that of the single sheet case). On the other hand, at very large distances between samples the flame front speed equals that of the single sample case. Therefore, it is in a region of approximately 1.3 cm of separation between samples for oxygen levels close to the ambient one where we observe a maximum in the propagation speed of the flame front. This is mainly caused by the increase of the radiative fluxes that in burning multiple samples play an important role [51, 52]. Our contribution to this topic, besides the development of a fully predictive model as detailed below, has consisted in providing new experimental data obtained at different oxygen atmospheric levels (up to 100%). In addition, our data shed light into the controversial raised by several authors questioning that the flame spread rate of all parallel sheets will be the same due to having end samples with no nearby neighbours. Experimentally we do observe the same burning rate for all samples, including those at the end of the array of vertical sheets. In those end samples, although the flame front speed is the same, its position is a little bit delayed in comparison with its location in those burning papers with sample neighbours at both sides.

Finally, Section 3.3 shows new experimental data related to the downward burning of inclined fuel samples. The main contribution of Section 3.3 consists of applying this study to different oxygen atmospheric levels, from molar fractions $X_{O2} = 22\%$ up to $X_{O2} = 70\%$. We have observed flow instabilities that arise when using angles close to the horizontal configuration in the latter case. This implies that tests done under the same experimental configurations may lead to substantially different values of the burning rate (i.e. the repeatability of the data is not achieved due to the unstable behaviour of the background flow). When the oxygen molar fraction increases, we experimentally observe that the onset of the instability corresponds to a higher angle with respect to the horizontal when the oxygen molar fraction increases. This is due to a combustion reaction with more vigorous flames that enhances the buoyancy effect and, hence, the intensity of the background flow.

4.3 Theoretical models

In this thesis we initially develop a very simple energy balance model in Section 3.1, which is based on the work of Bhattacharjee et al. [18]. Essentially, it uses a single control volume for defining the solid region and two additional control volumes for the gas zones

normal and parallel to the sample surface. Since a single value of temperature defines the state of each control volume, the calculation of energy fluxes is greatly simplified once using the characteristic lengths of the main phenomena involved in the combustion process. This very basic model allows us to estimate the value of the downward velocity when burning samples with one free lateral edge. Due to the simplifications carried out (e.g., ignore energy losses), the expression obtained may be understood as an upper bound of the flame front velocity in terms of an order of magnitude analysis. This is confirmed by making a comparison of the results predicted by the mathematical expression and those obtained experimentally. An important feature of such a simple model is that the predicted upper bound differs less than 76% from the measured value for a very wide range of atmospheric oxygen concentration values. This contrasts with the upper bound expressions found in more complex models with estimated flame front speeds larger than 150% the observed data within the same interval of oxygen molar fractions (see, e.g., Figure 3 in Ref. [56]). We stress that our model is based on de Ris' one, which assumes infinite fast reaction kinetics, so it is applicable to situations with high reaction kinetics.

The work presented in Section 3.2 makes a step forward in terms of modelling with respect to Section 3.1, since it discretizes the solid surface in small elements of 0.01 cm long. In addition, this model takes into account radiative heat fluxes, which are crucial when studying the simultaneous burning of parallel thin sheets of cellulose. It requires an iterative process, this being similar to that derived by Itoh and Kurosaki [52]. However, the main difference with this previous work is that our model is fully predictive. Its solution requires an iterative process that gives us the flame front speed value as well as the temperature distribution and heat fluxes along the direction of propagation on the sample surface.

Numerical results indicate that for a single sheet configuration (or, equivalently, for multiple parallel sheets separated a large distance), the global contribution from radiative heat fluxes is much less important than the global contribution from the convective heat fluxes (conductive heat fluxes through the solid phase are neglected). This justifies the classical assumption, implicitly accepted in Section 3.1, of ignoring the effect of the radiative heat transfer when the flame front propagation is far from extinction conditions.

As an example of the previous affirmation, Figure 4.1 shows the calculated heat fluxes received (and emitted) in the unburned zone of the sample. It can be clearly seen that the main contribution near the flame front (at $x = 0$) is from the convective heat flux. It is important to stress that our numerical model includes radiative effects in the simplest possible way, since all surfaces are assumed to emit as grey bodies and the gas phase is assumed to be totally transparent to radiation. Thus, we use some concepts, like ember (or, equivalently, pyrolysed material) whose radiative properties are highly simplified. As stated below, a more detailed model is required in further studies where must accurately describe key elements such as, for example, the flame emissivity.

In Section 3.2 we have also developed an analytical expression for the flame spread rate based on an energy balance equation similar to that of Section 3.1 with radiation effects. Indeed, this analytical model is a generalization of the classical de Ris' formula [27] explicitly including the contribution of radiative heat fluxes. Note that we understand

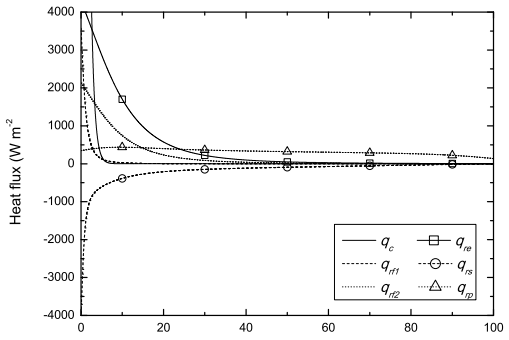

Figure 4.1: Heat fluxes received at the unburned sample simulated with the model employed in Section 3.2. q_c is the convective flux, q_{rf1} the radiative heat flux received from the flame, q_{rf2} the radiative heat flux received from the flame of a parallel burning paper separated 1.5 cm, q_{re} the radiative heat flux from the ember of the parallel sample, q_{rp} the radiative heat flux from the unburned parallel sample, and q_{rs} the radiative heat losses. The environment is a O_2 - N_2 atmosphere with $X_{O_2} = 21\%$.

the de Ris' model as an excellent expression for determining the flame front speed in the thermal regime of a single sheet burning downwards. As expected, the analytical model developed here performs as the de Ris' formula at the limit of one sample case. The main advantage of our analytical expression is its simplicity and ease of applicability. In comparison with the iterative model, however, the analytical one fails to reproduce the experimental trend of the flame front velocity as a function of the separation distance. This is very well reproduced with our generalization of the Itoh and Kurosaki model [52] not only when comparing with our own data but also with measured values obtained by Kurosaki et al. [51] who used a cellulose sample with different physical properties.

The approach taken in Section 3.3 for modelling the downward flame spread rate as a function of the angle of inclination of the sample is based on the comprehensive equations for both the gas and the solid phases. Those corresponding to the solid phase are simplified in order to get an analytical equation that is very similar to that derived in Section 3.2 but, now, including the effect of using different characteristic thermal lengths for both upward and downward faces of the paper samples (which are not obviously equal since the sample surface is inclined). In addition to this analytical approach to the flame front speed, we employ the comprehensive gas phase equations in order to derive a criterion for determining the instability threshold found when the downward burning sample is inclined more than a given angle θ_c. The phenomenon of reaching a critical angle beyond which the instability arises was already observed by Kashiwagi and Newman [62] using external radiant fluxes of different intensities. However, it is the first time that a criterion for determining the value of such a critical angle has been derived and whose validity has been confirmed experimentally. We note that the Nusselt number,

which is the core of this criterion, has been extensively used in heat transfer applications since it naturally arises from the analysis of the full equations that govern the gas phase with background flow at rest.

Finally, we point out the severe constraints related to the use of simple energy balance models in order to predict the flame front speed in complex cases. We are aware of the intrinsic limitations of this type of modelling so we do not intend to push its application beyond reasonable situations. It is clear that a deeper understanding of the flame front propagation will be achieved by employing fully coupled dynamical models that solve both the gas and solid phases. As noted in Section 1 this is the aim of our continuing research that it is now devoted to develop a fully detailed numerical combustion model of thin solid fuels. Such a model will simulate the behaviour of the background flow, species concentrations, temperature field, mass flux of volatiles, etc., thereby improving our knowledge of the combustion processes experimentally investigated.

Chapter 5

General conclusions

We have studied both experimentally and numerically the flame front speed in the downward burning of thin solid fuels accordingly with the three main objectives of the present work. Essentially, these were: 1) study the downward flame front speed of thin solid fuels in situations more complex (and hazardous) than the classical vertical configuration 2) generalize the classical analytical models in order to correctly predict the behaviour of those cases studied in 1), and 3) explain the convective instabilities found when burning inclined samples.

The effects of inhibiting the lateral edges by means of holding plates and of using lateral walls have been investigated in Section 3.1. The main conclusions extracted from this study are:

- At ignition, the vertical downward burning at the free edge (i.e., lateral part of the vertical sheet with no holding plates) is faster than that close to the inhibited one. This leads to an inclined front that finally propagates at a constant velocity.
- The flame spread rate normal to the inclined flame front when burning a sample with one free edge can be explained using de Ris' formula [27]. $V \sim \lambda_g/(\rho_s c_s \tau_s)(T_f - T_v)/(T_v - T_\infty)$.
- The main effect of having lateral holders is to reduce the lateral entrainment of oxygen, this effect being substantially more important than the heat losses towards the holding plate. Therefore, lateral holders tend to reduce the propagation speed of the flame front since they provoke a shortage of oxygen (especially in the case of sidewalls).
- An analytical expression based on the energy balance equation is derived, being an extension of the de Ris' expression for thin solid fuels that includes the effect of having a lateral free edge. This simple model provides a reasonable upper bound for the downward flame front speed, as it is confirmed experimentally.

The previous work has essentially dealt with the effect of having non-inhibited edges finally reaching a simplified analytical model. In Section 3.2 we have studied the flame

front speed when burning multiple parallel samples of thin solid fuels also experimentally and numerically. Besides being a more hazardous situation, one of the main reasons of choosing such a problem is that radiation plays an important role in this burning configuration and, therefore, it cannot be neglected as in classical studies of downward burning of a single sample. Thus, it requires, now, the development of more physically-realistic models in order to correctly capture the radiative heat transfer mechanism. The conclusions of this study are:

- The experimental data confirm that the flame front speed of downwards burning of an array of parallel sheets reaches a maximum at intermediate separation distances between samples. This separation distance where the maximum flame front velocity is reached varies as a function of the atmospheric oxygen molar fraction due to changes in the energy released in the combustion reaction.

- An analytical model based on a simple two-box energy balance formulation has been derived. The model may be understood as a generalization of the de Ris' expression by explicitly including the radiative heat fluxes. In multiple parallel samples, the energy fluxes generated by nearby samples have been also accounted for. A comparison of the results predicted by our analytical model with data reveals that it is, also here, a good estimator (upper bound) of the flame front speed (although it fails to reproduce the burning rate behaviour as a function of the separation distance between parallel sheets).

- We have generalized the energy balance model developed in Ref. [52] in order to be fully predictive. Thus, we avoid the use of parameters other than the physical properties of the sample and the experimental configuration. The results extracted from this more advanced model have been compared with our own measured data and, also, with observations obtained by other authors. The agreement with experimental data confirms the validity of this generalized model that can be applied to a wide range of environmental conditions.

Finally, we study the influence on the burning rate of the induced background flow due to buoyancy effects. In all previous cases (vertically downward burning) there was a buoyancy induced flow parallel to the sample and, therefore, there existed a buoyant flow opposed to the direction of the flame front propagation. For inclined samples, there is also a contribution normal to the sample that gains importance when the sample is more inclined. This implies that the opposed induced flow weakens and, therefore, the flame velocity is expected to increase. We analyse this phenomenon in Section 3.3 whose main conclusions are:

- The experimental data reveals that the normal contribution (relative to the sample surface) of the buoyant flow triggers an hydrodynamic instability. This is observed by obtaining a wide range of flame front speeds under the same experimental configuration. This unstable behaviour arises at more inclined angles of the sample (i.e., towards a more horizontal position) as the oxygen molar fraction decreases.

- We generalize the previous analytical models of Sections 3.1 and 3.2 based on simple energy balance equations in order to be applied in an inclined sample. The predicted values of the burning rate are confirmed to behave as upper bounds of the measured data.
- From applying the concepts of boundary layer theory to the Navier-Stokes equations of the gas phase, we have developed a criterion based on the Nusselt number that determines the critical angle beyond which the flow instability is obtained. The validity of this criterion is also confirmed experimentally at different oxygen atmospheric concentrations.

Bibliography

[1] A.E. Frey and J.S. T'Ien. A theory of flame spread over a solid fuel including finite-rate chemical kinetics. *Combustion and Flame*, 36:263–289, 1979.

[2] C.H. Chen. A numerical study of flame spread and blowoff over a thermally thin solid fuel in an opposed air flow. *Combustion Science and Technology*, 69:63–83, 1990.

[3] C. Kumar and A. Kumar. A computational study on opposed flow flame spread over thin solid fuels with side-edge burning. *Combustion Science and Technology*, 182:1321–1340, 2010.

[4] J.N. De Ris. *The spread of a diffusion flame over a combustible surface*. PhD thesis, Harvard University, Cambridge, MA, May 1968.

[5] I.S. Wichman. Theory of opposed-flow flame spread. *Progress in Energy and Combustion Science*, 18:553–593, 1992.

[6] C.W. Lautenberger. *A generalized pyrolysis model for combustible solids*. PhD thesis, University of California, 2007.

[7] H.C. Kung. A mathematical model of wood pyrolysis. *Combustion and Flame*, 18:185–195, 1972.

[8] T. Pujol and B. Comas. Bounds for downward flame spread rate in solid fuels and comparison to experiments. *Combustion Science and Technology*, 183(10):1083–1106, 2011.

[9] C. Di Blasi. The state of the art of transport models for charring solid degradation. *Polymer International*, 49:1133–1146, 2000.

[10] S. Bhattacharjee, M.D. King, and C. Paolini. Structure of downward spreading flames: a comparison of numerical simulation, experimental results and a simplified parabolic theory. *Combustion Theory and Modelling*, 8:23–39, 2004.

[11] F.C. Duh and C.H. Chen. A theory for downward flame spread over a thermally thin fuel. *Combustion Science and Technology*, 77:291–305, 1991.

[12] D.B. Spalding. Mass transfer in laminar flow. In *Proceedings of the Royal Society London A*, volume 221, pages 78–99, 1954.

[13] Ya.B. Zeldovich. Theory of combustion of unmixed gases. Technical Translation F-14360, NASA, 1973.

[14] J.B. Greenberg and P.D. Ronney. Analysis of lewis number effects in flame spread. *Int. J. Heat Mass Transfer*, 36(2):315–323, 1993.

[15] Y. Zhang, P.D. Ronney, E.V. Roegner, and J.B. Greenberg. Lewis number effects on flame spreading over thin solid fuels. *Combustion and Flame*, 90:71–83, 1992.

[16] T. Pujol, J. Fort, J.R. González, L. Montoro, and M. Pelegrí. Bounds for the speed of combustion flames: the effect of mass diffusion. *Physica A*, 387:1987–1998, 2008.

[17] K.K. Wu and C.H. Chen. Radiation effects for downward flame spread over a thermally thin fuel in a partial gravity environment. *Combustion Science and Technology*, 176:1909–1933, 2004.

[18] S. Bhattacharjee, R. Ayala, K. Wakai, and S. Takahashi. Opposed-flow flame spread in microgravity-theoretical prediction of spread rate and flammability map. *Proceedings of the Combustion Institute*, 30:2279–2286, 2005.

[19] F.A. Lastrina, R.S. Magee, and R.F. Alevy III. Flame spread over fuel beds: solid-phase energy considerations. *Proceedings of the Combustion Institute*, 13:935–948, 1971.

[20] R.A. Altenkirch, A.R. Rizvi, and R. Eichhorn. A dimensionless correlation of the flame spread rate down thermally thick fuels in the presence of free convection. In *1980 Eastern States Section Meeting of the Combustion Institute*, Princeton University, Princeton, NJ, 1980.

[21] K. Zik and E. Moses. Fingering instability in combustion: an extended view. *Physical Review E*, 60(1):518–531, 1999.

[22] I.S. Wichman, S.L. Olson, F.J. Miller, and S.A. Tanaya. Experimental evaluation of flame and flamelet spread over cellulosic materials using the narrow channel apparatus. *Fire and Materials*, 37(7):503–519, 2013.

[23] G.H. Markstein and J. de Ris. Flame spread along fuel edges. *Journal of Fire and Flammability*, 6:140–154, 1975.

[24] C. Di Blasi. Influences of sample thickness on the early transient stages of concurrent flame spread and solid burning. *Fire Safety Journal*, 25(4):287–304, 1995.

[25] A. Itoh and T. Kashiwagi. Measurement technique for determining the temperature distribution in a transparent solid using optical interferometry. *Applied Optics*, 26:954–958, 1987.

[26] T. Hirano, S.E. Noreikis, and T.E. Waterman. Postulations of flame spread mechanisms. *Combustion and Flame*, 22:353–363, 1974.

[27] J.N. De Ris. Spread of a laminar diffusion flame. In *Twelfth Symposium (International) on Combustion*, pages 241–252. The Combustion Institute, 1969.

[28] I. Milosavljevic and E.M. Suuberg. Cellulose thermal decomposition kinetics: Global mass loss kinetics. *Industrial & Engineering Chemistry Research*, 34(4):1081–1091, 1995.

[29] J. Warnatz, U. Maas, and R.W. Dibble. *Combustion*. Springer-Verlag, 3rd edition, 2001.

[30] R.A. Altenkirch, R. Eichhorn, and P.C. Shang. Buoyancy effects on flames spreading down thermally thin fuels. *Combustion and Flame*, 37(1):71–83, 1980.

[31] M.A. Delichatsios. Exact solution for the rate of creeping flame spread over thermally thin materials. *Combustion Science and Technology*, 44:257–267, 1986.

[32] A.C. Fernandez-Pello and F.A. Williams. A theory of downward flame spread over flat surfaces of solid combustibles. *Combustion and Flame*, 28:251–277, 1977.

[33] A.C. Fernandez-Pello, S.R. Ray, and I. Glassman. Flame spread in an opposed forced flow: the effect of ambient oxygen concentration. *Proceedings of the Combustion Institute*, 18:579–589, 1981.

[34] A.E. Frey and J.S. T'Ien. Near-limit flame spread over paper samples. *Combustion and Flame*, 26:257–267, 1976.

[35] H.W. Emmons and T. Shen. Fire spread in paper arrays. In *Thirteenth Symposium (International) on Combustion*, pages 917–926. The Combustion Institute, 1971.

[36] J.V.Jr. Creeden and M. Sibulkin. The effect of an uninhibited edge on downward flame propagation. *Combustion Science and Technology*, 14:123–124, 1976.

[37] M. Vedha-Nayagam, K. Saito, and R.A. Altenkirch. Edge effects in flame spreading down thermally thin solid fuels. *Chemical and Physical Processes in Combustion*, pages 2843–2849, 1986.

[38] W.E. Mell, S.L. Olson, and T. Kashiwagi. Flame spread along free edges of thermally thin samples in microgravity. *Proceedings of the Combustion Institute*, 28:2843–2849, 2000.

[39] W.A. Sirigniano. Theory of flame spread above solids. *Acta Astronautica*, 1:1285–1299, 1974.

[40] W.E. Mell and T. Kashiwagi. Effect of finite sample width on the transition and flame spread in microgravity. *Proceedings of the Combustion Institute*, 28:2785–2792, 2000.

[41] C. Di Blasi. Processes of flames spreading over the surface of charring fuels: the effect of the solid thickness. *Combustion and Flame*, 97:225–239, 1994.

[42] J. West, S. Bhattacharjee, and R.A. Altenkirch. A comparison of the roles played by natural and forced convection in opposed-flow flame spreading. *Combustion Science and Technology*, 83:233–244, 1992.

[43] C. Di Blasi, S. Crescitelli, G. Russo, and A.C. Fernandez-Pello. Model of the flow assisted spread of flames over a thin charring combustible. In *Twenty-Second Symposium (International) on Combustion*, pages 1205–1212. The Combustion Institute, 1988.

[44] K.K. Wu and C.H. Chen. A numerical analysis of ignition to steady downward flame spread over a thin solid fuel. *Combustion Science and Technology*, pages 933–964, 2003.

[45] X. Zhang and Y. Yu. Experimental studies on the three-dimensional effects of opposed flow flame spread over thin solid materials. *Combustion and Flame*, 158:1193–1200, 2011.

[46] S. Bhattacharjee, S. Takahashi, K. Wakai, and C.P. Paolini. Correlating flame geometry in opposed-flow flame spread over thin fuels. *Proceedings of the Combustion Institute*, 33:2465–2472, 2011.

[47] R.L. Alpert. Evaluation of the hazard of fire resistant materials using measurements from laboratory and parallel panel tests. *Fire Safety Science*, 7:41–57, 2003.

[48] J.N. de Ris and L. Orloff. Flame heat transfer between parallel panels. *Fire Safety Science*, 8:999–1010, 2005.

[49] S. Nam and R.G.Jr. Bill. A new intermediate-scale fire test for evaluating building material flammability. *Journal of Fire Protection Engineering*, 19:157–176, 2009.

[50] S.R. Wasan, P. Rauwoens, J. Vierendeels, and B. Merci. Study of vertical upward flame spread on charring materials—part ii: Numerical simulations. *Fire and Materials*, 35:261–273, 2011.

[51] Y. Kurosaki, A. Itoh, and M. Chiba. Downward flame spread along two vertical parallel sheets of thin combustible solid. *Proceedings of the Combustion Institute*, 17:1211–1219, 1979.

[52] A. Itoh and Y. Kurosaki. Downward flame spread along several vertical, parallel sheets of paper. *Combustion and Flame*, 60:269–277, 1985.

[53] J.S. Kim, J.N. de Ris, and K.W. Kroesser. Laminar free-convective burning of fuel surfaces. *Proceedings of the Combustion Institute*, 13:949–961, 1971.

[54] D.L. Urban, J.S. Goldmeer, and Z.G. Yuan. Interactions between flames on paralles solid surfaces. *NASA Conference Publication N10194*, pages 429–434, 1997.

[55] B. Comas and T. Pujol. Experimental study of the effects of side-edge burning in the downward flame spread of thin solid fuels. *Combustion Science and Technology*, 184(4):489–504, 2012.

[56] T. Pujol and B. Comas. Analytical expressions for the flame front speed in the downward combustion of thin solid fuels and comparison to experiments. *Physical Review E*, 84(2):026306, 2011.

[57] H.Y. Shih. Flame spread and interactions in an array of thin solids in low-speed concurrent flows. *Combustion Theory and Modelling*, 13(3):443–459, 2009.

[58] D.D. Drysdale. *An Introduction to Fire Dynamics*. Wiley, 3 edition, 8 2011.

[59] R.D. Benguria, J. Cisternas, and M.C. Depassier. Variational calculation for thermal combustion waves. *Physical Review E*, 52(4):4410–4413, 1995.

[60] N. Provatas, T. Alanissila, M. Grant, K.R. Elder, and L. Piche. Flame propagation in random-media. *Physical Review E*, 51(5):4232–4236, 1995.

[61] T. Pujol, J. Fort, L. Montoro, and J.J. Suñol. Generalized analytical expressions for the burning velocity in a combustion model with non-constant transport coefficients and several specific heats. *Physica A*, 388:4959–4972, 2009.

[62] T. Kashiwagi and D.L. Newman. Flame spread over an inclined thin fuel surface. *Combustion and Flame*, 26:163–177, 1976.

[63] O. Zik, Z. Olami, and E. Moses. Fingering instability in combustion. *Physical Review Letters*, 81:3868–3871, 1998.

[64] M.A. Delichatsios. Relation of opposed flow (creeping) flame spread with extinction/ignition. *Combustion and Flame*, 135(4):441–447, 2003.

[65] K. Annamalai and M. Sibulkin. Flame spread over combustible surfaces for laminar-flow systems. part i: Excess fuel and heat-flux. *Combustion Science and Technology*, 19(5-6):167–183, 1979.

[66] K. Annamalai and M. Sibulkin. Flame spread over combustible surfaces for laminar-flow systems. part ii: Flame heights and fire-spread rates. *Combustion Science and Technology*, 19(5-6):185–193, 1979.

[67] H. Schlichting. *Boundary-Layer Theory*, pages 271–350. McGraw-Hill, 7th edition, 1987.

[68] S. Levy and N.Y. Schenectady. Integral methods in natural convection flow. *Journal of Applied Mechanics*, 22:515–522, 1955.

[69] M. Sibulkin, W. Ketelhut, and S. Feldman. Effect of orientation and external flow velocity on flame spreading over thermally thin paper strips. *Combustion Science and Technology*, 9:75–77, 1974.

[70] J.S. Kim and J.N. de Ris. Laminar burning between parallel surfaces. *International Journal of Heat and Mass Transfer*, 17:439–451, 1974.

[71] D.D. Drysdale and A.J.R. Macmillan. The King's Cross fire: Experimental verification of the 'trench effect'. *Fire Safety Journal*, 18:75–82, 1992.

[72] D.D. Drysdale and A.J.R. Macmillan. Flame spread on inclined surfaces. *Fire Safety Journal*, 18:245–254, 1992.

[73] J.G. Quintiere. The effects of angular orientation on flame spread over thin materials. *Fire Safety Journal*, 36:291–312, 2001.

Appendix A

Publications

Combustion Science and Technology, 184: 489–504, 2012

Combustion Science and Technology, 185: 1820–1837, 2013

Physical Review E, 88: 063019, 2013

B. Comas and T. Pujol. Experimental study of the effects of side-edge burning in the downward flame spread of thin solid fuels. *Combustion Science and Technology*, 184: 489-504, 2012

http://dx.doi.org/10.1080/00102202.2011.648033

http://www.tandfonline.com/doi/abs/10.1080/00102202.2011.648033#.VAVzz_l_vTo

Received: 1 Aug 2011

Accepted: 6 Dec 2011

Published online: 13 Mar 2012

Abstract

A comparison between the downward flame spread rate for thermally thin samples with one or two inhibited edges is done in multiple situations. The effects of atmospheric composition as well as the width and thickness of a cellulosic-type fuel are tested experimentally. We have found that the normal velocity to the inclined flame front in a side-edge burning is very similar to the downward flame front speed when the sample is inhibited by both edges. Also, the effect of locating a sidewall close to the free edge of the sample is investigated. All these results may be important in order to validate or refute possible models of downward flame spread that take into account side effects.

Keywords

Downward combustion; Flame spread; Side burning

B. Comas and T. Pujol. Energy balance models of downward combustion of parallel thin solid fuels and comparison to experiments. *Combustion Science and Technology*, 185: 1820-1837, 2013

http://dx.doi.org/10.1080/00102202.2013.839556

http://www.tandfonline.com/doi/abs/10.1080/00102202.2013.839556

Received: 21 Jun 2013

Accepted: 26 Aug 2013

Accepted author version posted online: 09 Sep 2013

Published online: 04 Nov 2013

Abstract

We analyze the flame front speed in the downward combustion of multiple parallel samples of thermally thin fuels at normal gravity and far from extinction conditions. In contrast with the single sample case, where conduction through the gas-phase is the dominant heat transfer mechanism, in the multiple parallel samples case, radiative heat fluxes may become very relevant, which compromises the application of the well-known formula of de Ris for determining the burning rate. Here we study the downward combustion of multiple parallel sheets by (1) obtaining new experimental data at different oxygen atmospheric levels; (2) generalizing a previous comprehensive energy balance model now expected to be valid for a wide range of scenarios; and (3) deriving an analytical approximation for the burning rate that generalizes the classical de Ris formula for those cases where radiative effects cannot be neglected. The comparison with own as well as with external data reveals the strengths and weaknesses of these types of models.

Keywords

Downward combustion; Flame spread; Thin-solid fuel

PHYSICAL REVIEW E **88**, 063019 (2013)

Flame front speed and onset of instability in the burning of inclined thin solid fuel samples

Bruna Comas and Toni Pujol
Universitat de Girona, 17071 Girona, Spain
(Received 4 October 2013; published 30 December 2013)

We focus on the front propagation of diffusive flames obtained from the downward burning of inclined thermally thin solid fuels. This process consists of a pyrolysis reaction in the solid-phase and a combustion reaction in the gas phase. The solid-phase model is based on two coupled one-dimensional equations of temperature and solid density. We reduce the system into a single one-dimensional equation from which we obtain an analytical expression for the flame front speed. This expression may be understood as an upper bound of the burning spread rate in inclined samples. The gas-phase model is based on four coupled two-dimensional equations. These are employed to derive a criterion for determining the critical inclination angle beyond which the flame behavior becomes unstable. The comparison with the experiments confirms the validity of our predictions.

DOI: 10.1103/PhysRevE.88.063019 PACS number(s): 47.70.Pq, 47.70.Fw, 47.20.−k, 82.33.Vx

I. INTRODUCTION

Combustion is an exothermic process of chemically reacting flows that may produce either a premixed or a nonpremixed flame [1]. Premixed flames occur when both fuel and oxidizer are mixed before burning. In laminar flows of flat premixed gaseous flames, several methods applied to the one-dimensional reaction-convection-diffusion equations that correspond to the conservation equations of mass and energy lead to analytical approximations of the flame front speed [2–4].

On the other hand, diffusion (or, equivalently, nonpremixed) laminar flames arise when the mixing and burning occur simultaneously, like in the downward burning of a cellulosic type sample. In contrast with flat premixed gaseous flames, the combustion of thin solid fuels is, at least, a two-dimensional process, since it involves the mass flux of volatiles at the solid surface and the combustion reaction at the flame height. For such a process, analytical expressions for the speed of the flame front V_f have been obtained after reducing complex two-dimensional reaction-convection-diffusion equations into a single one-dimensional one [5,6]. Although some of these approximations successfully predict the downward flame speed, they fail to explain the burning spread rate over inclined samples where flame instabilities may arise [7].

In this work, we use the solid-phase equations in Sec. III to derive an analytical expression of the upper bound of the flame spread rate. This expression generalizes previous equations and it is valid for inclined surfaces. In Sec. IV we use the gas phase equations to obtain stationary solutions that allow us to calculate the Nusselt number at first-order approximation (equivalent to assume only the gravity component parallel to the surface) and at second-order approximation (equivalent to assume the gravity component normal to the surface). A given value of the ratio of these Nusselt numbers will provide an instability threshold when comparing with experimental data as shown in Sec. V. Here, our approach differs from Refs. [8,9] since it is based on the fundamental governing equations.

II. EXPERIMENTAL SETUP

The experiments were carried out in a combustion chamber, using a controlled atmosphere of 10^5 Pa with a mixture of O_2 and N_2. Figure 1 shows a schematic view of the experimental design. The combustion chamber could be inclined at the angle required for the test.

Cellulosic samples of half-thickness 0.0933 mm and surface density 0.0431 kg m^{-1} were used. The length and width of the samples were 24 × 4 cm, long enough to ensure steady spread and wide enough to minimize effects of lateral heat losses. More details about the samples and justification of the sizes can be found in Ref. [10].

Samples were dried for 2 h at 100 °C and stored for a minimum of 24 h before each experiment. Then they were held by aluminium holders, 2 mm thick and 40 mm wide, in the middle of the chamber; the chamber was closed and inclined to the desired angle. A vacuum was created inside the chamber and then it was filled with O_2 and N_2 at the desired concentration. Gases were mixed during three minutes with a fan and then they were left at rest for 2 min. Samples were ignited uniformly at the top with a coiled nichrome wire. Three repetitions with the same sample configuration and atmospheric concentration were done.

Every experiment was recorded with a high-definition camera at 50 Hz. Videos were later analyzed frame by frame to determine the position of the flame front and the existence (if observed) of an erratic flame behavior that may cause instabilities and produce a substantial variability of the flame front speed once the experiment is repeated under the same conditions. A typical image of the experiment can be seen in Fig. 2. Flame spread velocities were obtained through lineal regression of the front position with respect to time, with a correlation factor of 0.996 or better for all cases.

III. FLAME SPREAD RATE

The combustion of a vertical cellulosic-type sample ignited at the top produces a flame front that propagates downwards at a given speed V_f. For thermally thin solids, many authors have proposed analytical expressions for calculating V_f based either on an energy balance of the solid phase [11] or on an energy balance of the gas phase [6]. Here, we generalize the broadly accepted model of de Ris [12] based on the solid phase equations in order to study the flame spread rate of inclined samples. This model assumes unit Lewis number

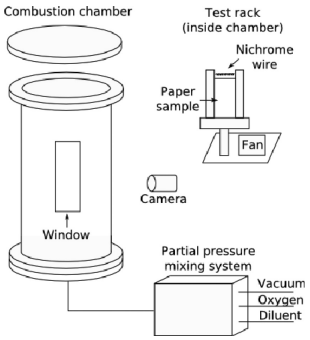

FIG. 1. Schema of the combustion chamber.

(equal thermal and mass diffusivities) and constant transport coefficients.

The burning process of cellulose consists of two main chemical reactions. The first is the endothermic pyrolysis reaction in the solid phase that releases fuel volatiles. The second is the exothermic combustion reaction in the gas phase (oxygen and fuel volatiles) that produces a diffusive flame. The transfer of heat from the flame to the virgin solid ahead preheats the sample, produces the pyrolysis, and sustains the propagation of the flame front.

The governing equations for the solid phase temperature T_s and solid phase density ρ_s are

$$c_s\rho_s\frac{dT_s}{dt} = -\overrightarrow{\nabla}\cdot\overrightarrow{J_s} - \frac{d\rho_s}{dt}[L_v + (c_s - c_g)(T_s - T_\infty)], \quad (1)$$

$$\frac{d\rho_s}{dt} = -A\rho_s e^{-E_s/(RT_s)}, \quad (2)$$

where c_s and λ_s, used in the conductive heat flux term, are the specific heat and conductivity of the solid, L_v is the heat of vaporization, c_g is the gas specific heat, and T_∞ is the room temperature. The term $\overrightarrow{J_s}$ in Eq. (1) includes radiative as well as conductive heat fluxes. In Eq. (2), E_s and A are the activation energy and the preexponential term of the pyrolysis reaction, respectively, with R the universal gas constant.

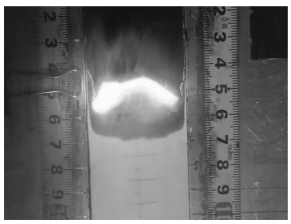

FIG. 2. Image from one experiment made at 30% of O_2, with an inclination of 70° with respect to the horizontal.

By applying the classical analysis of Benguria and collaborators [2] to the set of Eqs. (1) and (2), Ref. [13] obtained an upper bound of the flame front speed,

$$V_f < V_{f,\text{de Ris}} - 2\int_0^1 2\sqrt{F\theta_s}d\theta_s, \quad (3)$$

where

$$F = \frac{\alpha_s T_v A\rho_s e^{-E_s/(RT_s)}[L_v + (c_s - c_g)(T_v - T_\infty)\theta_s]d}{c_s^2\rho_{s\infty}^2(T_v - T_\infty)^2}, \quad (4)$$

with α_s the solid thermal diffusivity, T_∞ and T_v the room and the vaporization temperatures, respectively, θ_s a dimensionless variable defined as

$$\theta_s = \frac{(T_s - T_\infty)}{(T_v - T_\infty)}, \quad (5)$$

and d a function of θ_s such as $d = 0$ at $\theta_s = 1$ and $d = 1$ at $\theta_s = 0$.

In Eq. (3), the term

$$V_{f,\text{de Ris}} = \frac{2\lambda_g(T_{f,\text{ad}} - T_v)}{\tau c_s\rho_{s\infty}(T_v - T_\infty)} \quad (6)$$

corresponds to the de Ris equation with τ the solid thickness, λ_g the gas phase conductivity, and $T_{f,\text{ad}}$ the adiabatic flame temperature (excluding a $\pi/4$ multiplying factor that arises after solving the gas-phase equations).

Equation (3) applies only to the downward combustion of vertical samples. In this configuration, the background convective flow induced by density variations through the flame region opposes the direction of propagation of the flame front. However, as the angle of inclination of the sample increases, the convective flow parallel to the sample decreases in intensity and, therefore, the velocity of the flame front increases. Here, we develop an analytical expression that aims to include this effect.

According to Ref. [14], our model assumes no pyrolysis (constant solid density) ahead of the flame front. Then, in a coordinate system attached to the flame front, Eq. (1) applied to the preheated region (negative x') reduces to

$$c_s\rho_s V_f\frac{dT_s}{dx'} = \lambda_s\frac{d^2T_s}{dx'^2} - \frac{\partial J_s}{\partial y}. \quad (7)$$

The integration of Eq. (7) through the sample thickness (from $y = -\tau$ to $y = 0$) and with the dimensionless variables θ_s (5) and $x = x'/L_{gx+}$ with L_{gx+} as the characteristic gas phase thermal length along x (parallel to the solid surface) of the upper side + of the inclined sample leads to

$$V_f\frac{d\theta_s}{dx} = \frac{\alpha_s}{L_{gx+}}\frac{d^2\theta_s}{dx^2} - \frac{L_{gx+}}{\tau c_s\rho_s(T_v - T_{s\infty})}(J_{cv,y=0} - J_{cv,y=-\tau} + J_{rd,y=0} - J_{rd,y=-\tau}), \quad (8)$$

where J_{cv} and J_{rd} are the conductive and radiative heat fluxes on the upper $y = 0$ and lower $y = -\tau$ sides of the inclined sample. In Eq. (8), we have assumed a uniform temperature across the y direction within the paper sample, which agrees with the thin solid fuel case studied.

The conductive flux in the preheated region is commonly expressed in terms of exponentially decaying functions with a maximum value at the flame leading edge ($x = 0$) [14,15]. At this point, we assume the adiabatic flame temperature $T_{f,\mathrm{ad}}$ as the characteristic gas phase temperature and T_v as the characteristic solid temperature. Therefore, the conductive heat flux at the solid surface at $x = 0$ is equal to $\lambda_g(T_{f,\mathrm{ad}} - T_v)/L_{gy}$ with L_{gy} the characteristic thermal length along y. Thus, the upper $J_{cv,y=0}$ and lower $J_{cv,y=-\tau}$ conductive fluxes in the preheated region are

$$J_{cv,y=0} = -\frac{\lambda_g(T_{f,\mathrm{ad}} - T_v)}{L_{gy+}}e^{x},$$
$$J_{cv,y=-\tau} = \frac{\lambda_g(T_{f,\mathrm{ad}} - T_v)}{L_{gy-}}e^{xL_{gx+}/L_{gx-}}, \tag{9}$$

where L_{gy+}, L_{gy-}, and L_{gx-} are the characteristic gas phase thermal lengths along y or x in the upper $+$ or lower $-$ sides of the inclined sample.

The radiative flux emitted by the flame and absorbed at the virgin solid ahead of the flame front is obtained by using a simplified model in which both flame and paper are constant temperature planes that intersect at the flame leading edge. From the above, the integration of the radiative fluxes from $x = -L/L_{gx+}$ to $x = 0$, where L is the length of the paper, gives

$$\int_{-L/L_{gx+}}^{0}(J_{rd,y=0} - J_{rd,y=-\tau})dx = \varepsilon_f a\sigma T_f^4(F_{s-f}^{+} + F_{s-f}^{-})\frac{L}{L_{gx+}}, \tag{10}$$

where ε_f is the flame emissivity, a is the absorptivity of the paper, and T_f is the mean flame temperature. As pointed out in Ref. [15], T_f must be lower than the adiabatic value $T_{f,\mathrm{ad}}$ and here is taken as the mean value of the gas-phase temperature obtained in the one-dimensional flame model of Ref. [16]. The view factors from the paper plane to the flame plane are

$$F_{s-f}^{+,-} = \frac{1}{2}\left(1 + \frac{L_f}{L} - \sqrt{1 + \frac{L_f^2}{L^2} - 2\frac{L_f}{L^2}\cos\beta^{+,-}}\right) \tag{11}$$

with β^+ and β^- the angle between the flame plane and the paper plane in the upper and lower sides of the sample, respectively.

The integration of Eq. (8) from $x = -L/L_{gx+}$ to $x = 0$ gives

$$V_{f,g} = \frac{\alpha_s}{L_{gx+}}\frac{d\theta_s}{dx}\bigg|_{x=0} + \frac{2\alpha_s}{\tau}\frac{\lambda_g(T_{f,\mathrm{ad}} - T_v)}{\lambda_s(T_v - T_{s\infty})} \times\left[\frac{L_{gx+}}{L_{gy+}}(1 - e^{-L/L_{gx+}}) + \frac{L_{gx-}}{L_{gy-}}(1 - e^{-L/L_{gx-}})\right] \times\frac{\alpha_s}{\tau}\frac{\varepsilon_f a\sigma T_f^4 L}{\lambda_s(T_v - T_{s\infty})}(F_{s-f}^{+} + F_{s-f}^{-}). \tag{12}$$

Note that Eq. (12) for the case with no radiation and no conduction through the solid phase reduces to the classical de Ris Eq. (6) for $L_{gx+} = L_{gx-} = L_{gy+} = L_{gy-}$ and $L = \infty$ as it should. Also note that for our radiative calculation, the temperature of the virgin solid is assumed constant and equal to that for the room. This implies no net radiative losses that would tend to lower the velocity in Eq. (12). Therefore, Eq. (12) will overestimate the flame front speed and may be understood as an upper bound to the actual value. This is confirmed by comparison with the experiments as we show in Sec. V.

IV. INSTABILITY

The momentum and continuity gas phase equations for a steady diffusion laminar flame upon an inclined angle ϕ from the vertical are the starting point of the instability analysis. The classical analysis of these equations ignores the gravity component normal to the surface [17–19], either by considering only vertical combustion or low-enough inclination angles ϕ. Our analysis aims to find the critical point where instability arises, and since it is located at angles near $\pi/2$, we must maintain the gravity component normal to the surface. This implies a nontrivial equation for the normal momentum that cannot be solved analytically.

In this section the flame plane is modelled parallel to the surface of the paper ($\beta^+ = \beta^- = 180^\circ$ in Eq. (11)) in order to use Boussinesq approximation for the density. We note that the flame speed Eq. (12) decreases by less than 4% only when varying the β angles from 140° to 180° for the 30% oxygen concentration case. We have experimentally seen with the aid of lateral mirrors inside the combustion chamber that the flame plane does not substantially deviate from the surface until the angle is close to the horizontal, where the flame becomes unstable.

Continuity, momentum, and energy equations will be

$$\frac{\partial(\rho u)}{\partial x} + \frac{\partial(\rho v)}{\partial y} = 0, \tag{13}$$
$$u\frac{\partial u}{\partial x} + v\frac{\partial u}{\partial y} = \nu\frac{\partial^2 u}{\partial y^2} + g\cos\phi\frac{(\rho_\infty - \rho)}{\rho}, \tag{14}$$
$$u\frac{\partial v}{\partial x} + v\frac{\partial v}{\partial y} = \nu\frac{\partial^2 v}{\partial y^2} + g\sin\phi\frac{(\rho_\infty - \rho)}{\rho}, \tag{15}$$
$$u\frac{\partial(T - T_\infty)}{\partial x} + v\frac{\partial(T - T_\infty)}{\partial y} = \alpha\nabla^2(T - T_\infty), \tag{16}$$

where boundary-layer assumptions have been made [17,18,20]. In the above equations we have supposed constant transport properties, unit Lewis number, and velocities much less than the speed of sound. Equations (13), (14), (15), and (16) provide the starting point of a natural convection flux. From these equations we can reach the equations in integral form,

$$\nu\frac{\partial^2 u}{\partial y^2}\bigg]_0^\delta + g\cos\phi\frac{\rho_\infty - \rho}{\rho}\bigg]_0^\delta - g\sin\phi\int_0^\delta\frac{\partial}{\partial x}\left(\frac{\rho_\infty - \rho}{\rho}\right)dy = 0, \tag{17}$$
$$\frac{\partial}{\partial x}\int_0^\delta u(T - T_\infty)dy - \alpha\frac{\partial(T - T_\infty)}{\partial y}\bigg]_0^\delta = 0. \tag{18}$$

The detailed analysis from Eqs. (13), (14), and (15) to the equations in integral form is not given here for the sake of brevity and may be found in the literature [17,21]. For a downward (or inclined) spreading flame, the reference frame

is defined as traveling at the steady flame spread rate V_f. The boundary conditions of the fluid will be

$$\left.\begin{array}{l} u = V_f \\ \rho = \rho_f \\ T = T_f \end{array}\right\} \quad \text{for} \quad y = 0, \tag{19}$$

$$\left.\begin{array}{l} u = V_f \\ T = T_\infty \\ \rho = \rho_\infty \\ \frac{\partial u}{\partial y}, \frac{\partial (T - T_\infty)}{\partial y}, \frac{\partial [(\rho_\infty - \rho)/\rho]}{\partial y} = 0 \end{array}\right\} \quad \text{for} \quad y = \delta. \tag{20}$$

The assumed velocity profile is similar to the velocity profile obtained in the numerical model of Ref. [22],

$$u = u_1 \frac{y}{\delta}\left(1 - \frac{y}{\delta}\right)^2 + V_f, \tag{21}$$

where δ is the thickness of the boundary layer. The density profile is normalized from 1 to 0,

$$\frac{(\rho_\infty - \rho)\rho_f}{(\rho_\infty - \rho_f)\rho} = \left(1 - \frac{y}{\delta}\right)^2. \tag{22}$$

Setting these profiles in the integral equations (17) and (18) gives a set of differential equations that in dimensionless form are

$$\frac{6u_1'}{\delta'^2} = \mathrm{PrGrcos}\phi + \frac{1}{3}\sin\phi \mathrm{PrGr}\frac{d\delta'}{dx'}, \tag{23}$$

$$\frac{1}{30}\frac{d}{dx'}(u_1'\delta' \mathrm{Gr}) = 2\frac{\mathrm{Gr}}{\delta'}, \tag{24}$$

where the dimensionless quantities are $u_1' = u_1 L/\alpha$, $\delta' = \delta/L$, $x' = x/L$, with L being a characteristic length scale. The Grashof and Prandtl numbers are defined as follows:

$$\mathrm{Gr} = g\frac{\rho_\infty - \rho_f}{\rho*}\frac{L_f^3}{\upsilon*^2}, \tag{25}$$

$$\mathrm{Pr} = \frac{\upsilon*}{\alpha*}, \tag{26}$$

where the superscript * means that properties are evaluated at the reference temperature. The set of dimensionless equations (23) and (24) might be solved for an inclined plate first neglecting the term with $d\delta'/dx$ from both equations. This is equivalent to consider only the gravity component parallel to the surface. This first approximation gives

$$\delta_1' = \left(\frac{480}{\mathrm{PrGrcos}\phi}\right)^{1/4} x'^{1/4}, \tag{27}$$

$$u_{1,1}' = \left(\frac{40}{3}\right)^{1/2} (\mathrm{PrGrcos}\phi)^{1/2} x'^{1/2}, \tag{28}$$

The Nusselt number is the ratio of the heat transfer convected by the heat transfer conducted. For natural convection, it is a function of Prandtl and Grashof numbers [20]. It may be expressed as $\mathrm{Nu} = 2/\delta'$ [17]. Then

$$\mathrm{Nu}_1 = \frac{2}{480^{1/4}}(\mathrm{PrGrcos}\phi)^{1/4}. \tag{29}$$

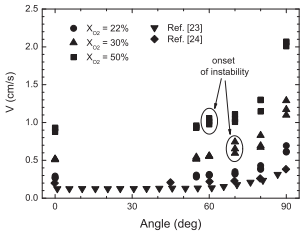

FIG. 3. Flame spread rate versus angle to vertical of the samples.

Taking into account the gravity component normal to the surface allows us to make a second approximation,

$$\delta_2' = \delta_1' \frac{\left[1 - \frac{1}{6}\tan\phi\left(\frac{480}{\mathrm{PrGrx'}}\right)^{1/4}\right]^{1/2}}{1 - \frac{1}{3}\tan\phi\left(\frac{480}{\mathrm{PrGrx'}}\right)^{1/4}}, \tag{30}$$

$$u_{1,2}' = u_{1,1}' + \frac{10^{3/4}}{3^{5/4}}\tan\phi\left(\frac{\mathrm{PrGrcos}\phi}{x'}\right)^{1/4} \times \frac{1 - \frac{1}{6}\tan\phi\left(\frac{480}{\mathrm{PrGrx'}}\right)^{1/4}}{\left[1 - \frac{1}{3}\tan\phi\left(\frac{480}{\mathrm{PrGrx'}}\right)^{1/4}\right]^2}, \tag{31}$$

where the second approximation to the Nusselt number gives

$$\mathrm{Nu}_2 = \mathrm{Nu}_1 \frac{1 - \frac{1}{3}\tan\phi\left(\frac{480}{\mathrm{PrGr}}\right)^{1/4}}{\left[1 - \frac{1}{6}\tan\phi\left(\frac{480}{\mathrm{PrGr}}\right)^{1/4}\right]^{1/2}}. \tag{32}$$

V. RESULTS

Figure 3 shows the experimental results of the flame spread rate as a function of the angle of inclination of the sample for (a) different values of room oxygen concentration (new data, three repetitions on every environmental conditions) and (b) ambient conditions obtained by Refs. [23] and [24]. In Ref. [7] there was also an experimental analysis of the flame front speed for different angles of inclinations but with an external heating supply. In contrast with the results of Kurosaki and coworkers [23,24], Kashiwagi and Newman [7] found that there exists a threshold angle of inclination beyond which the instabilities of the flow lead to large variations on the value of the flame front speed. This critical angle reduces as the value of the external heat supplied to the system increases. This effect is not clearly observed at near-ambient conditions without an external heat supply. However, at higher room oxygen concentration X_{O_2}, we do capture an onset of instability (see Fig. 3) that arises at lower angles of inclination as X_{O_2} increases. Note in Fig. 3 that the flame spread rate is almost constant for a wide range of angles of inclination until a point where the three repetitions of the experiments produce a variation of 20% or higher between flame spread values.

Although such an instability makes it difficult to reproduce the observed flame spread rate by means of an analytical model, a generalization of the de Ris expression (6) in order

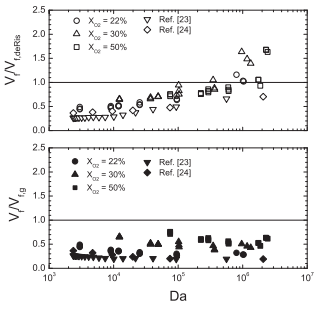

FIG. 4. Normalized values of flame front speed as a function of Damkohler number.

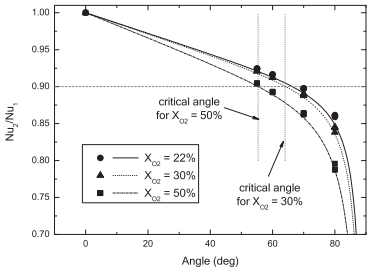

FIG. 5. Nu_2/Nu_1 for all X_{O_2} tested, experimental results, and expected curves.

to predict the trend of data is of great importance, especially at low oxygen concentrations. Figure 4 shows the normalized values of the flame front speeds shown in Fig. 3 as a function of the Damkohler number Da. In Fig. 4, $V_{f,\text{de Ris}}$ follows Eq. (6) and $V_{f,g}$ is obtained from Eq. (12) by using the characteristic gas phase thermal lengths as

$$L_{gx+} = \frac{\alpha_g}{V_{\text{acv}}\cos\phi + V_f}, \tag{33}$$

and $L_{gx-} = L_{gy+} = L_{gy-} = L_{gx+}(\phi = 0^\circ)$. In Eq. (33), α_g is the gas-phase thermal diffusivity and V_{acv} is the convective velocity itself, which is calculated as $V_{\text{acv}} = [g\alpha(\rho_\infty - \rho_f)/\rho*]^{1/3}$ (the formula is obtained equating buoyancy and inertia forces [22]). Note that $V_{\text{acv}}\cos\phi$ is the component parallel to the sample surface on the upper side. Below, the paper acts as a barrier for the upward convective flow and, for simplicity, we have employed $L_{gx-} = L_{gy+} = L_{gy-} = L_{gx+}(\phi = 0^\circ)$. The effect of the radiative flux from the flame is taken into account by using a constant value of $\beta^+ = \beta^- = 140^\circ$, although different values of these angles did not produce significant changes on the burning rate, which confirms the small relevance of radiative fluxes in the flame front propagation within the thermal regime [25]. Conduction through the solid in Eq. (12) has been also neglected, since it is not considered of importance in the burning of thin samples [5].

The Damkohler number is the ratio of the residence time for the gas mixture in the flow and the chemical time for the first-order Arrhenius-type reaction [26], being

$$\text{Da} = \frac{\alpha_g}{\rho_g}\frac{Y_F Y_O A_g e^{-E_g/RT_{f,\text{ad}}}}{(V_{\text{acv}}\cos\phi + V_f)^2}, \tag{34}$$

where $A_g(=3.57\times10^7\ \text{m}^3\ \text{kg}^{-1}\ \text{s}^{-1})$ is the preexponential factor, E_g $(=125\times10^5\ \text{J mol}^{-1})$ is the activation energy, and Y_O and Y_F are the room oxygen and fuel mass fractions, respectively. Following Ref. [26], the fuel mass fraction follows $Y_F = \text{Sc}\ln(1+B)/B^{0.15}$, where B is the mass transfer number and Sc is the viscous to mass diffusivity ratio. We note that higher values of the Damkohler number are obtained for higher values of inclination angle and/or higher values of room oxygen concentration level (fast reaction).

In Fig. 4, the normalized flame front speed data with respect to the de Ris expression shows a trend to increase as a function of the Damkohler number Da. A similar behavior was already observed in Ref. [26] for the downward ($\phi = 0^\circ$) combustion of thin solid fuels. Our simple analytical model (12) improves the classical one since the normalization of V_f with Eq. (12) tend to be almost independent on Da. However, Eq. (12) overpredicts the flame front speed for a factor of 1.3 to 5, depending on the data and angle employed. In contrast with the classical de Ris expression, however, Eq. (12) behaves as an upper bound whose range of values are even below than those obtained applying Eq. (3) (see Fig. 3 in Ref. [13]).

The onset of the instability can be tracked using the quotient of Nusselt numbers exposed in Sec. IV. Figure 5 shows the ratio of Nusselt numbers calculated as in Eq. (32) for all the situations tested and the theoretical behavior expected. There is a good agreement between the expected curves and experimental values of the quotient of Nusselt numbers; they differ less than 1.5%. The values of $\text{Nu}_2/\text{Nu}_1 = 0.9$ are chosen as the theoretical critical angle in Fig. 5, being 64.2° and 55.4° for $X_{O_2} = 30\%$ and 50%, respectively. This coincides with the experimental angles showing unstable values seen in Fig. 3. For the $X_{O_2} = 22\%$ case, there is no instability due to the low energy of the flame as also observed in thermally thicker samples [23,24].

The Grashof number is computed using as a reference length the flame length L_f, calculated using the formula obtained in Ref. [11], $L_f \approx 0.0345\{(T_f - T_v)/[(T_v - T_\infty)Y_{O2\infty}]\}^2\alpha/(V_{\text{acv}} + V_f)$, with the flame spread rate V_f being either the experimental value or the calculated using de Ris's formula $[V_f = (\pi/4)\lambda/(\tau\rho_s c_s)(T_f - T_v)/(T_v - T_\infty)$ [12], i.e., Eq. (12) for $\phi = 0^\circ$ with no radiation neither conduction through the solid phase]. The experimental values of the flame length were not used because of experimental difficulties. The temperature of flame used is the mean of temperatures of the flame zone computed as in Ref. [16]. The reference temperature used for calculating the transport

properties from the gas was the vaporization temperature ($T_v = 640$ K).

For nearly horizontal samples, the experiments show an unstable spread rate that may be triggered by curling of ashes and may be due to the flame in the lower side of the sample, as stated in Ref. [7]. The instability observed can be explained through the importance of the gravity component normal to the surface.

The importance of the normal component of gravity can be traced through the correction done to the Nusselt number Nu_2/Nu_1. After doing the tests, it has been seen that when this correction is greater than 10% of Nu_1, flame spread rates become unstable and expand for a large range of values.

VI. CONCLUSIONS

The flame spread down thermally thin inclined samples is controlled by heat transfer to the unburned part of the sample. For vertical or slightly inclined surfaces, the behavior can be explained using only the component of gravity parallel to the surface. The component of gravity normal to the surface of the sample gains importance as the surface becomes more horizontal and may trigger an instability. In this paper we have generalized the classical analytical expression of the flame front speed [12] in order to be valid for the downward burning of an inclined sample. We have also developed a method to show the importance of the normal component of gravity via the quotient of Nusselt numbers having and not having into account this component. We have found that the instability arises when the correction is greater than a 10%, this being valid for different X_{O_2} concentration values.

ACKNOWLEDGMENTS

B.C. acknowledges the support of a FPU grant from the MICINN. Some data were obtained by Adrià Carmona. We also thank Jordi Vicens and Sergi Saus for their technical assistance. This work has been partially funded by the Generalitat de Catalunya under Grant No. 2009-SGR-374 and the MICINN-FEDER under Grant No. FIS-2012-31307.

[1] D. Drysdale, *An Introduction to Fire Dynamics*, 3rd ed. (Wiley, New York, 2011).
[2] R. D. Benguria, J. Cisternas, and M. C. Depassier, Phys. Rev. E **52**, 4410 (1995).
[3] N. Provatas, T. Ala-Nissila, M. Grant, K. R. Elder, and L. Piche, Phys. Rev. E **51**, 4232 (1995).
[4] T. Pujol, J. Fort, L. Montoro, and J. J. Suñol, Physica A **388**, 4959 (2009).
[5] I. S. Wichman, Prog. Energy Combust. Sci **18**, 553 (1992).
[6] T. Pujol and B. Comas, Phys. Rev. E **84**, 026306 (2011).
[7] T. Kashiwagi and D. L. Newman, Combust. Flame **26**, 163 (1976).
[8] O. Zik, Z. Olami, and E. Moses, Phys. Rev. Lett. **81**, 3868 (1998).
[9] O. Zik and E. Moses, Phys. Rev. E **60**, 518 (1999).
[10] B. Comas and T. Pujol, Combust. Sci. Technol. **184**, 489 (2012).
[11] S. Bhattacharjee, S. Takahashi, K. Wakai, and C. P. Paolini, Proc. Combust. Inst. **33**, 2465 (2011).
[12] J. N. De Ris, in *Proceedings of the Twelfth Symposium (International) on Combustion, University of Poitiers, France, 1968*, edited by The Combustion Institute (The Combustion Institute, Pittsburgh, 1969), p. 241.
[13] T. Pujol and B. Comas, Comb. Sci. Technol. **183**, 1083 (2011).
[14] M. A. Delichatsios, Combust. Flame **135**, 441 (2003).
[15] A. Itoh and Y. Kurosaki, Combust. Flame **60**, 269 (1985).
[16] J. B. Greenberg and P. D. Ronney, Int. J. Heat Mass Transf. **36**, 315 (1993).
[17] J. S. Kim, J. N. de Ris, and K. W. Kroesser, Proc. Comb. Institute **13**, 949 (1971).
[18] K. Annamalai and M. Sibulkin, Combust. Sci. Technol. **19**, 167 (1979).
[19] K. Annamalai and M. Sibulkin, Combust. Sci. Technol. **19**, 185 (1979).
[20] H. Schlichting, *Boundary-Layer Theory*, 7th ed. (McGraw-Hill, New York, 1987).
[21] S. Levy and N. Y. Schenectady, Numer. Heat Transfer, Part A **40**, 841 (2001).
[22] F. C. Duh and C. H. Chen, Combust. Sci. Technol. **77**, 291 (1991).
[23] T. Hirano, S. E. Noreikis, and T. E. Waterman, Combust. Flame **22**, 353 (1974).
[24] M. Sibulkin, W. Ketelhut, and S. Feldman, Combust. Sci. Technol. **9**, 75 (1974).
[25] S. Bhattacharjee, R. Ayala, K. Wakai, and S. Takahashi, Proc. Combust. Inst. **30**, 2279 (2005).
[26] A. C. Fernandez-Pello, S. R. Ray, and I. Glassman, in *Proceedings of the Eighteenth Symposium (International) on Combustion, University of Waterloo, Canada, 1980*, edited by The Combustion Institute (The Combustion Institute, Pittsburgh, 1981), p. 579.